University of Nevada, Reno

Characterization of Field-Produced HMA Mixtures from Nevada for Mechanistic-Empirical Pavement Design

A thesis submitted in partial fulfillment of the
requirements for the degree of Master of Science in
Civil and Environmental Engineering

by

Teresa Christine Feaster

Dr. Elie Hajj/Thesis Advisor

August, 2012

University of Nevada, Reno

THE GRADUATE SCHOOL

We recommend that the thesis
prepared under our supervision by

TERESA CHRISTINE FEASTER

entitled

Characterization Of Field-Produced HMA Mixtures From Nevada For Mechanistic-Empirical Pavement Design

be accepted in partial fulfillment of the
requirements for the degree of

MASTER OF SCIENCE

Elie Y. Hajj, Ph.D., Advisor

Peter Sebaaly, Ph.D., Committee Member

Rajarantnam V. Siddharthan, Ph.D., Committee Member

James Carr, Ph.D., Graduate School Representative

Marsha H. Read, Ph. D., Dean, Graduate School

August, 2012

ABSTRACT

The Nevada Department of Transportation (NDOT), with the help of the Western Regional Superpave Center (WRSC) began steps toward implementing the Mechanistic-Empirical Pavement Design Guide (MEPDG). NDOT is transitioning from AASHTO 1993 design methods to the newer state of the practice method. The MEPDG incorporates the mechanistic-empirical (M-E) pavement models to predict pavement damage as a function of specific traffic, materials and environmental inputs. The use of M-E based methods makes it possible to optimize the design and to more fully ensure that specific distress types will be limited to values less than the failure criteria within the design life of the pavement structure.

To begin implementation 26 field produced mixtures have been sampled from behind the paver, since 2005, throughout the state of Nevada. Each mixture has a Contract designation and will be evaluated using laboratory performance testing for the binders viscosity, dynamic modulus, rutting regression coefficients using the Repeated Load Triaxial (RLT), and fatigue regression coefficients using the Flexural Beam Fatigue tester. Currently the MEPDG prediction models are nationally calibrated and require local or regional calibration to predict pavement performance more accurately. This implementation study is the first steps toward local calibration for Nevada.

Each of the laboratory evaluations will be grouped using a 95% confidence interval to see if the Contracts can all be grouped together or separate groups for binder grade, District divisions within NDOT, Type 2 or 2C mixtures, or by aggregate and/or

binder source. Viscosity groups found include binder grade, a District and two binder sources. Dynamic modulus values could be grouped together by District division and six different binder and aggregate sources each. Rutting coefficients were grouped by District, two binder sources, and an aggregate source. Fatigue coefficients can be grouped together for all the Contracts tested and by binder grade. Each of the Contracts for a group will be averaged for the corresponding input and provided to NDOT as inputs into the MEPDG to begin local calibration.

ACKNOWLEDGMENTS

I would like to acknowledge all of those who have helped me achieve this goal of finishing a Master's degree. First and foremost my family which includes my parents for always supporting me 100% in everything I do, my sister for always being there for me when I need any advice, and my brother for being the one person who I could always count on to be there for me whenever I needed him.

My fellow colleagues in the program, who have helped me in so many ways, who have now become my friends I am forever thankful to. These people include, in no particular order, Christine, Nathan, Matt, Alvaro, Juan, Piratheep, Kevin, Cristian, Nate Mena, Zia, and Zahi.

I would not have made it through this process without my closet friends being there for me. These people include Lindsay, Tory, Brittany, Jessica, Sara, Dave, Jordan, Krystin, Michon, Chris, Tabitha, Emily, Chanse, LeAnna, Cameron, and Jenny. These are the few people who have kept me sane throughout this long process.

I also owe gratitude to Dr. Sebaaly and Dr.Hajj for guiding me through this process and helping me to achieve a Masters.

TABLE OF CONTENTS

Abstract i

Acknowledgments iii

List of Tables vi

List of Figures vii

Chapter 1: Introduction 1

1.1: Objective 2

Chapter 2: Background 3

2.1 Design Method Comparison 3

2.1.1 AASHTO 1993 Design Guide 3

2.1.3 AASHTO 2002 MEPDG 5

2.2: MEPDG Design Process 7

2.2.1 Prediction Models 8

2.2.2 Rutting Model Calibration 9

2.2.3 Fatigue Model Calibration 11

2.3 Calibration Factors for Polymer-Modified Asphalts 15

2.4 National Calibration Deficiencies 15

2.5 Local Calibration Experiences 16

Chapter 3: Research Project Scope 19

Chapter 4: Laboratory Testing 21

4.1: Descriptions 21

4.1.1: Binder Viscosity 21

4.1.2: Dynamic Modulus 22

4.1.3 Repeated Load Triaxial 25
4.1.4 Flexural Beam Fatigue 28
4.2 Results 31
4.2.1 Binder Viscosity 31
4.2.2 Dynamic Modulus 33
4.2.3 Repeated Load Triaxial 35
4.2.4 Flexural Beam Fatigue 36
Chapter 5: Analysis 37
5.1 Witczak Model 37
5.2 A-VTS Comparison 38
5.3 Recommendations to Begin Local Calibration 38
Chapter 6: Conclusions and Recommendations 40
References 44
Tables 47
Figures 56

LIST OF TABLES

Table 1. List of Contracts Sampled for NDOT MEPDG Implementation 48
Table 2. Contract Grouping Information 49
Table 3. Binder Measurements from the DSR 50
Table 4. A-VTS Values 51
Table 5. Binder Viscosity Groupings 51
Table 6. Dynamic Modulus Shift Factors 52
Table 7: Dynamic Modulus Groupings 53
Table 8. Rutting Laboratory Regression Coefficients 54
Table 9: Rutting Laboratory Regression Grouping Coefficients 54
Table 10. Fatigue Laboratory Regression Coefficients 55
Table 11: Fatigue Laboratory Regression Grouping Coefficients 55
Table 12. MEPDG Level 3 A-VTS Values 55

LIST OF FIGURES

Figure 1. MEPDG Stages of Design 57
Figure 2. Nevada map with District Boundaries and Contract Location by County 58
Figure 3. .45 Power Gradation Plots for Contracts 3214, 3239, 3247, 3257, 3248, and 3260..... 59
Figure 4. .45 Power Gradation Plots for Contracts 3312, 3274, 3325, 3331, 3323, and 3330..... 60
Figure 5. .45 Power Gradation Plots for Contracts 3329, 3338, 3348-TR, 3358, 3358, 3350, and 3368 61
Figure 6. .45 Power Gradation Plots for Contracts 3372, 3373, 3383, 3348-PM, 3378, and 3382 62
Figure 7. .45 Power Gradation Plots for Contracts 3399-NR and 3399-RAP 63
Figure 8. Rutting Permanent Deformation Levels 63
Figure 9. Flexural Beam Fatigue Loading Frame and Degrees of Freedom 64
Figure 10. Binder Viscosity Results for sampled Nevada Binders 65
Figure 11. Binder Viscosity Results for PG64-28NV Mixtures 65
Figure 12. Binder Viscosity Results for PG76-22NV Mixtures 66
Figure 13. Binder Viscosity Results for District 2 66
Figure 14. Binder Viscosity Results for District 3 67
Figure 15. Binder Viscosity Results for Valero Binder Source 67
Figure 16. Binder Viscosity Results for Paramount Binder Source 68
Figure 17. Dynamic Modulus Results for all Sampled Nevada Mixtures at 70°F 69
Figure 18. Dynamic Modulus Results for all Sampled Nevada Mixtures at 104°F 70
Figure 19. Dynamic Modulus Results for the Averages of PG64-28NV and PG76-22NV Mixtures (a) 70°F (b) 104°F 71
Figure 20. Dynamic Modulus Results for the PG64-28NV Mixtures at 70°F 72
Figure 21. Dynamic Modulus Results for the PG64-28NV Mixtures at 104°F 73
Figure 22. Dynamic Modulus Results for the PG76-22NV Mixtures at 70°F 74
Figure 23. Dynamic Modulus Results for the PG76-22NV Mixtures at 104°F 75
Figure 24. Dynamic Modulus Results for Type 2 Mixtures at 70°F 76
Figure 25. Dynamic Modulus Results for Type 2 Mixtures at 104°F 77
Figure 26. Dynamic Modulus Results for Type 2C Mixtures at 70°F 78
Figure 27. Dynamic Modulus Results for Type 2C Mixtures at 104°F 79
Figure 28. Dynamic Modulus Results for District 2 Mixtures at 70°F 80
Figure 29. Dynamic Modulus Results for District 2 Mixtures at 104°F 81
Figure 30. Dynamic Modulus Results for District 3 Mixtures at 70°F 82

Figure 31. Dynamic Modulus Results for District 3 Mixtures at 104°F 83
Figure 32. Dynamic Modulus Results for Aggregate Source Bertagnolli Mixtures at 70°F 84
Figure 33. Dynamic Modulus Results for Aggregate Source Bertagnolli Mixtures at 104°F 85
Figure 34. Dynamic Modulus Results for Aggregate Source Blue Diamond Mixtures at 70°F 86
Figure 35. Dynamic Modulus Results for Aggregate Source Blue Diamond Mixtures at 104°F .. 87
Figure 36. Dynamic Modulus Results for Aggregate Source Hunewill Mixtures at 70°F 88
Figure 37. Dynamic Modulus Results for Aggregate Source Hunewill Mixtures at 104°F 89
Figure 38. Dynamic Modulus Results for Aggregate Source Lockwood Mixtures at 70°F 90
Figure 39. Dynamic Modulus Results for Aggregate Source Lockwood Mixtures at 104°F 91
Figure 40. Dynamic Modulus Results for Aggregate Source PE 83-02 Mixtures at 70°F 92
Figure 41. Dynamic Modulus Results for Aggregate Source PE 83-02 Mixtures at 104°F 93
Figure 42. Dynamic Modulus Results for Aggregate Source Sloan Mixtures at 70°F 94
Figure 43. Dynamic Modulus Results for Aggregate Source Sloan Mixtures at 104°F 95
Figure 44. Dynamic Modulus Results for Binder Source Ergon Mixtures at 70°F 96
Figure 45. Dynamic Modulus Results for Binder Source Ergon Mixtures at 104°F 97
Figure 46. Dynamic Modulus Results for Binder Source Idaho Mixtures at 70°F 98
Figure 47. Dynamic Modulus Results for Binder Source Idaho Mixtures at 104°F 99
Figure 48. Dynamic Modulus Results for Binder Source KPA Mixtures at 70°F 100
Figure 49. Dynamic Modulus Results for Binder Source KPA Mixtures at 104°F 101
Figure 50. Dynamic Modulus Results for Binder Source Paramount Mixtures at 70°F 102
Figure 51. Dynamic Modulus Results for Binder Source Paramount Mixtures at 104°F 103
Figure 52. Dynamic Modulus Results for Binder Source SEM Mixtures at 70°F 104
Figure 53. Dynamic Modulus Results for Binder Source SEM Mixtures at 104°F 105
Figure 54. Dynamic Modulus Results for Binder Source Valero Mixtures at 70°F 106
Figure 55. Dynamic Modulus Results for Binder Source Valero Mixtures at 104°F 107
Figure 56. Rutting Results for all Sampled Nevada Mixtures (a)104°F (b) 114.8°F (c) 136.4°F 108
Figure 57. Rutting Results for all PG64-28NV Mixtures (a)104°F (b) 114.8°F (c) 136.4°F 109
Figure 58. Rutting Results for all PG76-22NV Mixtures (a)104°F (b) 114.8°F (c) 136.4°F 110
Figure 59. Rutting Results for all Type 2 Mixtures (a)104°F (b) 114.8°F (c) 136.4°F 111
Figure 60. Rutting Results for all Type 2C Mixtures (a)104°F (b) 114.8°F (c) 136.4°F 112
Figure 61. Rutting Results for District 2 Mixtures (a)104°F (b) 114.8°F (c) 136.4°F 113
Figure 62. Rutting Results for District 3 Mixtures (a) 104°F (b) 114.8°F (c) 136.4°F 114

Figure 63. Rutting Results for Binder Source SEM Mixtures (a) 104°F (b) 114.8°F (c) 136.4°F 115
Figure 64. Rutting Results for Binder Source Paramount Mixtures (a) 104°F (b) 114.8°F (c) 136.4°F..... 116
Figure 65. Rutting Results for Aggregate Source Lockwood Mixtures (a) 104°F (b) 114.8°F (c) 136.4°F..... 117
Figure 66. Fatigue Results for Sampled Mixtures in Nevada (a) 55°F (b) 70°F (c) 85°F 118
Figure 67. Fatigue Results for PG76-22NV Mixtures in Nevada (a) 55°F (b) 70°F (c) 85°F..... 119
Figure 68. Witczak Model Comparison To Measured E* 120
Figure 69. MEPDG Level 3 Comparison to Measured A Values..... 120
Figure 70. MEPDG Level 3 Comparison to Measured VTS Values 121
Figure 71. Shifting Predicted to Measured using a Beta Factor 121

CHAPTER 1: INTRODUCTION

The Nevada Department of Transportation (NDOT) currently uses the 1993 American Association of State Highway and Transportation Officials (AASHTO) Guide for Design of Pavement Structures. As the asphalt industry evolves so do the methods of design. To adjust for current trends NDOT's goal is to implement the Mechanistic-Empirical Pavement Design Guide (MEPDG) in the near future for flexible pavements. The MEPDG incorporates the mechanistic-empirical (M-E) pavement models to predict pavement damage as a function of specific traffic, materials and environmental inputs. The use of M-E based methods makes it possible to optimize the design and to more fully ensure that specific distress types will be limited to values less than the failure criteria within the design life of the pavement structure.

The MEPDG uses performance based models nationally calibrated using the Long-Term Pavement Performance (LTPP) database under the National Cooperative Highway Research Program (NCHRP) Project 1-37A (1). The LTPP database includes pavement sections throughout the United States, however only one flexible pavement section in Nevada was included in the national calibration process (1). Therefore it is necessary to calibrate these models for specific state and regional conditions because of the difference in materials, environmental conditions, and construction practices (2). The primary objective of model calibration is to reduce bias because a biased model will consistently produce either over-designed or under-designed pavements (3).

1.1: Objective

The objective of this study is to provide NDOT with recommendations for implementing the MEPDG for flexible pavements using local calibration factors. To begin implementation NDOT has established a research plan with the University of Nevada, Reno's Western Regional Superpave Center (WRSC), which began in 2005, to use laboratory mixture evaluations to create a database of input values to be used in the distress models of MEPDG for local calibration. Recommendations will be given based off results from Binder Viscosity, Dynamic Modulus, Repeated Load Triaxial, and Flexural Beam Fatigue testing. Suggestions of possible groupings for the input values will be categorized based off districts within NDOT, binder grade, Type 2 or 2C mixtures, and binder source and/or aggregate source.

CHAPTER 2: BACKGROUND

2.1 Design Method Comparison

2.1.1 AASHTO 1993 Design Guide

AASHTO's 1993 pavement design guide is an empirical design method based on performance equations developed using 1950's AASHO Road Test data with some refinements in material input parameters, design reliability, and empirical procedures for rehabilitation design (4,5). Although refinements have been added, the AASHTO design guide has serious limitations including (1):

- Traffic loading deficiencies: Heavy truck traffic design volume levels have increased tremendously (about 10 to 20 times) since the design of the pavements used in the interstate system in the 1960's. Pavements today need to be designed for 50 to 200 million trucks versus 5 to 15 million trucks previously designed for. Design life has also increased to 30-40 years versus 20 years. Designing for this level requires extrapolation of the design methodology and may result in either "under-designed" or "over-designed" projects.
- Rehabilitation deficiencies: Procedures in the 1993 Guide are completely empirical and very limited, especially in consideration of heavy traffic. Most projects today include rehabilitation design.
- Climatic effects deficiencies: Because the AASHO Road Test was conducted at one specific geographic location, it is impossible to address the effects of different climatic conditions on pavement performance.

- Subgrade deficiencies: One type of subgrade was used for all test sections at the Road test, but many types exist nationally that result in different performance of highway pavements.
- Surfacing material deficiencies: only one hot mix asphalt (HMA) mixture and one portland cement concrete (PCC) mixture were used at the Road Test.
- Base course deficiencies: Only two unbound dense granular base/subbase materials were included in the main flexible and rigid pavement sections of the AASHO Road Test (limited testing of stabilized bases was included for flexible pavements). Today, various stabilized types of higher quality are used routinely, especially for heavier traffic loadings.
- Truck characterization deficiencies: Vehicle suspension, axle configurations, and tire types and pressures were representative of the types used in the late 1950's. Many of these are outmoded (tire pressures of 80 psi versus 120 psi today), resulting in deficient pavement designs to carry these loadings.
- Construction and drainage deficiencies: Pavement designs, materials, and construction were representative of those used at the time of the Road Test. No subdrainage was included in the Road Test sections, but positive subdrainage has become common in today's highways.
- Design life deficiencies: Because of the short duration of the Road Test, the long-term effects of climate and aging of materials were not addressed. Direct consideration of the cyclic effect on materials response and aging will lead to improved design life reliability.

- Performance deficiencies: Earlier AASHTO procedures relate the thickness of the pavement surface layers to serviceability. However, research and observations have shown that many pavements need rehabilitation for reasons that are not related directly to pavement thickness (e.g., rutting, thermal cracking, faulting). These failure modes are not considered directly in the previous versions of the AASHTO Guide, which may be leading to more premature failures.

2.1.3 AASHTO 2002 MEPDG

The MEPDG Guide embraces a design philosophy which includes the following major tenants (1):

- The Guide generally applies validated, state-of-the-practice technologies.
- The Guide provides designers with the versatility to consider a wide variety of design and material options.
- The Guide provides an equitable design basis from the standpoint of pavement type selection.
- The Guide addresses both new and rehabilitation design issues.
- The Guide and associated software are user friendly.
- The Guide provides for three hierchical levels of design inputs that allow the designer to match the level of effort of the importance of the project. The input levels also allow for using improved procedures that may be developed in the future.
    - Level 1: Inputs provide the highest level of accuracy and, thus, would have the lowest level of uncertainty or error. Level 1 inputs would

typically be used for designing heavily trafficked pavements or wherever there are dire safety or economic consequences of early failure. Level 1 material input require laboratory or field testing, such as dynamic modulus testing of hot-mix asphalt concrete, site-specific axle load spectra data collections, or nondestructive deflection testing. Odbtaining Level 1 input requires more resources and time than other levels.

- Level 2: Inputs provide an intermediate level of accuracy and would be closes to the typical procedures used with earlier editions of the AASHTO Guide. This level would be used when resources or testing equipment's are not available for test required for Level 1. Level 2 inputs typically would be user-selected, possibly from an agency database, could be derived from a limited testing program, or could be estimated through correlations. Examples would be estimating asphalt concrete dynamic modulus from binder, aggregate, and mix properties, or using site-specific traffic volume and traffic classification data in conjunction with agency-specific axle load spectra.
- Level 3: Inputs provide the lowest level of accuracy. This level might be used for design where there are minimal consequences of early failure (e.g., lower volume roads). Inputs typically would be user-selected values or typical averages for the region. An example includes default unbound resilient modulus values.

Using the MEPDG has many benefits over the AASHTO 1993 design guide. MEPDG allows for the use of significant material properties while the 1993 Guide used a loosely defined layer coefficient. The MEPDG also allows the designer to determine the required thickness of asphalt bound material to limit fatigue cracking. The AASHTO design procedure is based only on 2 years of performance data, so long-term climatic effects could not be considered, while the MEPDG includes technology that directly considers aging of materials, month by month, over the design period (1). Using mechanistic procedures will reduce life cycle costs significantly over an entire highway network.

2.2: MEPDG Design Process

The design approach consists of three major stages shown in Figure 1. Stage 1 consists of the development of input values for the analysis. Input values consist of foundation analysis (stiffness determination, volume change, frost heave, thaw weakening, and drainage concerns), pavement material characterization, traffic input, and the Enhanced Integrated Climate Model (EICM) is utilized (1). The EICM is a powerful climatic effects tool which is used to model temperature and moisture within each pavement layer and the subgrade. Using hourly climatic data from weather stations across the country (temperature, precipitation, solar radiation, cloud cover, and wind speed), the temperature and moisture predictions from the EICM are calculated hourly over the design period and used in various ways to estimate material properties for the foundation and pavement layers throughout the design life (1).

Stage 2 of the design process is the structural/performance analysis. Beginning with an initial trial design that can be created by the designer, obtained from an existing design procedure, or from a general catalog, the analysis approach is iterative (6). The trial section is analyzed incrementally over time using the pavement response and distress models, and the outputs of the analysis are accumulated damage, the expected amount of distress, and smoothness over time. If the trial design does not meet the performance criteria, modifications are made and the analysis re-run until a satisfactory result is obtained (1). Stage 3 of the process includes those activities required to evaluate the structurally viable activities such as an engineering analysis and life cycle cost analysis of the alternatives (1).

2.2.1 Prediction Models

Pavement distress prediction models, or transfer functions, are the key components of any M-E design and analysis procedure, and the accuracy depends on an effective process of calibration and subsequent validation with independent data sets (3). The term "calibration" refers to the mathematical process through which the total error or difference between the observed and the predicted values for a quantity is minimized. It is a systematic process to eliminate the bias and minimize the difference between the observed or measured performance from the actual pavements and predicted results from an empirical or mechanistic model (7). All performance models in the MEPDG were calibrated on a global level to observed field performance over a representative sample of pavement test sites throughout North America. The Long Term Pavement Performance (LTPP) test sections were used extensively in the calibration process, because of the

consistency in the monitored data over time and the diversity of the test sections spread throughout North America (3). Since pavement preservation and maintenance, construction and material specifications, and materials vary across the United States and are not considered directly in the MEPDG, local calibration allows for these parameters to be included indirectly (3).

Most of the sections used to calibrate the MEPDG included conventional or neat HMA mixtures. NDOT specifies polymer modified asphalt binders in all their mixtures. NCHRP Projects 9-30 and 1-40B and the Asphalt Institute report showed that the use of calibration factors based primarily on neat mixtures will over estimate the amount of distress of polymer-modified asphalt layers (8,9,10). The MEPDG includes, for flexible pavements, transfer functions for fatigue, rutting, thermal cracking, and roughness. For this study, fatigue and rutting transfer functions will be the primary focus.

National calibration and validation of the MEPDG was conducted under NCHRP 1-37A (11). Under this project, both rutting and fatigue models were calibrated using 134 test sections with variable site conditions in the United States.

2.2.2 Rutting Model Calibration

Rutting is the accumulation of rutting in all the layers of the pavement structure and appears as a longitudinal depression along the wheel path. Rutting can cause roughness issues, hydroplaning, and other safety concerns. The MEPDG model, before calibration, is shown in Equation 2.1.

$$\frac{\varepsilon_p}{\varepsilon_r} = 10^{K_1} T^{K_2} N^{K_3} \quad (2.1)$$

where:

ε_p= Accumulated plastic strain at N repetitions of load (in/in)
ε_r= Resilient strain of the asphalt material as a function of mix properties, temperature and time rate of loading (in/in)
K_1, K_2, K_3= Non-linear regression coefficients before national calibration, where K_1=-3.1552, K_2=1.734, K_3=0.39937
T= Temperature (°F)

The main purpose of calibrating the rutting model was to modify the K factors in order to reduce the prediction error that was associated with the original MEPDG model. To calibrate the model, each K value is multiplied by a calibration factor. Additionally, a k_Z factor was introduced and is a function of the total AC layer thickness. The rutting model with the addition calibration factors is shown in Equation 2.2.

$$\frac{\varepsilon_p}{\varepsilon_r} = k_Z \times \beta_{r1,National} \times 10^{K_1} T^{K_2 \times \beta_{r2,National}} N^{K_3 \times \beta_{r3,National}} \quad (2.2a)$$

$$k_z = (C_1 + C_2 \times depth) \times 0.328196^{depth} \quad (2.2b)$$

$$C_1 = -0.1039 \times H_{ac}^2 + 2.4868 \times H_{ac} - 17.342 \quad (2.2c)$$

$$C_2 = 0.0172 \times H_{ac}^2 - 1.7331 \times H_{ac} + 27.428 \quad (2.2d)$$

where:

k_Z= Function of total asphalt layer thickness (H_{ac}, in) and depth (in) to computational point, to correct for the confining pressure at different depths

$\beta_{r1,National}$, $\beta_{r2,National}$,$\beta_{r3,National}$= National calibration coefficients

Calibration of the rutting model was achieved by optimizing the error for the total rut on all layers by running simulation runs using the MEPDG software. The final national calibration factors were found to be: $\beta_{r1,National}$= 0.509, $\beta_{r2,National}$=0.9, $\beta_{r3,National}$=1.2. The final nationally calibrated model is shown in Equation 2.3.

$$\frac{\varepsilon_p}{\varepsilon_r} = k_Z \times 10^{-3.4488} T^{1.5606} N^{0.479244} \quad (2.3)$$

After national calibration, regional calibration is still needed to refine the models to fit the conditions for each specific region. Local calibration coefficients were added to the nationally calibrated model which is shown in Equation 2.4.

$$\frac{\varepsilon_p}{\varepsilon_r} = k_Z \times \beta_{r1} \times 10^{-3.4488} T^{1.5606 \times \beta_{r2}} N^{0.479244 \times \beta_{r3}} \quad (2.4)$$

where:

β_{r1}, β_{r2},β_{r3}= Local calibration coefficients

2.2.3 Fatigue Model Calibration

Due to repeated traffic loading, a series of interconnected cracks caused by fatigue failure of the HMA surface (or stabilized base) occur resulting in fatigue cracks. In thin pavements, cracking initiates at the bottom of the HMA layer, where the tensile stress is the highest, and propagates to the surface as one or more longitudinal cracks. This is referred to as “bottom-up” fatigue cracking. “Top-down” cracking, usually occurring in thick pavements, results from high localized tensile stresses resulting from

tire-pavement interaction and asphalt binder aging. After repeated loading, the longitudinal cracks connect forming a pattern that resembles the back of an alligator. The fundamental fatigue failure model used is shown in Equation 2.5 (12).

$$N_f = K_1 \left(\frac{1}{\varepsilon_t}\right)^{K_2} \left(\frac{1}{E}\right)^{K_3} \quad (2.5)$$

N_f= number of repetitions to fatigue cracking
ε_t= tensile strain at the critical location
E= stiffness of the material
K_1, K_2, K_3= laboratory regression coefficients before the national calibration

$$K_1 = 0.00432 \times C, C = 10^M, M = 4.84\left(\frac{V_b}{V_a + V_b} - 0.69\right)$$

$$K_2 = 3.291$$

$$K_3 = 0.854$$

The main purpose of the MEPDG national calibration was to change the K factors in order to reduce the prediction error. Equation 2.6 displays the fatigue model with the national calibration factors.

$$N_f = \beta_{f1,National} \times K_1 \left(\frac{1}{\varepsilon_t}\right)^{K_2 \times \beta_{f2,Natinal}} \left(\frac{1}{E}\right)^{K_3 \times \beta_{f3,National}} \quad (2.6)$$

where:

$\beta_{f1,National}$, $\beta_{f2,National}$,$\beta_{f3,National}$= National calibration coefficients

National calibration coefficients are introduced to eliminate the bias and scatter in predictions. $\beta_{f1,National}$ was optimized as a function of the total asphalt concrete thickness to compensate for the crack propagation phase of the fatigue cracking phenomena. Trial

runs were conducted using the MEPDG software and $\beta_{f2,National}$ and $\beta_{f3,National}$ were found to be 1.2 and 2.5, respectively. The final nationally calibrated alligator cracking model is shown in Equation 2.7.

$$N_f = 0.00432 \times C \times \beta_{f1,National} \times 0.007566 \times \left(\frac{1}{\varepsilon_t}\right)^{3.9492} \left(\frac{1}{E}\right)^{1.281} \quad (2.7)$$

where:

C= Laboratory to field adjustment factor

The fatigue cracking damage transfer function used in the calibration of the MEPDG alligator (bottom-up) fatigue cracking was assumed to take the form of a mathematical sigmoidal function given in Equation 2.8.

$$F.C. = \left(\frac{6000}{1+e^{C_1 - C_2 \times \log D}}\right) \times \left(\frac{1}{60}\right) \quad (2.8)$$

where:

F.C.= Fatigue cracking (% of lane area)
D= Damage in percentage
C_1, C_2= Regression coefficients

The alligator fatigue cracking transfer function was calibrated based off the assumption that fatigue cracking would be at 50% at a damage of 100%. The calibrated model for the bottom-up fatigue cracking is expressed in Equation 2.9.

$$F.C. = \left(\frac{6000}{1+e^{(C_1 \times C_1' + C_2 \times C_2' \times \log 10((D \times 100))}}\right) \times \left(\frac{1}{60}\right) \quad (2.9)$$

where:

C_1=1.0
C_2=1.0
C'_2=-2.40874-39.748*(1+H_{ac})$^{-2.856}$
C'_1=-2*C'_2

For longitudinal (surface-down) fatigue cracking the model used in the MEPDG is shown in Equation 2.10.

$$F.C. = \left(\frac{1000}{1+e^{C_1 - C_2 \times \log D}}\right) \times 10.56 \quad (2.10)$$

F.C.= Fatigue cracking (% of lane area)
D= Damage in percentage
C_1, C_2= Regression coefficients

The longitudinal cracking transfer function was calibrated in the same way as the alligator transfer function and is displayed in Equation 2.11.

$$F.C. = \left(\frac{1000}{1+e^{(7-3.5\times \log 10(Damage*100))}}\right) \times 10.56 \quad (2.11)$$

After national calibration, additional local calibration for each region or state is recommended to refine the models for each specific region to fit their conditions. Equation 2.12 shows the modified fatigue model to include local calibration parameters.

$$N_f = 0.00432 \times C \times \beta_{f1} \times 0.007566 \times \left(\frac{1}{\varepsilon_t}\right)^{3.9492\times\beta_{f2}} \left(\frac{1}{E}\right)^{1.281\times\beta_{f3}} \quad (2.12)$$

where:

β_{f1}, β_{f2},β_{f3}= Local calibration coefficients

2.3 Calibration Factors for Polymer-Modified Asphalts

Nevada requires the use of polymer modified asphalt (PMA) for all flexible pavements. The Asphalt Institute (AI) determined calibration factors for PMA mixtures for rutting and fatigue cracking. For rutting, the AI determined the k_{r1} coefficient was the only parameter to be adjusted for the neat HMA and PMA sections, as it minimized the difference between the predicted and measured rut depths over time. For rutting, Equation 2.15 shows the relationship determined for neat HMA sections to PMA sections. Similar to rutting, the $_{kf1}$ coefficient was found to minimize the difference between the predicted and measured fatigue cracking over time. The AI determined the $_{kf1(PMA)}$ value could be estimated from $_{kf1(NeatHMA).}$ Equation 2.14 provides an estimate for calibration coefficient for PMA mixtures based on neat HMA mixtures. (13)

$$k_{r1(PMA)} = 1.13k_{r1(NeatHMA)} \tag{2.13}$$

$$-\log\left(k_{1f(PMA)}\right) = \left(-\log\left(k_{f1(NeatHMA}\right)\right)^{0.8} \tag{2.14}$$

2.4 National Calibration Deficiencies

Using the nationally calibrated models without regional or local calibration will significantly affect a pavement design. For an example a PG64-22 neat mixture will be compared to a PG64-28NV mixture. Assuming all loading and environmental factors are the same, a design for fatigue will be described. The neat mixture will result in a stiffer dynamic modulus at a specified frequency compared to the polymer mixture. Assuming the initial design of the HMA has the same thickness for both mixtures, the polymer mixture will experience a higher tensile strain at the bottom of the HMA layer. Using the

nationally calibrated model, the higher strain will result in a lower number of cycles to failure. When in reality, the polymer modified mixture would increase the number of cycles to failure compared to the neat mixture. To compensate for the higher strain, the designer would increase the thickness of this pavement section using the polymer mixture and the national calibrated fatigue model. With local calibration, the over designing of pavement sections can be resolved, because the initial fatigue model would be shifted to more accurately predict failures for that region.

2.5 Local Calibration Experiences

Many states are in the process, or have completed implementing MEPDG using local calibration factors. The Arizona Department of Transportation implemented a 3 year study, conducted at Arizona State University, to establish a database to support MEPDG implementation. A database of five binder types for viscosity-temperature susceptibility relationships and 27 dynamic modulus curves was created (14). The Oklahoma Department of Transportation began a 2 year study to create a database for MEPDG implementation. They created a database using three types of binder from three different sources measuring complex shear modulus (G*) and phase angle (δ) from the Dynamic Shear Rheometer. Also, a database was created of dynamic modulus and flow number values of five mixtures (15).

Bahia et al. suggested that actual values of G* and δ at various testing temperatures be used as inputs into the MEPDG rather than simply the binder's PG grade, as this approach would lead to a more reliable estimate of pavement performance. A Maryland study of the sensitivity of the predicted performance to the calibration

coefficients was conducted. It was found that a small variation in any one of the calibration coefficients in the asphalt concrete rutting model had a substantial impact on the performance predictions, and for alligator fatigue cracking the β_2 and β_3 predictions were very sensitive to calibration (17). Schwartz et al. studied asphalt concrete properties in their sensitivity analysis which included: air voids, effective binder content, gradation, and binder type. These properties were found to have a significant influence on the dynamic modulus values. Fatigue cracking was found to increase with binder grade and an increase in air void content, but was found to decrease with high binder content. The Authors also found rutting increased with binder grade, higher binder content, and an increase in air void content and concluded additional research was necessary for the concrete rutting model (17).

The Florida Department of Transportation performed a sensitivity analysis on material property inputs at different hierarchical levels to determine how much time and effort should be focused on establishing a specific input before beginning local calibration (18). Variables with high sensitivity based on predicted performance were found to be: AC dynamic modulus, layer thickness, base modulus, and subgrade modulus. The Authors found that the pavement with a higher AC modulus were predicted to perform better. Data collection for inputs into the MEDG was determined from field AC cores. Binder content, gradation, effective bitumen content, air voids content, and resilient modulus were identified as significant properties. For implementation, manuals of design tables, and charts derived from MEPDG runs will be developed so they match current FDOT design method formats. (18)

The Minnesota Department of Transportation conducted a sensitivity analysis on flexible pavements were evaluated at a 20 year design life and two traffic levels, 10 and 1 million ESALs (19). For 10 million ESAL analyses, longitudinal cracking, rutting, and alligator cracking were found to be highly sensitive to AC layer thickness. For the 1 million ESAL pavement analyses, all three were found to still be highly sensitive to AC layer thickness in addition to longitudinal and alligator cracking being sensitive to soil type. (19)

The Wisconsin Department of Transportation (WisDot) conducted an analyses on nineteen pavement structures throughout the state focusing on AC dynamic modulus and flow number enabling a Level 1 evalaution (20). MEPDG analyses were performed using a number of pavement thicknesses while adjusting AC binder content and air voids and compared to actual constructed pavement structure. The comparison showed variation in air voids and binder content did not impact the failure of pavements designed with current WisDOT procedures. (20)

CHAPTER 3: RESEARCH PROJECT SCOPE

In the process of implementing the MEPDG, the Nevada Department of Transportation (NDOT) began a study in 2005 with the University of Nevada, Reno's (UNR) Western Regional Superpave Center (WRSC). Multiple field produced mixtures were collected, each year since 2005, throughout the state in five gallon steel buckets from behind the paver, which is then designated by a contract number. Nevada uses two polymer-modified binder grades which include PG64-28NV and PG76-22NV. Two contacts included in this study used PG64-28PM, one used PG64-28TR (tire rubber), and additionally one contract included 15% recycled asphalt pavements (RAP). Table 1 shows the list of contracts collected, the binder grade of the mixture, the county location where the mixture was sampled, percent binder (Pb) contents by dry weight of the mixture (DWM) and mile posts of the project.

NDOT's goal is to have WRSC create a database of Level 2 inputs based off Level 1 analysis of laboratory testing for performance models, which includes binder viscosity, dynamic modulus, repeated load triaxial and flexural beam fatigue testing. The purpose of sampling mixtures all throughout Nevada was to see if any of the MEPDG laboratory input values could be grouped together. NDOT is divided into three districts so the data will be evaluated to see if it can be grouped by district, binder grade, type of mixture (2 or 2C), binder sources and/or aggregate sources. Figure 2 shows the division line of the districts in Nevada along with the contracts separated by county. Figures 3 through 7 provide the gradation plots for all 26 contracts using a .45 power chart. Type 2 and 2C mixtures have 100% passing 1" sieve, with 90-100% and 88-95% passing the ¾"

sieve, respectfully. These grouping will then be used to calibrate the performance models. This will allow NDOT to easily and efficiently implement MEPDG practices.

CHAPTER 4: LABORATORY TESTING

All mixtures were stored in sealed metal buckets until being prepared for laboratory testing. The mixture was heated at 275°F for four hours and split following AASHTO R47 (21). As these are field mixtures they are already short-term aged, so they were immediately put back in the oven at the compaction temperature for compaction. All PG64-28NV and PG76-22NV mixtures were compacted at 295°F and 305°F, respectively. Once compaction temperature was reached the mixtures were compacted for their corresponding laboratory tests which are described below.

4.1: Descriptions

4.1.1: Binder Viscosity

Binder Viscosity is evaluated using data from the Dynamic Shear Rheometer (DSR) following AASHTO T315 (21). The DSR uses two parallel plates, one oscillating and the other fixed. A shear stress is applied to an asphalt binder sample at 10 rad/s, and the shear strain and phase lag of the sample are measured. The complex shear modulus (|G*|) can then be computed. Using the complex shear modulus and phase angle the binders viscosity can be computed from Equation 4.1. Short-term aged binders are used in MEPDG viscosity calculations. The viscosity will be used in further analysis discussed below.

$$\eta = \frac{G^*}{10}\left(\frac{1}{\sin\delta}\right)^{4.8628} \quad (4.1)$$

where:

G*= binder complex shear modulus, Pa

δ= binder phase angle, °
η= viscosity, Pa.s

4.1.2: Dynamic Modulus

Dynamic Modulus (|E*|) represents the stiffness property of HMA mixes assuming linear viscoelastic properties. To measure the Dynamic Modulus a sinusoidal (haversine) axially compressive stress is applied to a cylindrical specimen at a given temperature and loading frequency. The applied stress and resulting recoverable axial strain response of the specimen are measured and used to calculate the dynamic modulus. Following NCHRP 9-29 protocol (22), each specimen was evaluated at four temperatures (4.4, 21.1, 37.8, and 54°C) and six frequencies (0.1, 0.5, 1, 5, 10, and 25 Hz) for each temperature. Samples are compacted using the Superpave Gyratory Compactor (SGC) and cored and cut to a sample size of 6 inches in diameter and 7 inches in height with air voids of 7±1%. The testing data is used to create a master curve which is used to evaluate the structural response of the asphalt pavement under various combinations of traffic loads, speed, and environmental conditions (1).

The Dynamic Modulus Master Curve is developed following AASHTO PP62 (21). The general form of the dynamic modulus master curve used in the MEPDG is a sigmoid function shown in Equation 4.2.

$$\log|E^*| = \delta + \frac{\alpha}{1+e^{\beta+\gamma log t_r}} \quad (4.2)$$

where:

|E*|=the dynamic modulus, psi

α, β, δ and γ= the fitting parameters; and
t_r= reduced time at the reference temperature

The reduced time is computed using shift factors based off of binder viscosity or as a function of temperature. If binder viscosity data is not available the reduced time is computed following Equations 4.3 and 4.4.

$$t_r = \frac{t}{a(T)} \tag{4.3}$$

$$log(t_r) = log(t) - log[a(T)] \tag{4.4}$$

where:

t_r= reduced time at reference temperature
t= reduced time at a given temperature of interest
a(T)= shift factor as function of temperature
T= temperature of interest

Using binder viscosity the reduced time can be computed from Equation 4.5.

$$log(t_r) = log(t) - c\left(log(\eta) - log\left(\eta_{T_r}\right)\right) \tag{4.5}$$

where:

t_r= time of loading at reference temperature
t= time of loading at a given temperature of interest
c= constant
η=binder viscosity at a given temperature of interest, 10^6 poise
η_{Tr}= binder viscosity at reference temperature T_r (in Rankine)

The viscosity of the asphalt binder at the temperature of interest is a critical input parameter for the dynamic modulus equation and the determination of shift factors. The viscosity of the asphalt binder at the temperature of interest is determined from the ASTM viscosity temperature relationship defined by Equation 4.6 (1).

$$loglog\eta = A + VTSlogT_R \quad (4.6)$$

where:

η= viscosity, cP
T_R=temperature, Rankine
A= regression intercept
VTS= regression slope of viscosity temperature susceptibility

The parameters of the ASTM VTS (A-VTS) equation are found by linear regression of the above equation. The resulting regression parameters can then be used to calculate the viscosity for any temperature. The final form of the dynamic modulus curves are shown in Equations 4.7 and 4.8, for shifting as a function of temperature or binder viscosity, respectively.

$$\log|E^*| = \delta + \frac{\alpha}{1+e^{\beta+\gamma(logt-log[a(T)])}} \quad (4.7)$$

$$\log|E^*| = \delta + \frac{\alpha}{1+e^{\beta+\gamma\left\{logt-c\left[10^{A+VTSlogT}-10^{A+VTSlogT_R}\right]\right\}}} \quad (4.8)$$

where:

|E*|=the dynamic modulus, psi
α, β, δ and γ= the fitting parameters

t= time of loading at a given temperature of interest
a(T)= shift factor as function of temperature
c= constant
T_R=reference temperature, Rankine
T= temperature of interest, Rankine
A= regression intercept
VTS= regression slope of viscosity temperature susceptibility

4.1.3 Repeated Load Triaxial

A major distress in the early life of pavements is permanent deformation referred to as rutting. This type of distress is an unrecoverable deformation characterized by longitudinal depressions in the wheel path of the roadway which accumulates under repeated loading (23). Using the relationship shown in Equation 4.9, the accumulated permanent strain as a function of the number of load repetions is used to characterize permanent deformation.

$$\varepsilon_p = aN^b \tag{4.9}$$

where:

ε_p= the accumulated permanent strain due to dynamic vertical loading
N=number of load applications that produced ε_p
a, b= regression constants that depend on the material and stress state conditions

MEPDG uses an empirical rutting model developed using data from the repeated load triaxial (RLT) test to predict rutting in the HMA layer as shown in Equations 4.10 and 4.11.

$$\frac{\varepsilon_p}{\varepsilon_r} = k_1 \times K_1 \times T^{K_2} \times N^{K_3} \tag{4.10}$$

$$RD_{HMA} = \varepsilon_p \times H_{AC} \tag{4.11}$$

where:

ε_p= permanent strain within the HMA layer (in/in)
ε_r= elastic vertical strain within the HMA layer (in/in)
N= number of load repetitions
T= temperature of the HMA layer (°F)
K_1, K_2, and K_3= experimentally determined coefficients from RLT test
k_1=depth correction function
RD_{HMA}= total rutting generated in the HMA layer (in)
H_{AC}= thickness of the HMA layer (in)

The RLT subjects an HMA sample, with the same dimensions and target air voids as the dynamic modulus sample, to a repeated haversine axial compressive pulse load (deviator stress) of 0.1 second loading and 0.6 second of rest time at a specified temperature. The RLT measures the permanent axial deformation in the HMA mixture as it is subjected to triaxial stress conditions. For this study a deviator stress of 45 psi and a confining pressure of 30 psi using compressed air to better simulate field conditions was applied to the HMA samples. The test is restricted to run a maximum of 12,000 cycles, and two independently monitored linear variable differential transducers (LVDT) placed 180° apart continuously measure axial deformations and the permanent vertical strain as a function of load cycles over the middle four inches of the sample. Testing was conducted at three temperatures to account for different resilient strain levels encountered in the pavement. The resulting cumulative permanent strain can be characterized by the primary, secondary, and tertiary stages. The primary stage exhibits high initial levels of rutting due to the rapidly increasing permanent strain and the decreasing rate of plastic deformations. The secondary stage demonstrates a high rate increase in shear deformation resulting in a small rate of rutting at a constant rate of change. The tertiary stage is a

result of a high level of permanent axial strain predominately associated with a decreasing rate of plastic or shear deformations. The primary and secondary stages are associated with volumetric changes, while the tertiary stage exhibits no change in volume. Figure 8 shows the three stages graphically.

The transition point from the secondary to the tertiary is stage is where the Flow Number (FN) occurs. The FN is reported as the number of load cycles at which tertiary flow begins and is determined using the Francken method. This method uses a combination of a power law function with an added exponential function and is obtained using a complex regression mathematical model shown in Equation 4.12 (24).

$$\varepsilon_p(N) = AN^B + C(e^{DN} - 1) \quad (4.12)$$

where:

ε_p= the axial permanent strain
N= number of loading cycles
A, B, C, D= regression constants

After obtaining the regression constants, the first derivative of Equation 4.12 with respect to N, shown in Equation 4.13, is taken to generate the strain rate. The second derivative of the Francken model is then computed at each cycle to obtain the rate of change of the slope of permanent strain as shown in Equation 4.14. Where the rate of change of slope changes signs from negative to positive indicates the inflection point in the permanent strain versus number of cycle's curve where the FN is measured (25).

$$\frac{\delta\varepsilon_p(N)}{\delta N} = \left(A \cdot B \cdot N^{(B-1)}\right) + (C \cdot D \cdot e^{DN}) \quad (4.13)$$

$$\frac{\delta^2\varepsilon_p(N)}{\delta N^2} = A \cdot B \cdot (B-1)N^{(B-2)} + (C \cdot D^2 \cdot e^{DN}) \quad (4.14)$$

4.1.4 Flexural Beam Fatigue

Fatigue cracking occurs in the pavement layer as a load related distress. The action of repeated traffic loads induces tensile and shear stresses in the bound layers, which eventually lead to a loss in the structural integrity of a stabilized layer. Repeated load or fatigue initiates cracks at points where the critical tensile strains and stresses occur (1). In order to evaluate fatigue cracking in the laboratory, flexural beam fatigue testing was used.

Following ASTM D7460, flexural beam fatigue testing was performed using a four-point bending test to evaluate the fatigue properties of an asphalt mixture (26). Since fatigue cracking occurs in the later life of the pavement, samples were long termed aged, following AASHTO R30, for five days at 85°C in a forced draft oven (21). Samples were compacted in a modified Hveem compactor to dimensions of 3x3x16 inches (wxhxl). Samples were then aged and cut to 2.5x2x15 inches for testing. A cyclic haversine load is applied, in the downward direction, to the center of the beam sample at 10 Hz with free rotation and horizontal translation at all load and reaction points. Figure 9 shows the loading frame and also depicts the degrees of freedom for movement. Testing was performed using strain control by subjecting the sample to loading while maintaining a constant level of displacement throughout testing. The displacement is measured at the center of the beam and is calculated using Equation 4.15.

$$\delta = \frac{\varepsilon_t[(3\times L^2)-(4\times a^2)]}{12\times h} \quad (4.15)$$

where:

δ=maximum deflection at center of beam (m)
ε_t=maximum tensile strain (m/m)
a= space between inside clamps, L/3, (0.1190 m)
h= average specimen height (m)
L= length of beam between outside clamps (0.3570 m)

Failure is measured as a 50% reduction in the stiffness measured at the 50th cycle of testing, known as the number of cycles to failure (N_f). The stiffness is a function of the maximum tensile stress and maximum tensile strain of the material which can be calculated using Equation 4.16, using the values specified in Equation 4.15 and calculated from Equation 4.17.

$$S = \frac{\sigma_t}{\varepsilon_t} \quad (4.16)$$

$$\sigma_t = \frac{3\times a\times P}{b\times h^2} \quad (4.17)$$

where:

S=flexural beam stiffness (Pa)
σ_t=maximum tensile stress (Pa)
a=center to center spacing between clamps (0.1190 m)
P=load applied by actuator (N)
b= average specimen width (m)
h=average specimen height (m)

The failure point occurs at the maximum or peak value of the Normalized Modulus × Cycles, computed following Equation 4.18, when plotted versus the Number of Cycles.

$$NM = \frac{S_i \times N_i}{S_o \times N_o} \quad (4.18)$$

where:

NM= normalized modulus×cycles (Pa/Pa)
S_i= flexural beam stiffness at cycle I (Pa)
N_i= cycle i
S_o= initial flexural beam stiffness (Pa), estimated at approximately 50 cycles
N_o= actual cycle number where initial flexural beam stiffness is estimated

When the duration of testing exceeds this point, the failure point can be extrapolated following Equation 4.19.

$$\ln(-\ln(SR)) = \gamma \times \ln(N) + \ln(\lambda) \quad (4.19)$$

where:

ln(-ln(SR))= the natural logarithm of the negative of the natural logarithm of SR
SR= flexural beam stiffness ratio, beam stiffness at cycle i/initial beam stiffness
N= number of cycles
γ= the slope of the linear regression of the ln(-ln(SR)) versus ln(N)
ln(λ)= the intercept of the linear regression of the ln(-ln(SR)) versus ln(N)

The failure point is estimated by solving Equation 4.19 for the number of cycles where the flexural beam stiffness ratio (SR), is equal to 0.5 or 50% of the initial beam stiffness.

Testing was performed at three temperatures and a minimum of three strain levels to get varying levels of the mixtures stiffness. To predict the number of load repetitions to fatigue cracking, MEPDG uses the model shown in Equation 4.20, which is a function of tensile strain and mix stiffness.

$$N_f = k_1 \left(\frac{1}{\varepsilon_t}\right)^{k_2} \left(\frac{1}{E}\right)^{k_3} \quad (4.20)$$

where:

N_f= number of repetitions to fatigue cracking
ε_t= tensile strain at the critical location
E= stiffness of the material
k_1, k_2, k_3= laboratory regression coefficients

4.2 Results

Laboratory testing results and statistical analysis will be discussed in this section. Summary tables or figures will be provided for discussion. Statistical analysis will be analyzed for laboratory predicted performance using 95% confidence interval (CI). Attempted groupings using statistical analysis will include all the Contracts tested, districts, binder grade, type of mixture, binder source, and/or aggregate source if applicable. Table 2 lists the Contacts with their corresponding information to be used for grouping. It should be noted that District 1 is all PG76-22NV binders except for Contract 3382. This Contract was considered an outlier and was removed from the analysis when grouping for District 1. Therefore any recommended groupings based off District 1 and PG76-22NV will be the same.

4.2.1 Binder Viscosity

Viscosity measurements were computed for two replicates at three temperatures for each binder. Table 3 shows the results for the binders that were available. A total of 17 binders were compared. Since the complex shear modulus (G*) and phase angle (δ) are measures of the binder, aggregate source was not considered in the grouping analysis.

Using the A-VTS values, shown in Table 4, each binder's viscosity was calculated for the four E* testing temperatures (40, 70, 100, 130°F) and plotted. Confidence bands were used to determine if groupings could be determined using a 95% level. Viscosity (η) will be plotted in centipoise versus temperature in Rankine to stay consistent with the use for dynamic modulus shifting. For groupings that are found, average A-VTS values will be provided.

As shown in Figure 10, binder viscosity cannot be grouped together for all the contracts collected as a general group for Nevada as a whole. About half of the 17 contracts are not within the 95% CI. This is to be expected with two different binder grades. Fourteen of the 17 binders evaluated were PG64-28NV binders. Figure 11 shows that half of the Contracts still are not within the CI and a further breakdown for grouping is needed. The three remaining PG76-22NV binders, shown in Figure 12, fall within the 95% CI and can be grouped together. Table 5 provides the grouping to be used for PG76-22NV binders which also applies to District 1. Nine Contacts were analyzed in District 2 and three to four of the Contracts were not within the confidence band at various temperatures shown in Figure 13. A grouping could be considered for District 2, but further breakdown of groupings should also be considered. District 3 included four contacts shown in Figure 14. At different temperatures, one Contract falls out of the CI, but overall a grouping can be used with the values shown in Table 5.

Only two binder sources were analyzed for the PG64-28NV binders since three or more Contracts could be included. Valero was used for three Contracts (one from District 2 & two from District 3). All three contracts fell within the confidence band, as

seen in Figure 15, and can be grouped together using the parameters shown in Table 5. Paramount was used on eight of the nine contacts in District 2. By eliminating the different binder source, a grouping can be established. Figure 16, shows the Contracts using Paramount binder, only two of the eight distinctly fall out of range of the CI. Table 5 provides the groupings for Paramount binder.

4.2.2 Dynamic Modulus

Dynamic modulus (E*) inputs into the MEPDG are critical. Level 1 requires a mixtures dynamic modulus at a minimum of three temperatures and three frequencies each. Twenty-six projects were used for the dynamic modulus analysis. Table 6 shows the fitting parameters for these contracts. Statistical analysis was performed, using the fitting parameters to predict E*master curves at 70°F and 104°F, to find possible groupings for dynamic modulus inputs.

When comparing all 26 Contracts, shown in Figures 17 and 18, about half are not within the 95% confidence band. In order to have a more accurate E* inputs, further groupings will be analyzed. Figure 19 shows the master curves of the averages for the PG64-28 and PG76-22NV mixtures. There is a clear difference between the two so these will be analyzed for possible groupings. Seventeen of the mixtures analyzed were PG64-28NV, while the other nine are PG76-22. Figures 20 through 23 show the PG64-28NV and PG76-22NV mixtures, respectively. For the contracts using PG64-28, only about half of the master curves are within the 95% CI at 70°F and it worsens at 104°F. There is a clear gap between the nine PG76-22NV mixtures, both at 70 and 104°F, leaving almost no contracts to completely fall within the confidence bands.

Seven of the Contracts analyzed were Type 2, while the other 19 were Type 2C. Figures 24 through 26 show that the Type 2 and Type 2C cannot be grouped for dynamic modulus. While District 1, cannot be grouped together Districts 2 and 3 had better results as seen in Figures 28 through 31 for two temperatures each, respectively. Two of the eleven contracts analyzed for District 2, were not within the confidence bands, and for District 3, one of the five contracts is not within the 95% CI at different frequency measurements. Table 7, provides the average fitting parameters to be used for E* groupings for District's 2 and 3. Further analysis will be conducted to find groupings for dynamic modulus inputs.

Variations in the E*, since the binder grade was not the only explanation, may be attributed to the differing binder and aggregate sources used for the Contracts. Analyses will include comparing each individual source with the other also being a factor (i.e. one binder source with multiple aggregate sources). Six aggregate sources, of the 17, were evaluated because they included two contracts or more and are displayed in Figures 32 through 43, Also, only six of the seven binder sources were analyzed for the same reason and are shown in Figures 44 through 55. Based off these figures, aggregate source, regardless of binder sources, groupings can be made and are provided in Table 7. Caution should be taken with Bertagnolli and Lockwood pits, because Paramount was the only binder source evaluated for these two aggregate sources. Groupings based off binder source show an even stronger similarity than the aggregate source master curves. All curves, despite different aggregate sources, were within the 95% confidence bands. Table 7 provides dynamic moduli fitting parameters for these sources.

4.2.3 Repeated Load Triaxial

Laboratory regression coefficients for the 17 Contracts evaluated using the RLT are given in Table 8. These coefficients were used to compute the ratio of the permanent strain to the resilient strain at 104, 114.8, and 136.4°F for the statistical analysis since these coefficients are used as the input into the MEDG. Figure 56 concludes that all 17 Contracts cannot be grouped together since almost half do not fall within the 95% confidence level. Figure's 57 and 58 separate the 17 contracts into PG64-28NV and PG76-22NV binder grades, respectively. Each of these groups still resulted in half of the Contracts not being within the confidence bands.

Type 2 and 2C could not be grouped as seen in Figures 59 and 60, since about half of the Contracts were not within the 95% CI for each type. District's 2 and 3 groupings are shown in Figures 61 and 62. District 2 is consistent with the results found from previous groupings in that half of the contracts are not within the statistical limits. However, the four contracts analyzed for District 3 appear to be within the 95% CI. Table 9 provides a grouping of the regression coefficients, but caution must be used because the four contracts analyzed had a wide variation in their results.

Three of the four PG76-22NV Contracts used SEM as the binder source. Figure 63 shows these four Contracts fall inside their 95% confidence band. Each of these three Contracts used different aggregate sources. Therefore a grouping is provided in Table 9 for SEM binder source. Looking at the PG64-28NV provider Paramount, 9 contracts with six different aggregate sources were plotted shown in Figure 64. Six to seven contracts are within the 95% confidence band at the three temperatures for a given number of

cycles, leading to the conclusion, the binder source Paramount can be grouped together and is also included in Table 9. The only aggregate source of the 17 contracts that included at least three Contracts was Lockwood. Figure 65 shows that the three Contracts fall within the confidence band. A grouping is provided in Table 9, however Paramount was the only binder source included in this analysis and should be considered when using this group.

4.2.4 Flexural Beam Fatigue

Only eight contracts have currently been evaluated so groupings will be limited for fatigue inputs. Table 10 provides the laboratory regression coefficients determined for these eight contracts. The regression coefficient will be used to predict the number of cycles to failure at 55, 70, and 80°F for strain levels of 400, 750, and 1000 microns each. Dynamic modulus values at the respective temperature and a frequency of 10Hz was also used. Figure 66 provides all eight Contracts for the three temperatures with their 95% confidence bands. At certain cycles a grouping can be established, and is provided in Table 11, but this should be used carefully as it is very limited. Three of the Contracts tested are PG64-28NV mixtures, but due to high variability 95% confidence levels could not be evaluated. Figure 67 provides the plots for the five PG76-22NV Contracts. It can be seen that these contracts fit well within a 95% CI, and that a grouping can be established which is provided in Table 11. Due to limited fatigue data further groupings cannot be analyzed.

CHAPTER 5: ANALYSIS

5.1 Witczak Model

Level 3 Input for dynamic moduli values are determined using the Witczak equation shown in Equation 5.1 (27). This equation predicts the E* using a regression that's a function of gradation, volume of air and effective binder, frequency and viscosity.

$$\log E^* = -1.25 + 0.029\rho_{200} - 0.0018(\rho_{200})^2 - 0.0028\rho_4 - 0.058V_a - 0.822\frac{V_{beff}}{V_{beff}+V_a} + \frac{3.872-0.0021\rho_4+0.004\rho_{38}-0.000071(\rho_{38})^2+0.0055\rho_{34}}{1+e^{(-0.603313-0.313351\log(f)-0.393532\log(\eta))}} \quad (5.1)$$

where:

E*=dynamic modulus of mix, 10^5 psi
η= viscosity of binder, 10^6 Poise
f= loading frequency, Hz
ρ_{200}= % passing #200 (0.075 mm) sieve
ρ_4= cumulative % retained on #4 (4.76 mm) sieve
ρ_{38}= cumulative % retained on 3/8 in (9.5 mm) sieve
ρ_{34}= cumulative % retained on ¾ in (19 mm) sieve
V_a= air void, % by volume
V_{beff}= effective binder content, % by volume

Comparing 1,092 measured dynamic modulus values to their predicted Witczak E*, for 17 mixtures with two to three replicates resulted in an overall good fit as shown in Figure 68. The statistical values R^2 adjusted and Se/Sy are 0.89 and 0.34, suggesting the Witczak model provides a good predicted measure of the dynamic modulus. NDOT can use Level 3 input for dynamic modulus values and still obtain reasonable results.

5.2 A-VTS Comparison

The MEPDG has default values for A-VTS using Level 3 analysis. However these default values are for neat binders. Since Nevada uses polymer modified binders only, these values are not representative of the materials used in Nevada. Table 12 displays the default A-VTS values for PG64-28 and PG76-22 binders in the MEPDG (1). Comparing these default values to the 17 measured A-VTS values there is a drastic difference as visible in Figures 70 and 71. It is not recommended for NDOT to use Level 3 for A-VTS values.

5.3 Recommendations to Begin Local Calibration

To begin implementing the groups recommended from this study, actual field performance will have to be compared to the laboratory predicted failures. Using an MEPDG software program, actual field conditions, such as layer thickness and traffic for each Contract will be input to begin calibration. The groupings suggested from this study will also be used as inputs. The predicted distresses after running the M-E analysis will be calibrated by shifting the predictions using a beta (β) factor. An example, of the shifting is shown in Figure ?. The beta factors are what shifts the performance models from nationally calibrated to locally calibrated.

Measured field data is crucial to the calibration process. The pavement management system used by NDOT will have to use the same approach to measure distresses throughout the years included in the calibration process. Staying consistent will give the most accurate values for local calibration. Traffic for each Contract will also have to be collected. MEPDG is capable of incorporating a load spectra analysis into the

predictions. NDOT however does not have these traffic measurement capabilities. A move toward this traffic analysis will allow for NDOT to achieve more accurate calibration factors.

CHAPTER 6: CONCLUSIONS AND RECOMMENDATIONS

Using laboratory performance testing of up to 26 field mixtures (Contracts) throughout Nevada, groupings were compiled for inputs into the MEPDG. Binder Viscosity measurements, dynamic moduli values, and regression coefficients for rutting and fatigue were evaluated for compilation for all of Nevada, binder grade, District, binder source and/or aggregate source using 95% confidence intervals. These groupings will allow NDOT to use more reliable inputs into the MEPDG based off current practices being used in Nevada. Grouping conclusions are as follow:

- All Contracts Tested for Nevada:
    - No performance measures based off 95% confidence level could be grouped together. A fatigue grouping was provided for Nevada, but is analyzed with limited mixtures.
- Binder Grade:
    - Binder Viscosity measurements (complex shear modulus and phase angle) could be grouped together for PG 76-22NV binders based off three Contacts
    - Dynamic Moduli inputs cannot be grouped based solely off of binder grade. Seventeen mixtures were examined for PG64-28NV binder, while the remaining nine were PG76-22NV.
    - Rutting regression coefficients could not be grouped together using 13 and four Contracts for PG64-28NV and PG76-22NV, respectively.

  - Fatigue regression coefficients are provided for PG76-22NV binders after analyzing 5 Contracts.

- Type 2 or Type 2C
  - Dynamic modulus and rutting regression coefficients could not be grouped for the type of mixture. Fatigue was not analyzed due to limited data.
- District
  - District 1 groupings are the same as the PG76-22NV conclusions, since the one outlier PG64-28NV contract was removed from the District analysis
  - Using four contracts and a 95% CI, District 3 can be grouped for binder viscosity measurements
  - District's 2 and 3 can both be grouped for Dynamic Moduli inputs. District 2 consisted of 11 Contracts for the analysis, and District 3 consisted of five.
  - Rutting regression coefficients can be grouped together for District 3, but the variation between the four contracts analyzed was large so extra attention should be paid when using these coefficients for large errors.
- Binder Source
  - Paramount and Valero can individually be grouped for binder viscosity measurements
  - Six binder sources were found to be strong groupings for Dynamic Moduli, all falling within their respective 95% confidence intervals

  - SEM and Paramount binder sources can be grouped for rutting regression coefficients. Both sources included multiple aggregate sources within their analysis

- Aggregate Source
  - Six groupings of aggregate sources were found for dynamic moduli inputs based off two or more contracts.
  - Lockwood was grouped together for Rutting, however all three contracts analyzed used Paramount as a binder source. This should be considered when using this group

These grouping should help in implementing MEPDG practices into the State of Nevada's pavement design procedures. As this study is ongoing, new Contracts have been collected and laboratory evaluations need to continue for the remaining testing and new contracts sampled. Since contracts have been collected beginning in 2005, calibration of the performance models can be started since there is 7 years of in-service pavement performance. The calibration is an iterative process that should continually be updated throughout the design life of the pavement.

As the MEPDG is a state of the practice design method, the inputs included in the analysis are more advanced. NDOT should look into a geographical information system (GIS), which will create a stronger database system for their pavement analysis needs. The MEPDG considers rutting as an accumulation amongst the pavement layer, base, and subgrade. To account for this, NDOT should perform periodic trench studies of the Contracts included in

the calibration process, since the rutting coefficients in this study only include the HMA layer. To further increase accuracy of the calibration factors, it is recommended NDOT monitor load-spectra traffic data to replace the estimation of AADTT and ESALs.

REFERENCES

1. "Guide for Mechanistic-Empirical Design of New and Rehabilitated Pavement Structures." Chapaign, Illinois: Transportation Research Board, 2004. <http://onlinepubs.trb.org/onlinepubs/archive/mepdg/guide.htm>
2. Banerjee, A., J.P. Aguiar-Moya, and J.A. Prozzi. "Calibration of Mechanistic-Empirical Pavement Design Guide Permanent Deformation Models: Texas Experience with Long Term Pavement Performance." *Transportation Research Board: Journal of the Transportation Research Board,* No. 2094, Transportation Research Board of the National Academies, Washington, D.C.,2009, pp.12-20.
3. American Association of State Highway and Transportation Officials (AASHTO). "Guide for the Local Calibration of the Mechanistic-Empirical Pavement Design Guide" 2010.
4. *AASHTO Guide for Design of Pavement Structures* (1986). American Association of State Highway and Transportation Officials, Washington, D.C.
5. *AASHTO Guide for Design of Pavement Structures* (1993). American Association of State Highway and Transportation Officials, Washington, D.C.
6. Darter, M.I., H.L. Von Quintus, Y.J. Jiang, E.B. Owus-Antwi, and B.M. Killingsworth (1997). *Catalog of Recommended Design Features* (CD-ROM). NCHRP Project 1-32. TRB, National Research Council, Washington, D.C.
7. *Mechanistic-Empirical Pavement Design Guide: A Manual of Practice*, interim ed. AASHTO, Washington, D.C., July 2008.
8. Von Quintus, Harold L., et al., *Experimental Plan for Calibration and Validation of Hot-Mix Asphalt Mixture Performance Models for Mix and Structural Design*, Unpublished Final Report , NCHRP Project 9-30, NCHRP, National Academies of Sciences, Washington, D.C., January 2004.
9. Von Quintus, Harold L., et al.. *Local Calibration Adjustments for the HMA Distress Prediction Models in the Mechanistic-Empirical Design Guide Software*, Technical Memorandum 1-40B/I.3.1, Phase 1, Task 3, NCHRP Project 1-40B, "Local Calibration Guidance for the Recommended Guide for the Mechanistic-Empirical Design of New and Rehabilitated Pavement Structures." National Cooperative Highway Research Program, Washington, D.C., November 2005.
10. Asphalt Institute, *Quantifying the Effects of PMA for Reducing Pavement Distress*, Information Series IS-215, First Edition. Asphalt Institute, Lexington, Kentucky, 2005.
11. El-Basyouny, M.M., and M. Witczak."Development of Fatigue Cracking Models for the 2002 Design Guide." Paper Presented at the Annual Meeting of the Transportation Research Board, Washington D.C., 2005.
12. Monismith, C.L., Epps, J.A., and Finn, F.N., "Improved Asphalt Mix Design," Proc. of Asphalt Paving Technologists, Vol., 54, San Antonio, Texas, 1985.

13. Von Quintus, H., J. Mallela, L. Titus-Glover, "Calibration Factors for Polymer-Modified Asphalts Using M-E Based Design Methods", *Asphalt Institute Report No. ER-235*. First Edition, 2008.
14. Souliman, M.I., M. Mamlouk, C.E. Zapata, and C.E. Cary. "Data Collection to Support Implementation of the Mechanistic-EmpiricalPavement Design Guide for County Roads." *Transportation Research Board: Journal of the Transportation Research Board,* No. 2225, Transportation Research Board of the National Academies, Washington, D.C.,2011, pp.67-77.
15. Cross, M., Z. Hossain, and M. Zaman. "Development of Flexible Database for Local Calibration of MEPDG: Annual Report for FY 2009." Oklahoma Department of Transportation. November, 2009.
16. Bahia, H., Hanz, A. Krebs, S. and Fenley, L. (2009). "Opportunities for WHRP to Support WisDOT Efforts to Implement the MEPDG (DRAFT)," White Paper, Wisconsin Department of Transportation and Wisconsin Highway Research Program, Wisconsin.
17. Schwartz, C. (2007). "Implementation of the NCHRP 1-37A Design Guide." Report No. SP0077B41. Maryland State Highway Administration, Lutherville, MD.
18. Fernando, F.G., Oh, J., and Ryu, D. (2007). *Phase I of MEPDG Implementation in Florida*. Report D04491/PR1528-1. Texas Transportation Institute, College Station, TX.
19. Cochran, G., Funk, N., Hoegh, K., Khazanovich, L., Marasteanu, M., and Velasquez, R. (2009). *Implementation of the MEPDG for New and Rehabilitated Pavement Structures for Design of Concrete and Asphalt Pavements in Minnesota.* Report MN/RC 2009-06. Minnesota Department of Transportation, St. Paul, MN.
20. Williams, C.R., Robinette, C.J., Bausano, J., and Breakah, T. (2007). *Testing of Wisconsin Asphalt Mixtures for the Forthcoming AASHTO Mechanistic-Empirical Pavement Design Procedure*. Report No. WHRP 07-06. Wisconsin DOT, Madison, WI.
21. American Association of State Highway and Transportation Officials (AASHTO). Standard Specifications for Transportation Materials and Methods of Sampling and Testing. 30th Edition, Washington, D.C., 2010.
22. Witczak, M.W., Kaloush, K., Pellinen, T., El-Basyouny, M., and Von Quintus, H., "Simple Performance Test for Superpave Mix Design," NCHRP Report 465, Transportation Research Board, Washington, D.C., 2002.
23. McGennis, R.B., Anderson, R.M., Kennedy, T.W., and Solamanian, M., "Background of Superpave Asphalt Mixture Design and Analysis'" *Report No. FHWA-SA-95-003, Federal Highway Administration*, Washigton D.D., 1994.

24. Francken, L., "Permanent Deformation Law of Bituminous Road mixes in Repeated Load Triaxial Compression," *Proceeding of Fourth International Conference on the Structural Desgn of Asphalt Pavements*, University of Michigan, Ann Arbor, MI, 1977.
25. Ulloa, A. Calderon., "Characteristics of Dynamic Triaxial Testing of Asphalt Mixtures," Masters Thesis, University of Nevada, Reno, 2009.
26. American Society for Testing and Materials (ASTM)."Determining Fatigue Failure of Compacted Asphalt Concrete Subjected to Repeated Flexural Bending. D 7640". American Society for Testing and Materials. 2010 Annual Book of ASTM Standards.
27. Bari, J., Witczak, M.M. "Development of a New Revised Version of the Witczak E* Predictive Model for Hot Mix Asphalt Mixtures", *Journal of the Association of Asphalt Paving Technologists*, Vol. 75, 2006, pp 381-424.

TABLES

Table 1. List of Contracts Sampled for NDOT MEPDG Implementation

Contract	Binder Grade	Year of Sampling	County	Pb (DWA)	Mileposts
3214	PG76-22NV	2005	Clark	4.3	US 95 - CL 62.22
3239	PG64-28NV	2005	Lyon	6.5	US 395- DO 0.00 to 12.04
3248	PG64-28NV	2005	Humboldt	6.6	I 080-HU 29.35 to 42.35
3257	PG76-22NV	2005	Clark	5	SR 160-CL 14.37 to CL 21.79, SR 160-CL 11.09 to CL 21.82
3247	PG76-22NV	2006	Clark	5.1	SR 160- CL 0.00 to 1.14
3260	PG76-22NV	2006	Clark	4.8	US 095- CL 77.51-79.92
3274	PG76-22NV	2006	Clark	4.8	SR 159-CL 22.94 to 25.72
3312	PG 76-22NV	2007	Clark	5.4	SR 160
3325	PG76-22NV	2007	Clark	5.5	US-095-1 CL17.08 to CL20.62
3331	PG76-22NV	2007	Clark	4.5	IR 015 CL 118.50 to CL 123.77
3323	PG64-28NV	2007	Churchill	6	US50A- CH 0.71 to CH 8.64
3330	PG64-28NV	2007	Humboldt	5.6	IR 080-HU 11.97 to 17.92
3329	PG64-28NV	2008	Elko	5.2	IR 080-EL 83.33 to EL 115.54
3338	PG64-28NV	2008	Douglas & Carson	4.8	US 50-DO 13.07 to 14.58, US 50-CC 0.00 to 7.63
3348	PG64-28NV(TR)	2008	Pershing	4.8	IR 80-PE 26.21 to PE 37.68
3358	PG64-28NV	2008	Washoe	5.7	US 395 WA 31.70 to US 395 WA 38.37
3348	PG64-28PM	2008	Pershing	5.4	IR 80-PE 26.21 to PE 37.68
3350	PG64-28PM	2008	Lander & Eureka	5.8	IR80-LA 15.89 to 26.97
3368	PG76-22NV	2009	Lyon	5.6	US 50 LY 18.84 to LY 29.46
3372	PG64-28NV	2009	Humboldt	5	IR 080-HU 17.48 to 29.51
3373	PG64-28NV	2009	Pershing	6	IR80-PE-0.00 to 16.96
3383	PG76-22NV	2010	Clark	4.6	CL-23.37 to CL-28.33, CL-28.15,CL-21.27 to CL 28.15 and CL 28.49 to CL-31.68
3378	PG64-28NV	2010	Washoe	4.7	SR 430
3382	PG64-28NV	2010	Lincoln & Nye	4.3	SR318-LN 30.00 to NY 10.00
3399	PG64-28NV	2010	Washoe	5.8	SR 430
3399	PG64-28 RAP	2010	Washoe	4.5	SR 430

Table 2. Contract Grouping Information

Contract	Binder Grade	District	Binder Source	Aggregate Source	Type
3214	PG76-22NV	1	KPA	Sloan	2C
3239	PG64-28NV	2	Paramount	Hunewill	2
3248	PG64-28NV	3	KPA	HU 82-01	2C
3257	PG76-22NV	1	Ergon	Blue Diamond	2
3247	PG76-22NV	1	Ergon	Blue Diamond	2C
3260	PG76-22NV	1	Ergon	Blue Diamond	2C
3274	PG76-22NV	1	Ergon	Spring Mountain	2C
3312	PG 76-22NV	1	SEM	Tecopa Pit	2
3325	PG76-22NV	1	SEM	Blue Diamond	2C
3331	PG76-22NV	1	SEM	Sloan	2C
3323	PG64-28NV	2	Paramount	CH 10-03	2
3330	PG64-28NV	3	Idaho	Hunewill	2C
3329	PG64-28NV	3	Idaho	EL 84-15 & EL 14-01	2C
3338	PG64-28NV	2	Paramount	Bertagnolli	2
3348	PG64-28NV(TR)	2	Paramount	PE 83-02	2C
3358	PG64-28NV	2	Paramount	Lockwood	2C
3348	PG64-28PM	2	Valero	PE 83-02	2C
3350	PG64-28PM	3	Valero	HU 83-08	2C
3368	PG76-22NV	2	Paramount	Bertagnolli	2
3372	PG64-28NV	3	Valero	Imlay Pit	2C
3373	PG64-28NV	2	Paramount	PE 81-11	2C
3383	PG76-22NV	1	Ergon	Lone Mountain	2C
3378	PG64-28NV	2	Paramount	Marietta	2C
3382	PG64-28NV	1	Mountain States	LN 16-02	2
3399	PG64-28NV	2	Paramount	Lockwood	2C
3399	PG64-28 RAP	2	Paramount	Lockwood	2C

Table 3. Binder Measurements from the DSR

Replicate		1			2			Average
Contract	Temp (°C)	G* (Pa)	Phase Angle δ (°)	Viscosity (cP)	G* (Pa)	Phase Angle δ (°)	Viscosity (cP)	Viscosity (cP)
3325	70	4940	63.2	858433	4890	63.2	849744	854,088
	76	2910	65.5	460422	2900	65.4	460622	460,522
	82	1740	67.7	253931	1740	67.5	255714	254,823
3331	64	7390	58.8	1579720	7320	58.9	1556750	1,568,235
	70	4410	59.2	923667	4360	59.3	908595	916,131
	76	2690	60.2	536154	2670	60.3	529592	532,873
3323	58	5510	62	1009391	5480	62	1003895	1,006,643
	64	3120	63	546857	3110	63.1	542757	544,807
	70	1820	64.6	298379	1810	64.8	294369	296,374
3330	58	5050	70.2	679184	5010	70.1	675872	677,528
	64	2660	71.6	343327	2640	71.6	340745	342,036
	70	1430	73.5	175447	1440	73.4	177120	176,283
3329	58	4260	69.5	585563	4240	69.5	582813	584,188
	64	2290	71	300709	2290	71	300709	300,709
	70	1270	72.8	158646	1270	72.7	159064	158,855
3338	58	6270	63	1098972	6130	63	1074434	1,086,703
	64	3520	64.8	572474	3460	64.7	564973	568,723
	70	2020	67.1	301110	2000	67	299202	300,156
3348_TR	58	6840	65.4	1086434	6750	65.5	1067990	1,077,212
	64	3790	66.4	579559	3750	66.4	573442	576,501
	70	2170	67.9	314498	2150	67.8	312678	313,588
3358	58	6910	63.6	1180522	6780	63.5	1163214	1,171,868
	64	3760	65.2	601902	3680	65.2	589095	595,499
	70	2090	67.7	305010	2050	67.5	301273	303,141
3348_PM	58	6960	63.6	1189064	6860	63.4	1181941	1,185,503
	64	3800	66	589855	3790	65.7	595057	592,456
	70	2100	69.3	290505	2120	68.9	297099	293,802
3350	58	8640	60.6	1689177	8640	60.6	1689177	1,689,177
	64	4840	61.5	907101	4850	61.4	913182	910,142
	70	2800	62.8	495051	2810	62.8	496819	495,935
3372	58	4950	63.3	856498	4960	63.4	854581	855,540
	64	2790	64.1	466822	2800	64.3	464667	465,745
	70	1620	65.1	260351	1620	65.3	258317	259,334
3373	58	5680	61	1089606	5700	60.9	1098610	1,094,108
	64	3230	62.8	571076	3240	62.7	575354	573,215
	70	1880	65.2	300951	1880	65.1	302136	301,543
3383	70	4580	52.6	1402542	4650	52.9	1396673	1,399,607
	76	3020	54.2	836092	3050	54.4	834161	835,127
	82	1990	56.5	481389	2010	56.8	478147	479,768
3378	58	4880	61.5	914598	4890	61.6	912267	913,433
	64	2810	61.7	521832	2820	61.7	523689	522,761
	70	1680	62.1	306381	1680	62.1	306381	306,381
3382	64	4960	60.2	988596	5000	60.3	991746	990,171
	70	2970	61.9	546548	2990	62	547746	547,147
	76	1790	64.2	298274	1800	64.2	299940	299,107
3399_NR	58	5280	61.1	1008129	5310	60.9	1023442	1,015,786
	64	3030	61.7	562687	3050	61.6	569001	565,844
	70	1800	62.8	318247	1810	62.9	318625	318,436
3399_RAP	58	5450	62.1	993913	5450	62.1	993913	993,913
	64	3090	62.7	548717	3090	62.7	548717	548,717
	70	1810	63.6	309225	1810	63.6	309225	309,225

Table 4. A-VTS Values

Contract	Binder Grade	A	VTS
3325	PG76-22NV	8.0551	-2.6093
3331	PG76-22NV	7.1506	-2.2846
3323	PG64-28NV	7.9994	-2.6018
3330	PG64-28NV	9.0041	-2.9684
3329	PG64-28NV	8.8086	-2.8997
3338	PG64-28NV	8.3539	-2.7287
3348	PG64-28NV(TR)	8.0344	-2.6137
3358	PG64-28NV	8.7084	-2.8556
3348	PG64-28PM	8.9753	-2.9516
3350	PG64-28PM	7.7296	-2.4989
3372	PG64-28NV	7.9022	-2.5687
3373	PG64-28NV	8.3636	-2.7321
3383	PG76-22NV	6.6334	-2.0947
3378	PG64-28NV	7.2415	-2.3299
3382	PG64-28NV	7.9950	-2.5931
3399	PG64-28NV	7.6078	-2.4606
3399	PG64-28 RAP	7.6652	-2.4816

Table 5. Binder Viscosity Groupings

Groupings		A	VTS
PG76-22NV		7.2797	-2.3295
District 3		8.3611	-2.7339
Binder Source	**Valero**	8.2024	-2.6731
	Paramount	7.9968	-2.6005

Table 6. Dynamic Modulus Shift Factors

		Sigmoidal E* Fitting Parameters				
Contract	**Binder Grade**	**δ**	**α**	**γ**	**β**	**c[1]**
3214	PG76-22NV	-0.1035	3.9676	0.3770	-0.9745	-
3239	PG64-28NV	0.9528	2.8333	0.5087	-0.5464	-
3248	PG64-28NV	0.7608	2.5265	0.5529	-0.7187	-
3257	PG76-22NV	0.6724	3.0231	0.4630	-0.7417	-
3247	PG76-22NV	0.3876	3.1504	0.4141	-0.6317	-
3260	PG76-22NV	0.7920	2.9133	0.5867	-0.8387	-
3274	PG76-22NV	0.7404	2.8034	0.5207	-0.9609	-
3312	PG76-22NV	0.8874	2.5399	0.5396	-0.6491	-
3325	PG76-22NV	0.9989	2.3910	0.6276	-0.3962	1.3697
3331	PG76-22NV	1.1423	2.3052	0.6335	-0.4363	1.6403
3323	PG64-28NV	0.8576	2.5637	0.5891	-0.3931	1.5203
3330	PG64-28NV	0.7671	2.6791	0.5671	-0.2778	1.3006
3329	PG64-28NV	0.5980	2.8738	0.5541	-0.3938	1.3801
3338	PG64-28NV	0.5226	2.8840	0.4996	-0.4067	1.4754
3348	PG64-28NV(TR)	0.8732	2.5593	0.5949	-0.5900	1.5496
3358	PG64-28NV	0.6624	2.6696	0.6136	-0.7289	1.4201
3348	PG64-28PM	0.6711	2.6762	0.5187	-0.8059	1.3927
3350	PG64-28PM	0.5485	2.8595	0.4812	-0.6793	1.6068
3368	PG64-28NV	0.6317	2.7884	0.4970	-0.6083	-
3372	PG64-28NV	0.9669	2.4531	0.5827	-0.5408	1.6381
3373	PG64-28NV	0.5978	2.8410	0.5286	-0.3486	1.4592
3383	PG76-22NV	0.9257	2.6148	0.5475	-0.3996	1.8713
3378	PG64-28NV	0.5781	2.7638	0.5983	-0.6087	1.8337
3382	PG64-28NV	1.0938	2.4010	0.5723	-0.1038	1.3988
3399	PG64-28NV	0.7264	2.6114	0.6112	-0.1229	1.6720
3399	PG64-28 RAP	0.5022	2.9439	0.5295	-0.5277	1.6568

1: c as "-" indicates shifting is a function of a(T)

$$\log|E^*| = \delta + \frac{\alpha}{1+e^{\beta+\gamma(logt-log[a(T)])}}$$

$$\log|E^*| = \delta + \frac{\alpha}{1+e^{\beta+\gamma\left\{logt-c\left[10^{A+VTSlogT}-10^{A+VTSlogT_R}\right]\right\}}}$$

Table 7: Dynamic Modulus Groupings

Groupings		Sigmoidal E* Fitting Parameters				
		δ	**α**	**γ**	**β**	**c[1]**
District	**2**	0.6887	2.7395	0.5536	-0.5170	1.5533
	3	0.7283	2.6784	0.5476	-0.5221	1.4814
Aggregate Source	**Bertagnolli**	0.5771	2.8362	0.4983	-0.5075	1.4754
	Blue Diamond	0.7127	2.8694	0.5229	-0.6521	1.3697
	Hunewill	0.8600	2.7562	0.5379	-0.4121	1.3006
	Lockwood	0.6303	2.7416	0.5848	-0.4598	1.5830
	PE 83-02	0.7722	2.6177	0.5568	-0.6979	1.4711
	Sloan	0.5194	3.1364	0.5052	-0.7054	1.6403
Binder Source	**Ergon**	0.7036	2.9010	0.5064	-0.7145	1.8713
	Idaho	0.6826	2.7765	0.5606	-0.3358	1.3403
	KPA	0.3286	3.2471	0.4649	-0.8466	-
	Paramount	0.6719	2.7661	0.5535	-0.4987	1.5810
	SEM	1.0095	2.4120	0.6002	-0.4939	1.5050
	Valero	0.7288	2.6629	0.5275	-0.6754	1.5459

1: c as "-" indicates shifting is a function of a(T)

$$\log|E^*| = \delta + \frac{\alpha}{1+e^{\beta+\gamma(logt-log[a(T)])}}$$

$$\log|E^*| = \delta + \frac{\alpha}{1+e^{\beta+\gamma\left\{logt-c\left[10^{A+VTSlogT}-10^{A+VTSlogT_R}\right]\right\}}}$$

Table 8. Rutting Laboratory Regression Coefficients

Contract	K1	K2	K3
3312	-4.9498	2.3913	0.3372
3325	-3.3057	1.5622	0.2987
3331	-6.7598	3.1787	0.4314
3383	-3.5733	1.7451	0.346
3329	-3.2295	1.5833	0.428
3338	-2.5082	1.3124	0.2973
3378	-4.539	2.1615	0.3868
3399-NR	-7.2994	3.5724	0.3145
3399-RAP	-4.8358	2.3886	0.3247
3382	-6.5822	3.1617	0.3602
3372	-5.8765	2.8753	0.3076
3350	-7.3905	3.5408	0.3088
3330	-6.7897	3.0991	0.5338
3323	-6.4597	3.0334	0.3697
3358	-8.8901	4.3681	0.2807
3373	-4.6552	2.3609	0.3144
3368	-2.523	1.3385	0.2327

$$\frac{\varepsilon_p}{\varepsilon_r} = k_1 \times K_1 \times T^{K_2} \times N^{K_3}$$

Table 9: Rutting Laboratory Regression Grouping Coefficients

		RLT Coefficients		
Groupings		**K1**	**K2**	**K3**
District 3		-5.4988	2.6665	0.3481
Binder Source	**SEM**	-5.0051	2.3774	0.3558
	Paramount	-4.9933	2.4577	0.3276
Aggregate Source	**Lockwood**	-7.0084	3.4430	0.3066

$$\frac{\varepsilon_p}{\varepsilon_r} = k_1 \times K_1 \times T^{K_2} \times N^{K_3}$$

Table 10. Fatigue Laboratory Regression Coefficients

Contract	K1	K2	K3	C
3260	0.122	3.823	1.167	5.27E-04
3274	755.119	4.777	3.385	5.18E-04
3312	7.15E-05	5.608	2.071	5.28E-04
3325	6.04E-09	6.647	1.919	5.41E-04
3329	6.512	3.202	1.142	5.49E-04
3331	315.638	4.287	2.994	5.24E-04
3358	83.726	5.158	3.862	5.36E-04
3350	7.889E-05	6.801	3.667	5.46E-04

$$N_f = CK_1\left(\frac{1}{\varepsilon_t}\right)^{K_2}\left(\frac{1}{E}\right)^{K_3}$$

Table 11: Fatigue Laboratory Regression Grouping Coefficients

Groupings	K1	K2	K3	C
Nevada	145.1395	5.0379	2.5261	0.0005
PG76-22NV	214.1758	5.0284	2.3075	0.0005

$$N_f = CK_1\left(\frac{1}{\varepsilon_t}\right)^{K_2}\left(\frac{1}{E}\right)^{K_3}$$

Table 12. MEPDG Level 3 A-VTS Values

Binder Grade	MEPDG	
	A	VTS
PG64-28	10.312	-3.44
PG76-22	9.751	-3.208

FIGURES

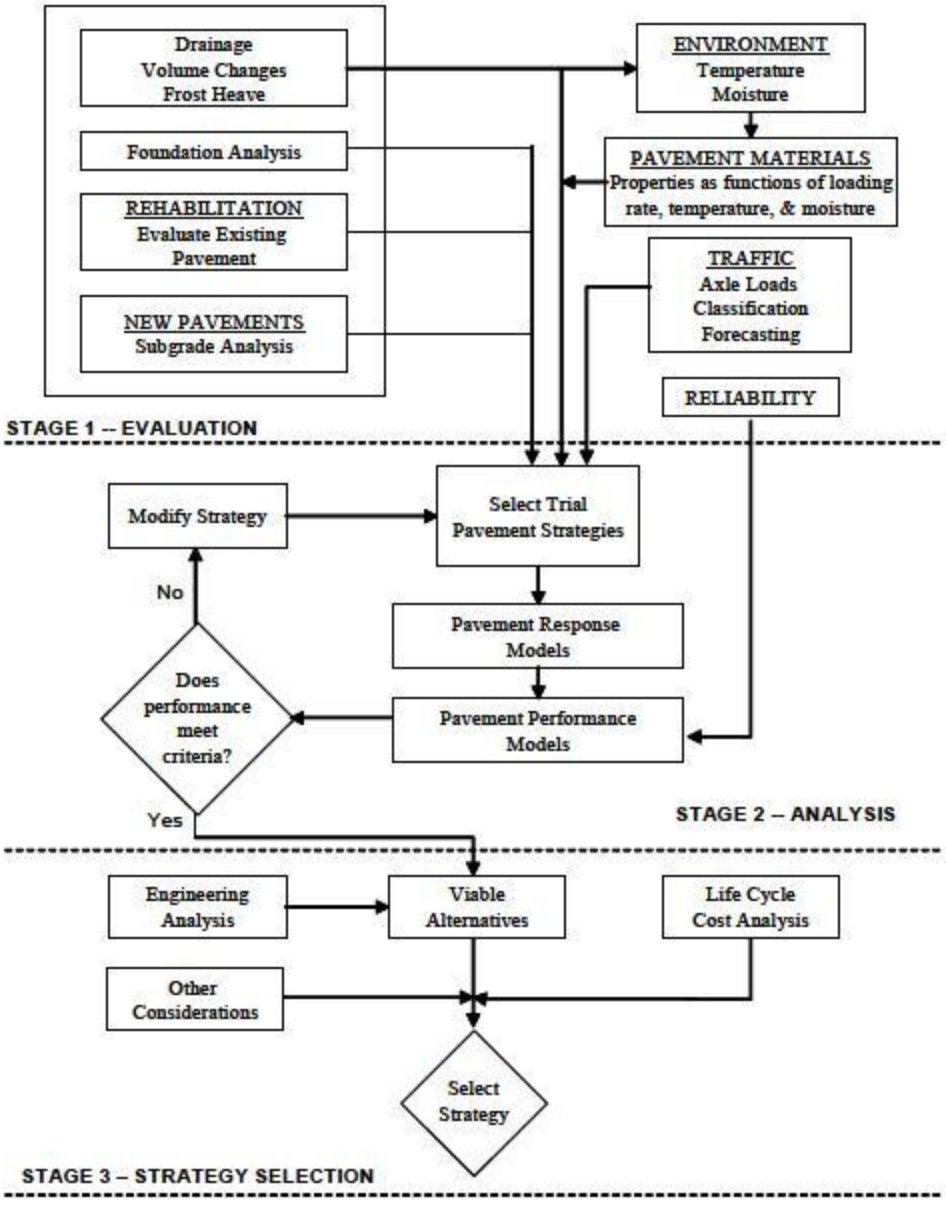

Figure 1. MEPDG Stages of Design

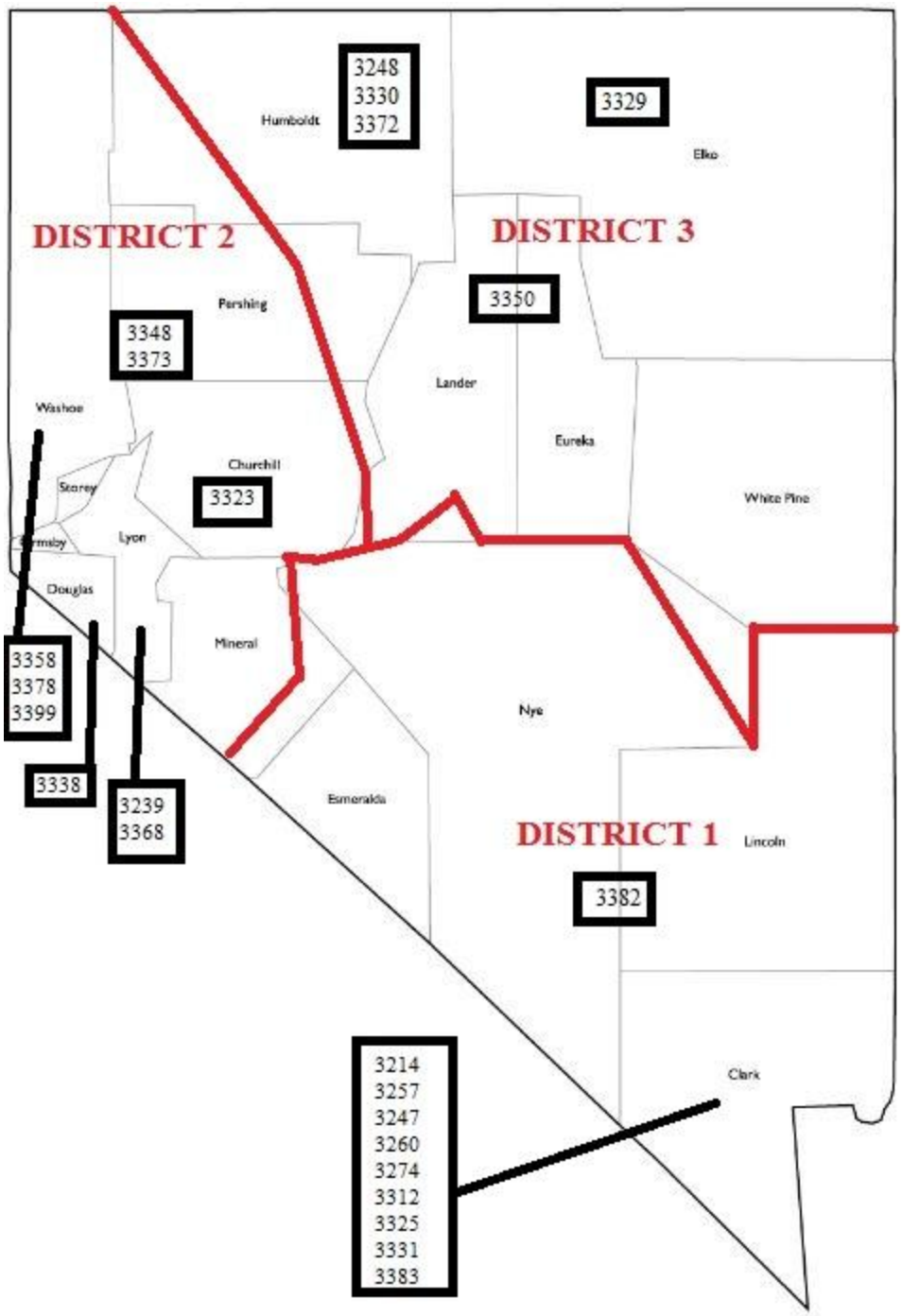

Figure 2. Nevada map with District Boundaries and Contract Location by County

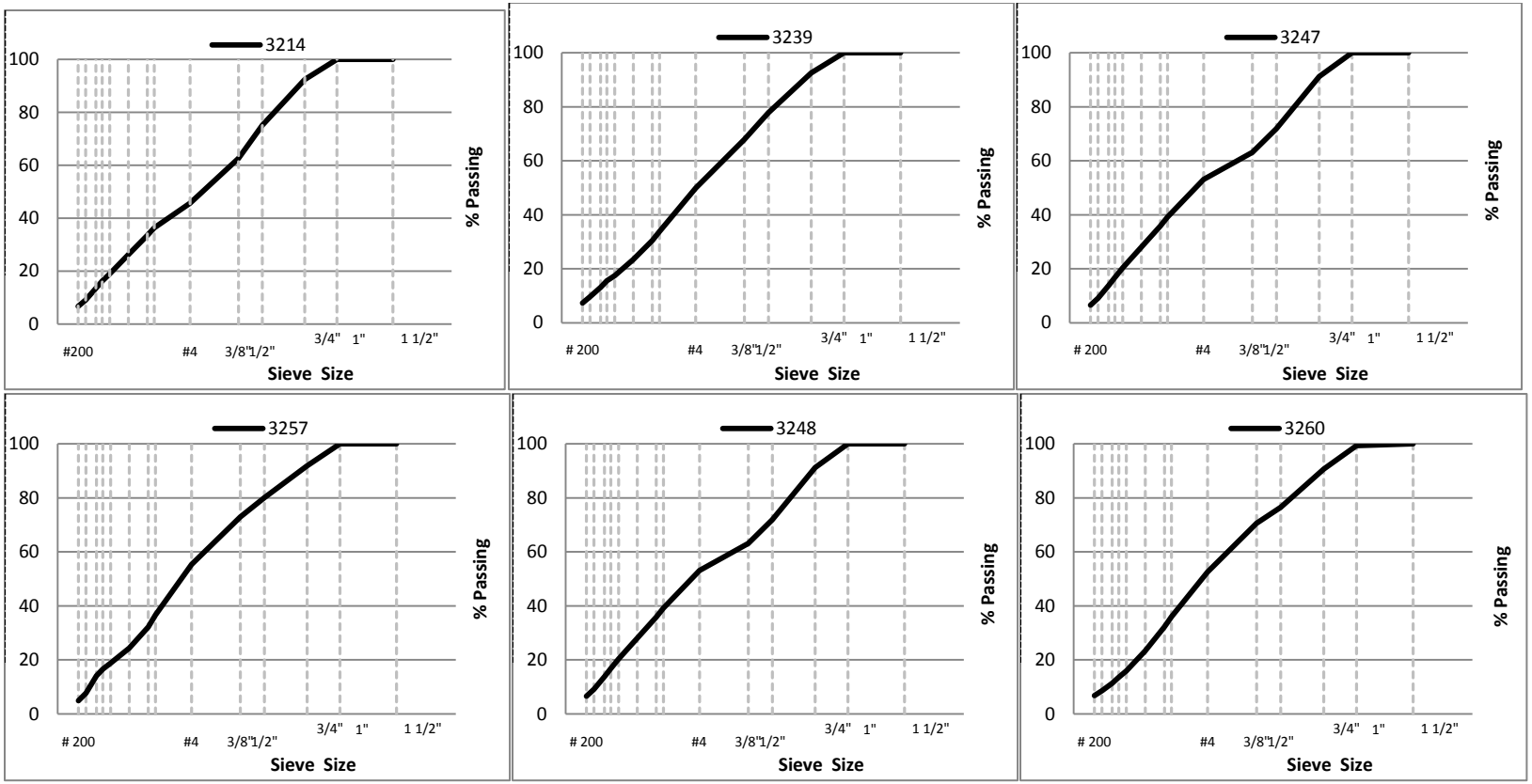

Figure 3. .45 Power Gradation Plots for Contracts 3214, 3239, 3247, 3257, 3248, and 3260

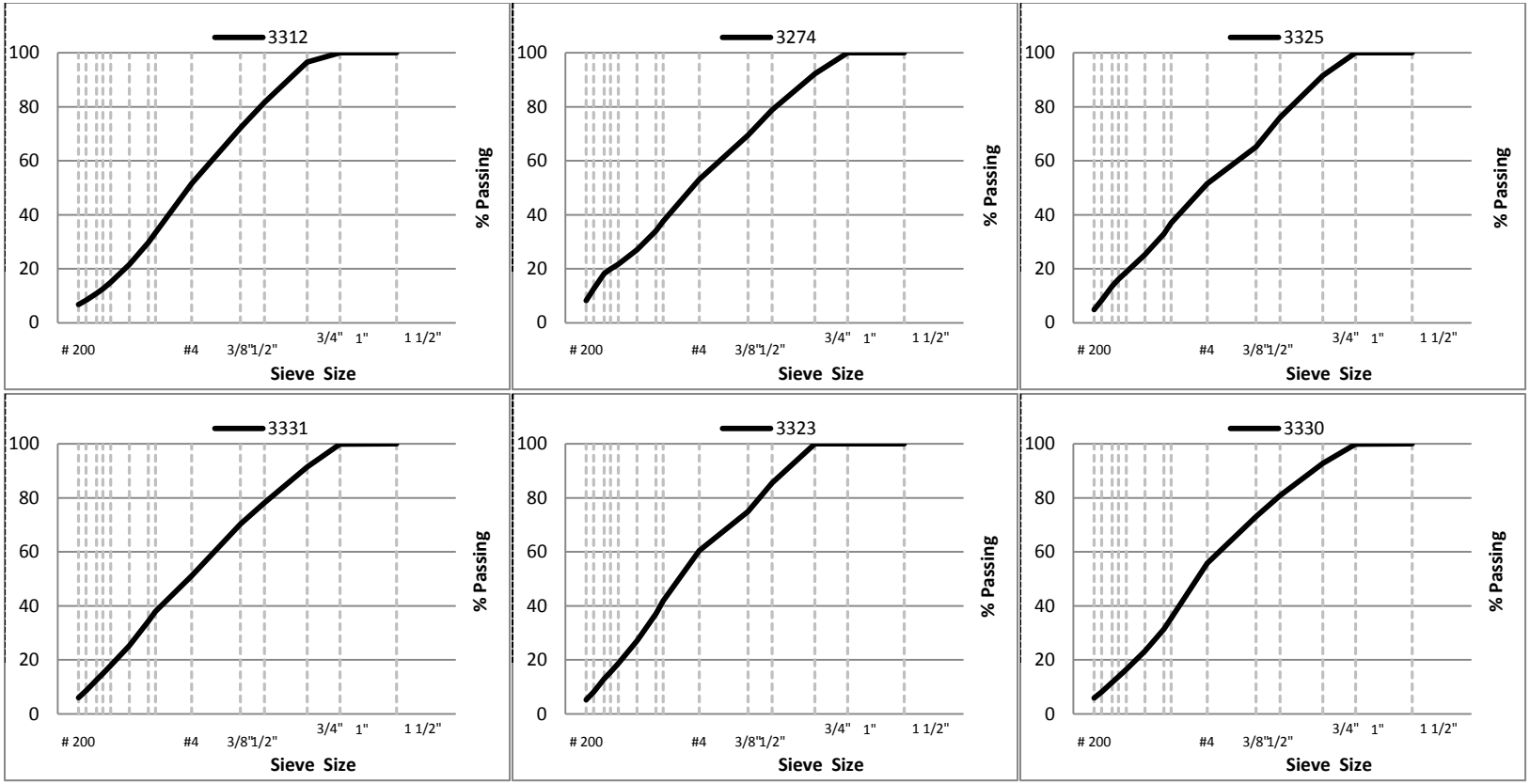

Figure 4. .45 Power Gradation Plots for Contracts 3312, 3274, 3325, 3331, 3323, and 3330

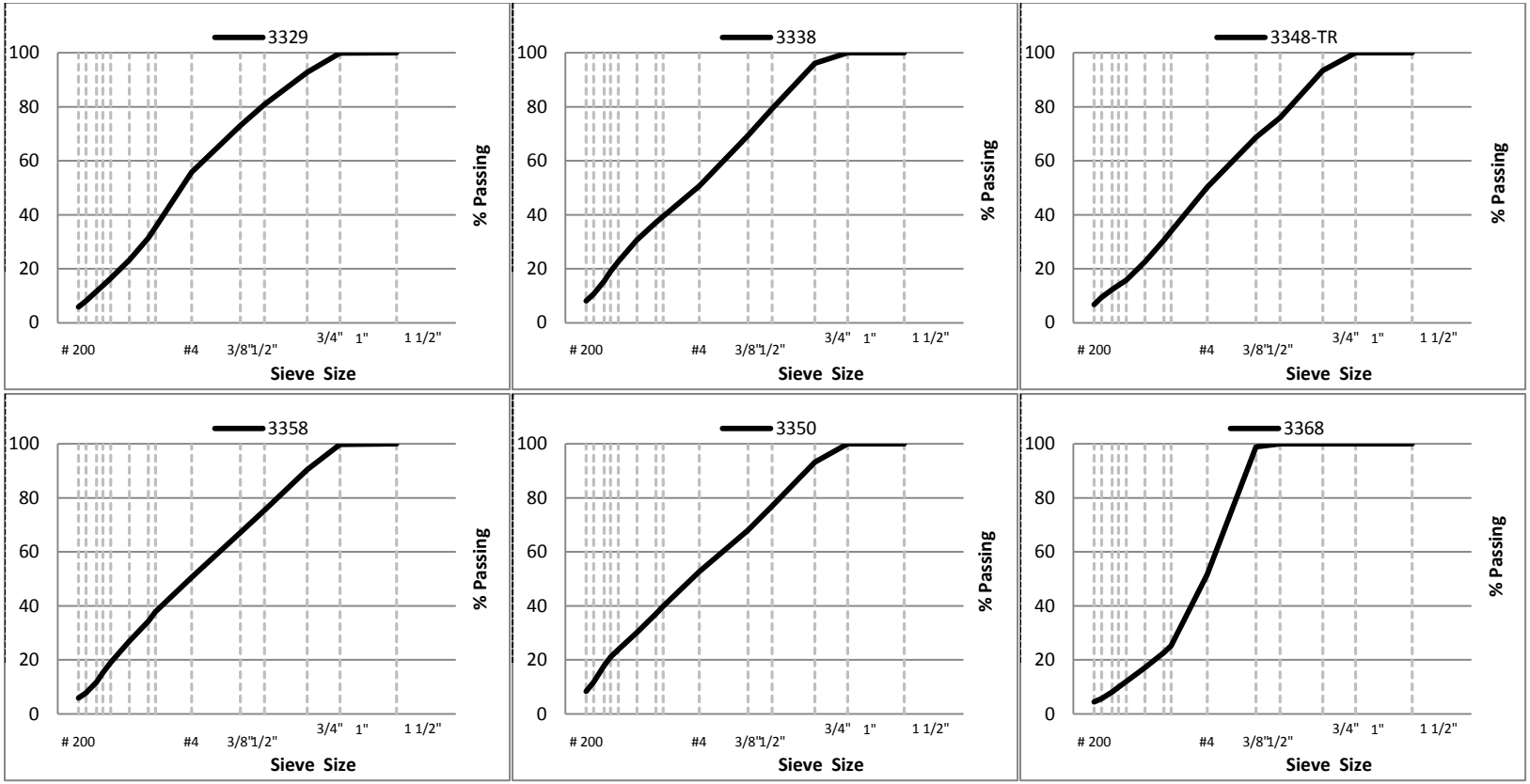

Figure 5. .45 Power Gradation Plots for Contracts 3329, 3338, 3348-TR, 3358, 3358, 3350, and 3368

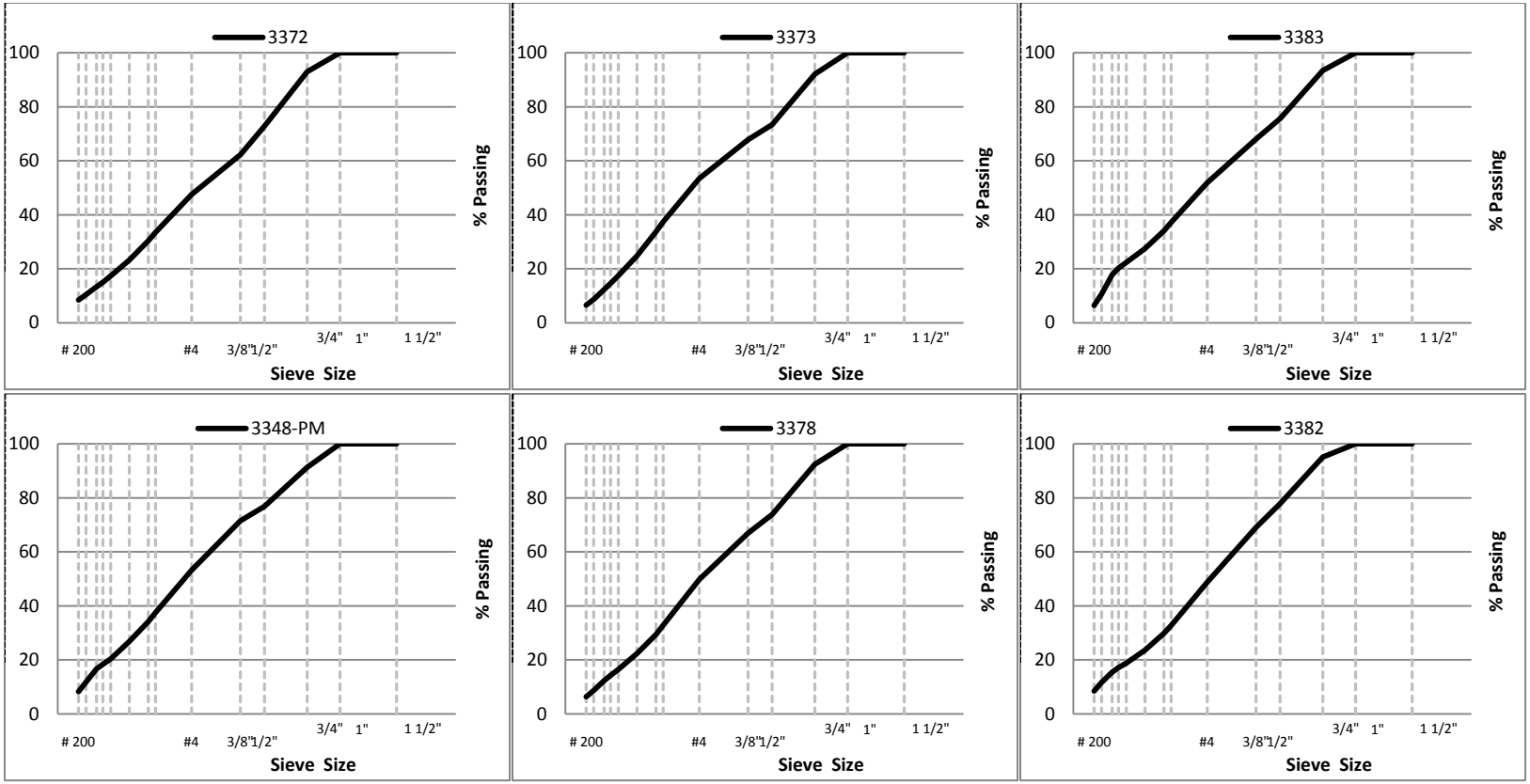

Figure 6. .45 Power Gradation Plots for Contracts 3372, 3373, 3383, 3348-PM, 3378, and 3382

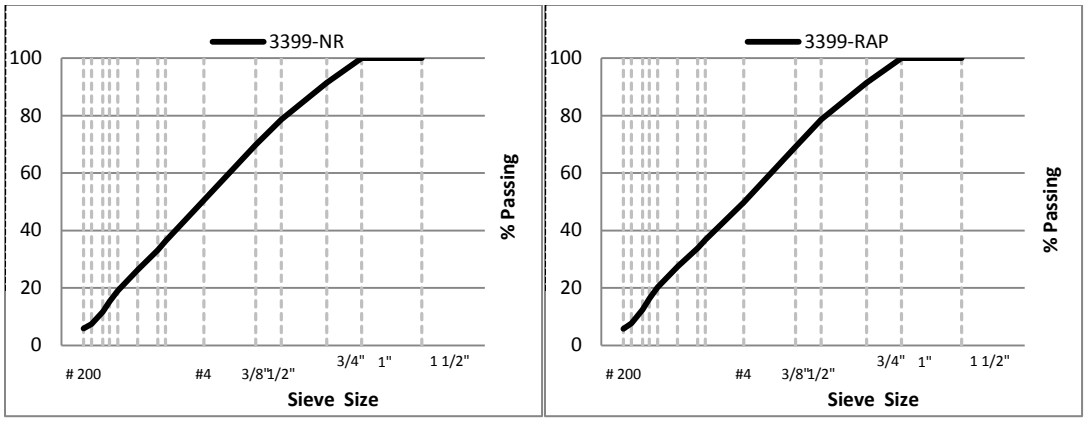

Figure 7. .45 Power Gradation Plots for Contracts 3399-NR and 3399-RAP

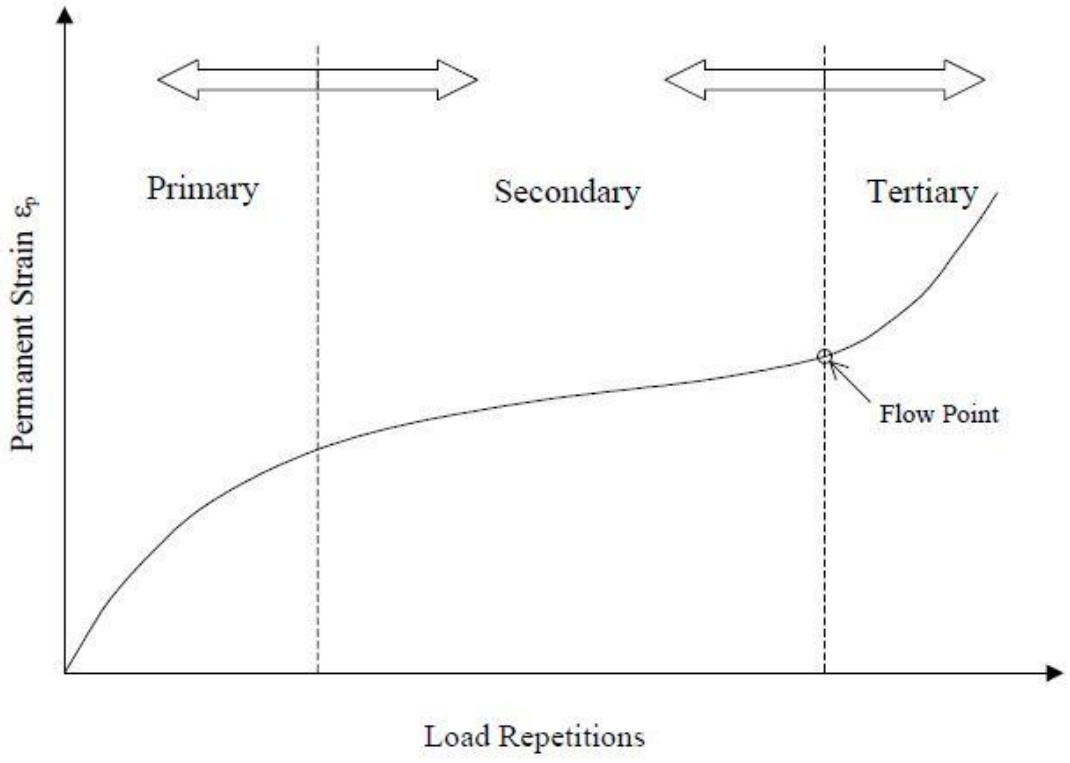

Figure 8. Rutting Permanent Deformation Levels

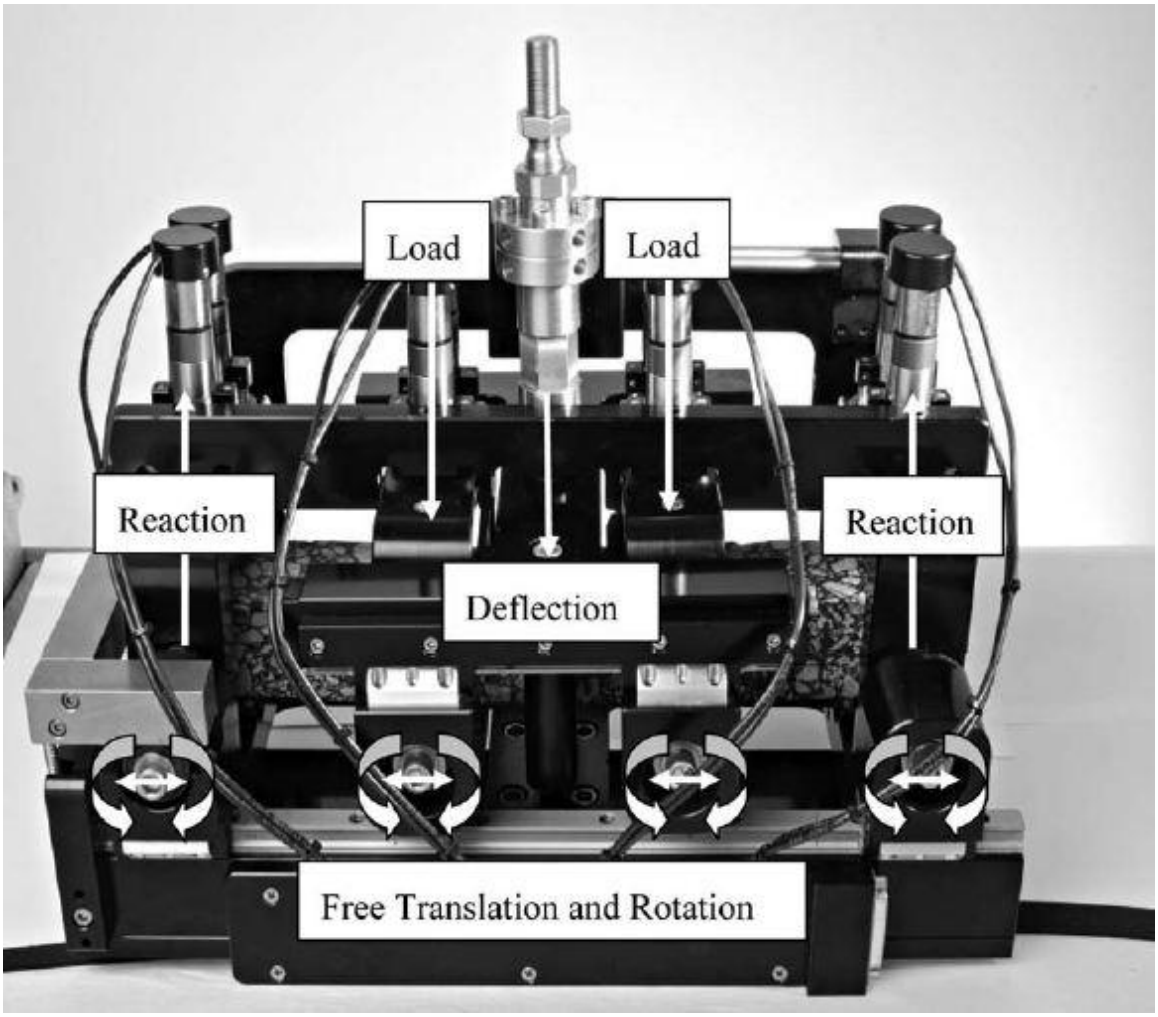

Figure 9. Flexural Beam Fatigue Loading Frame and Degrees of Freedom

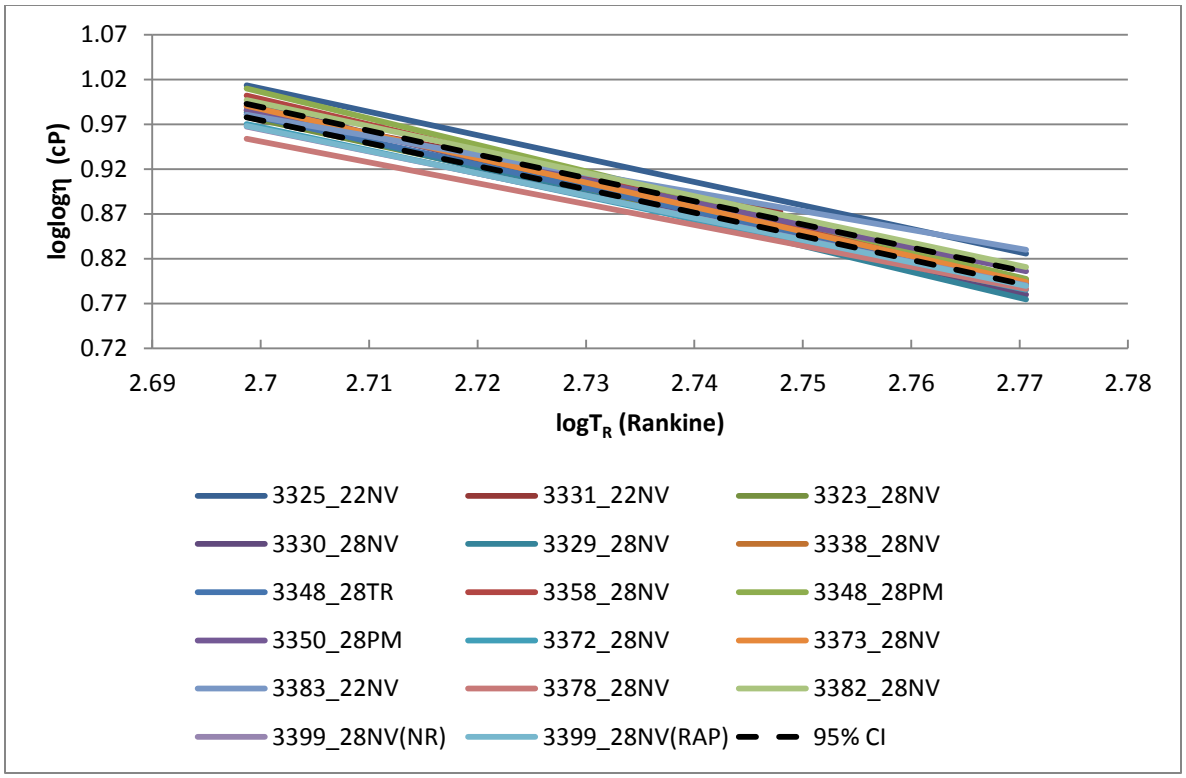

Figure 10. Binder Viscosity Results for sampled Nevada Binders

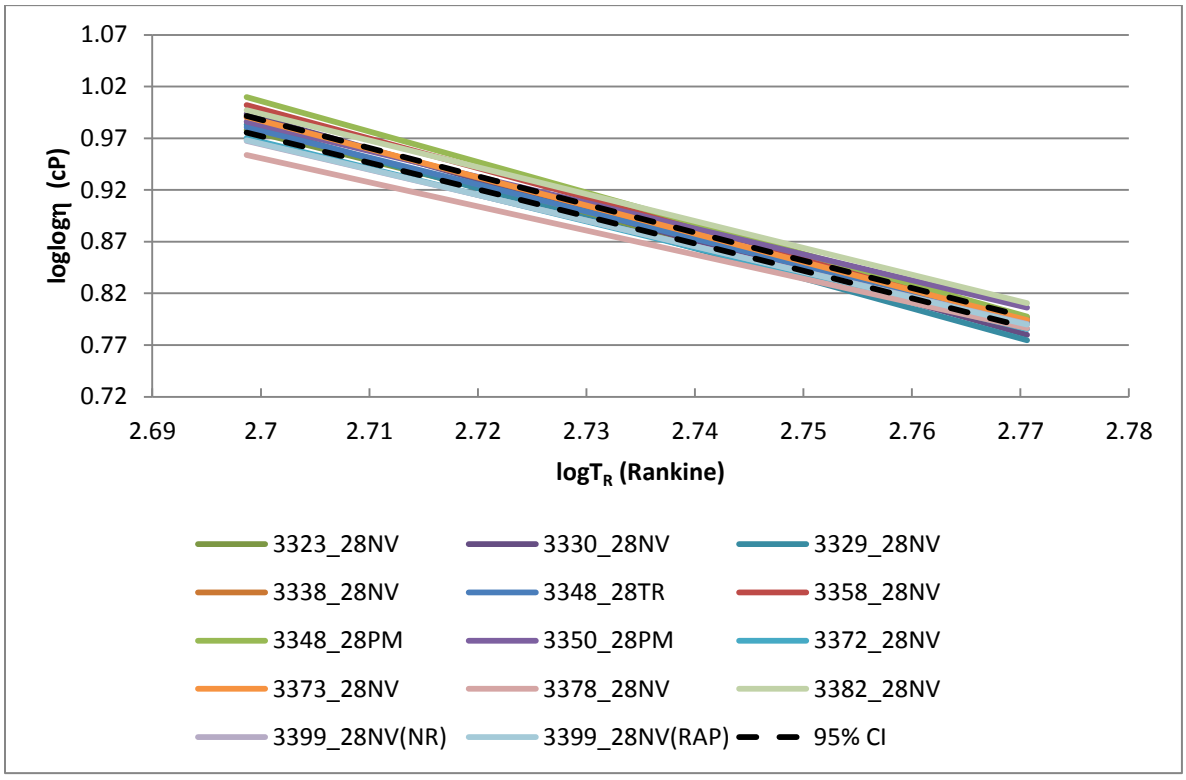

Figure 11. Binder Viscosity Results for PG64-28NV Mixtures

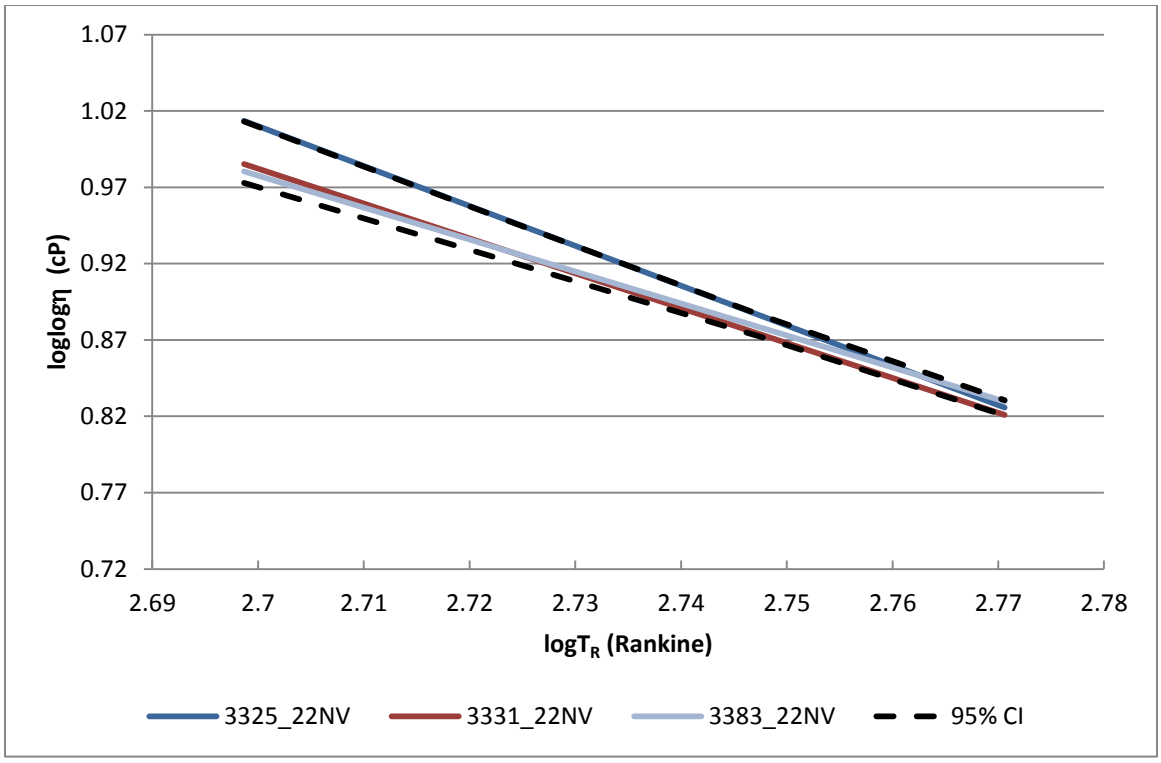

Figure 12. Binder Viscosity Results for PG76-22NV Mixtures

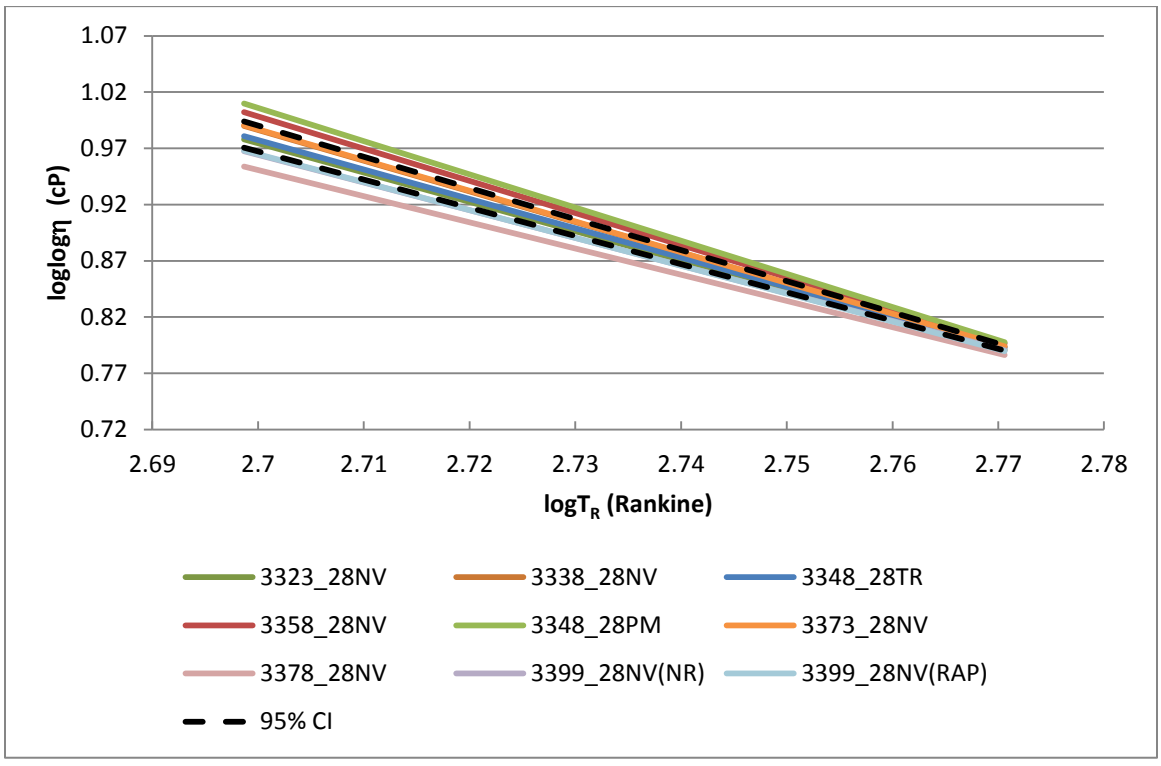

Figure 13. Binder Viscosity Results for District 2

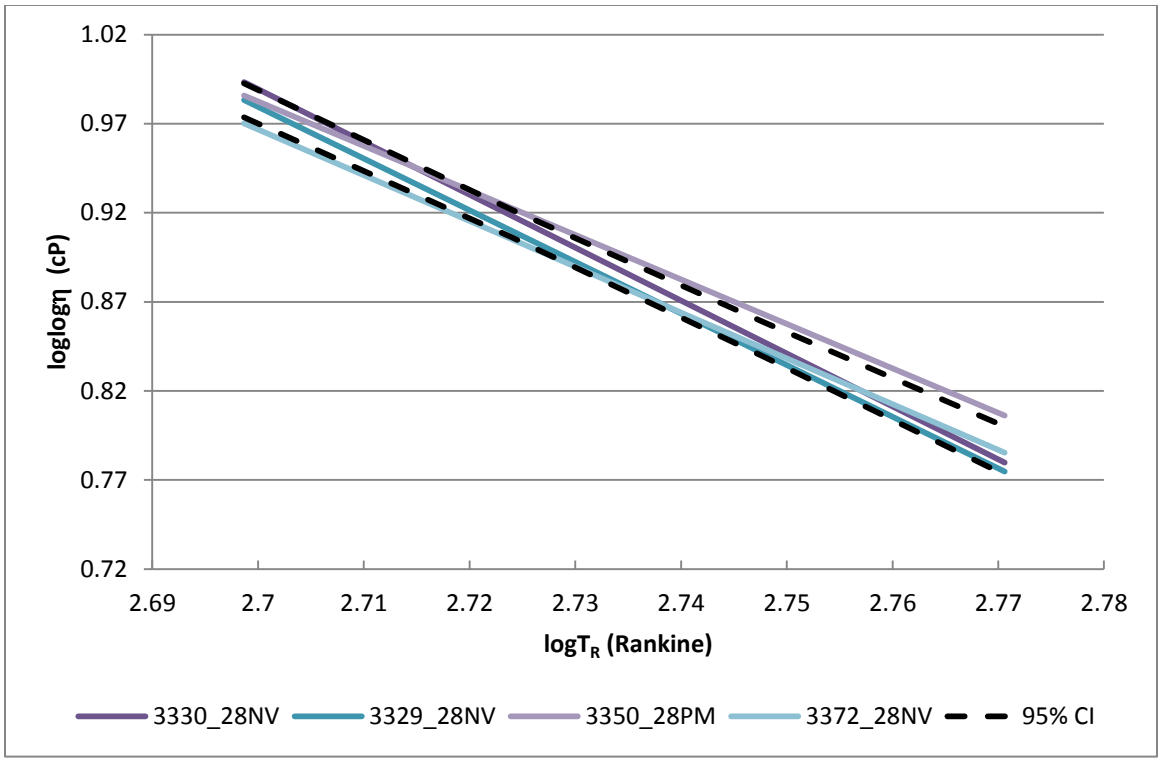

Figure 14. Binder Viscosity Results for District 3

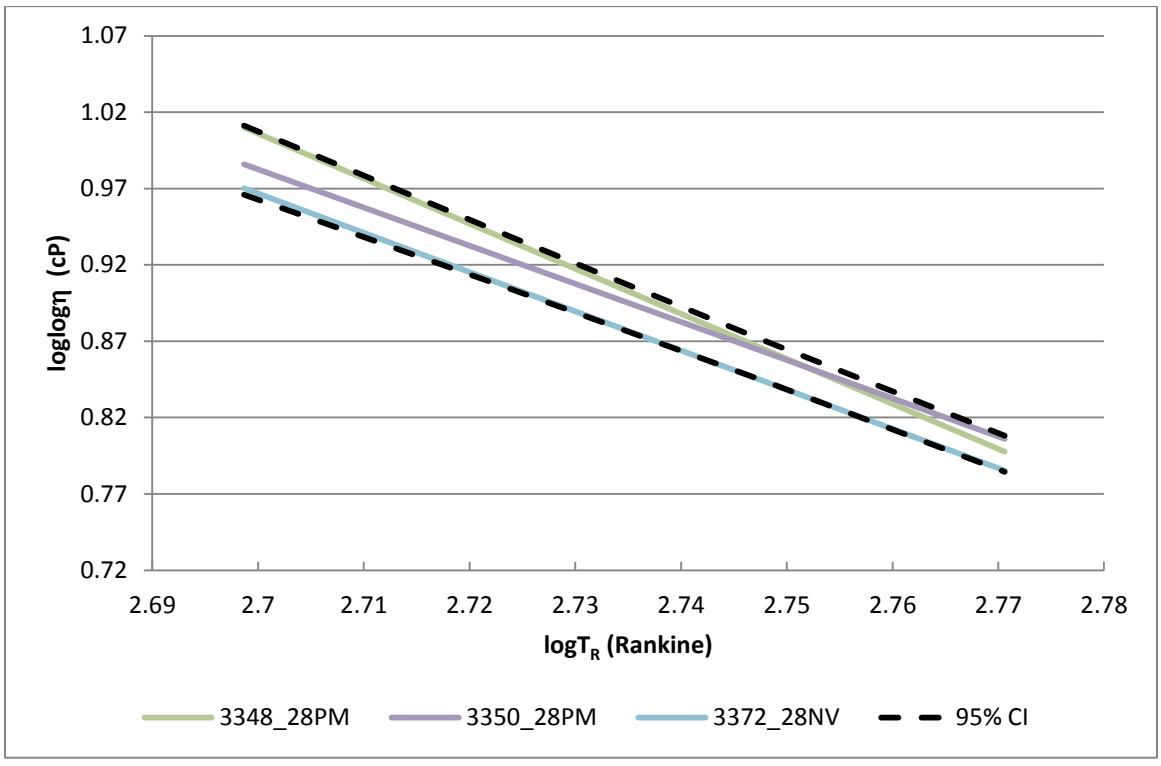

Figure 15. Binder Viscosity Results for Valero Binder Source

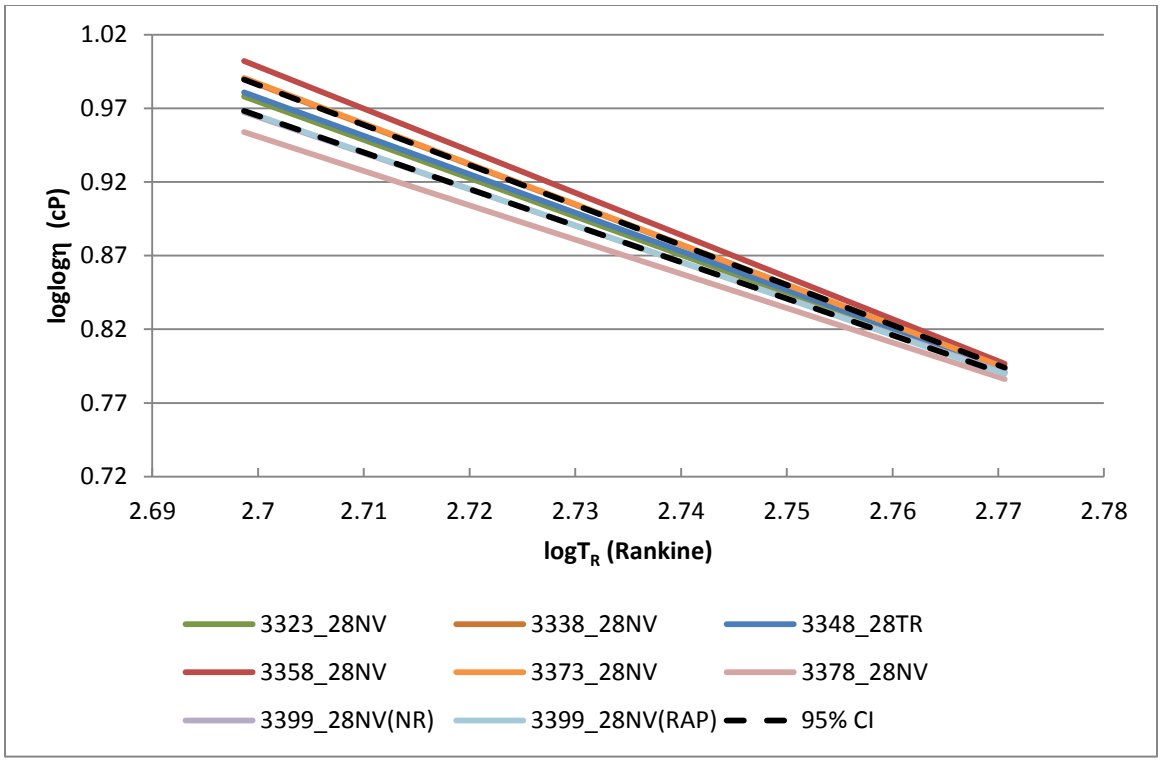

Figure 16. Binder Viscosity Results for Paramount Binder Source

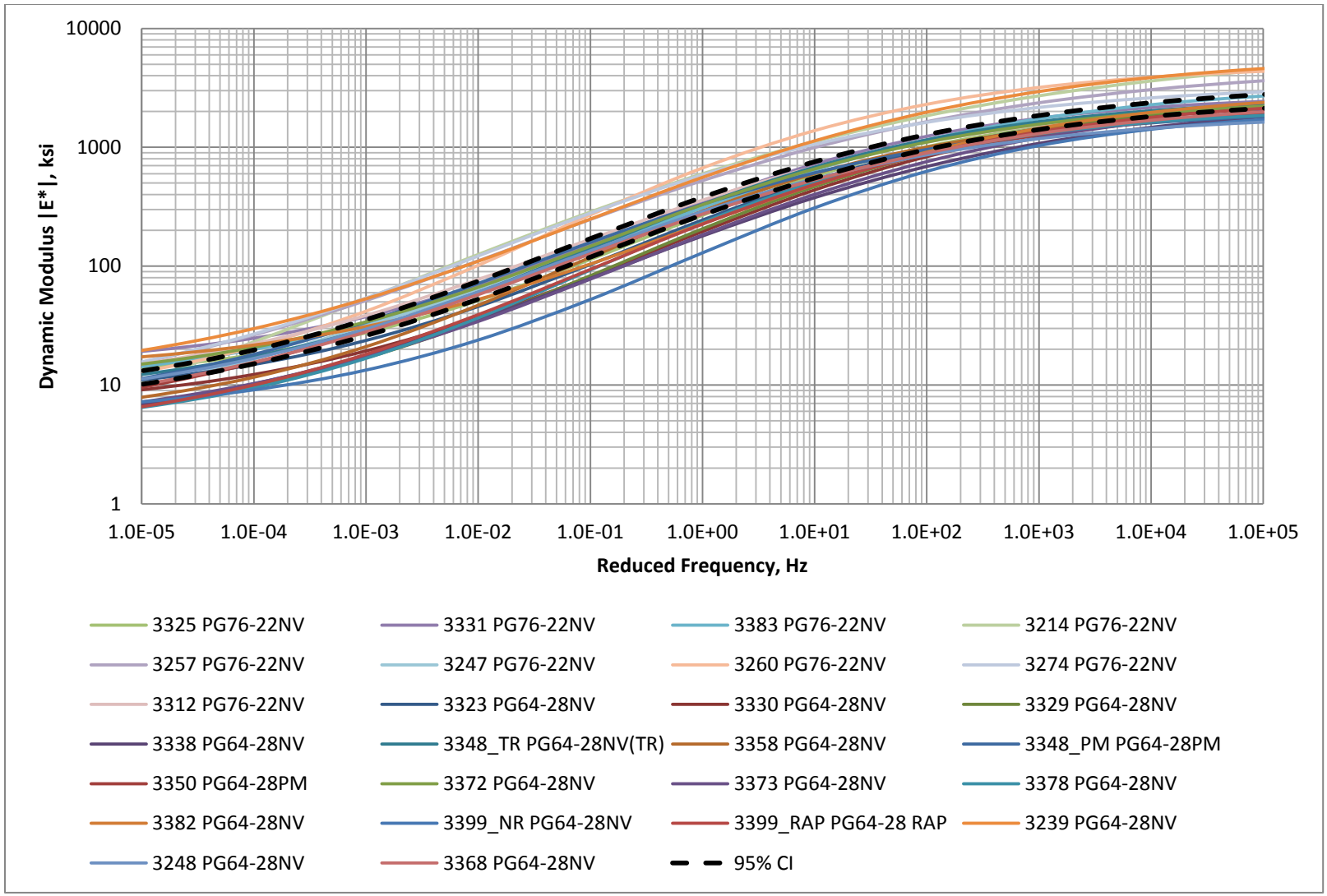

Figure 17. Dynamic Modulus Results for all Sampled Nevada Mixtures at 70°F

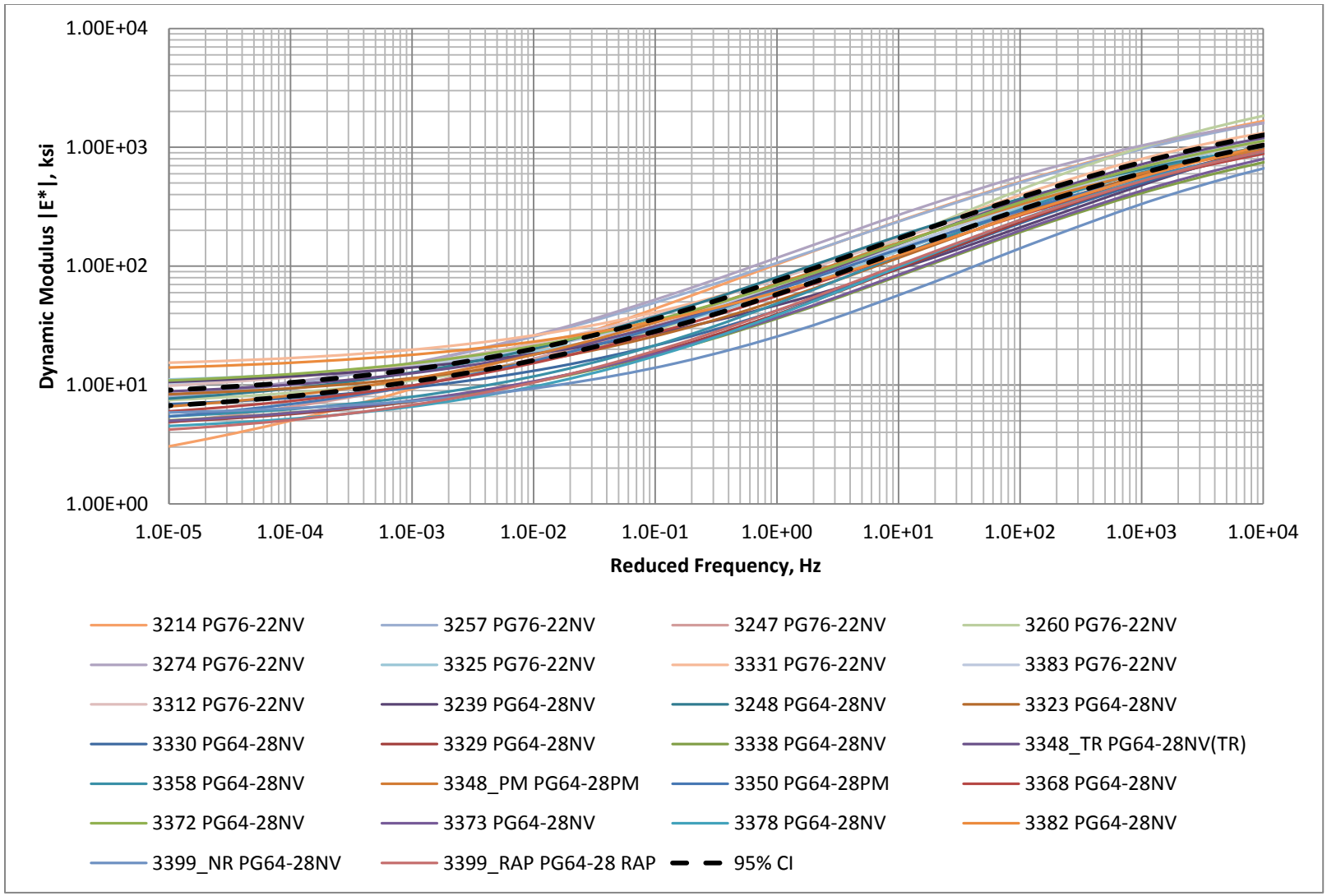

Figure 18. Dynamic Modulus Results for all Sampled Nevada Mixtures at 104°F

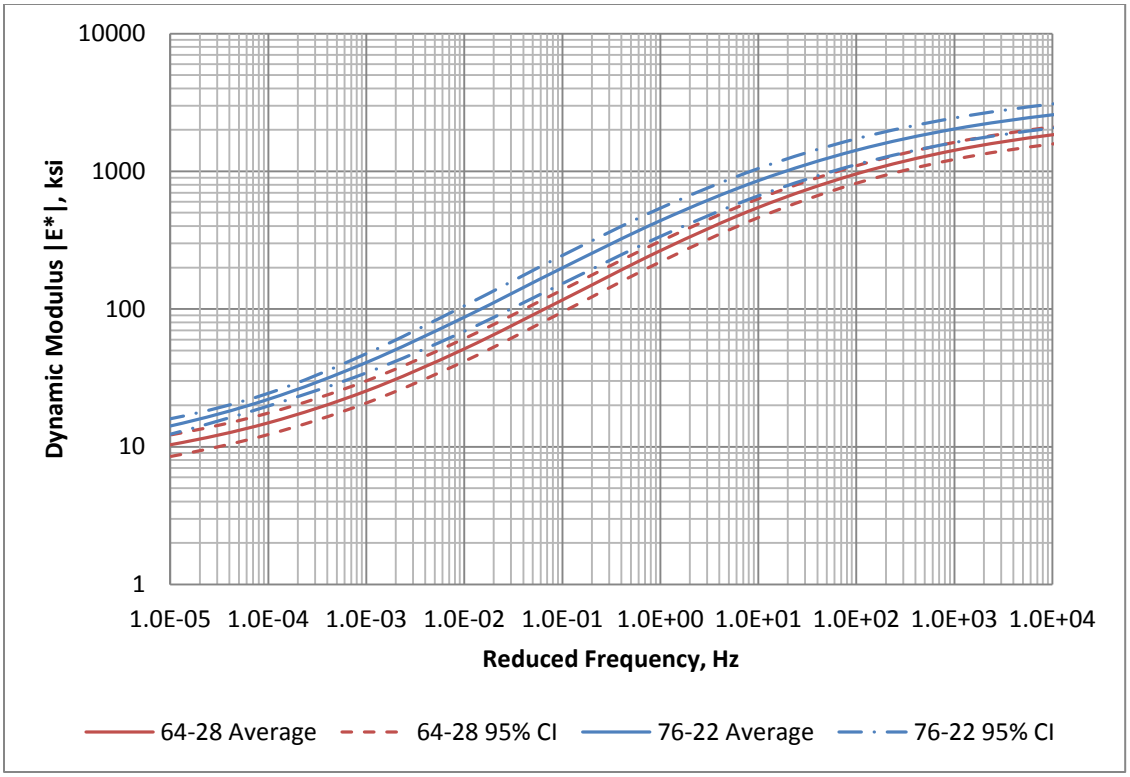

(a)

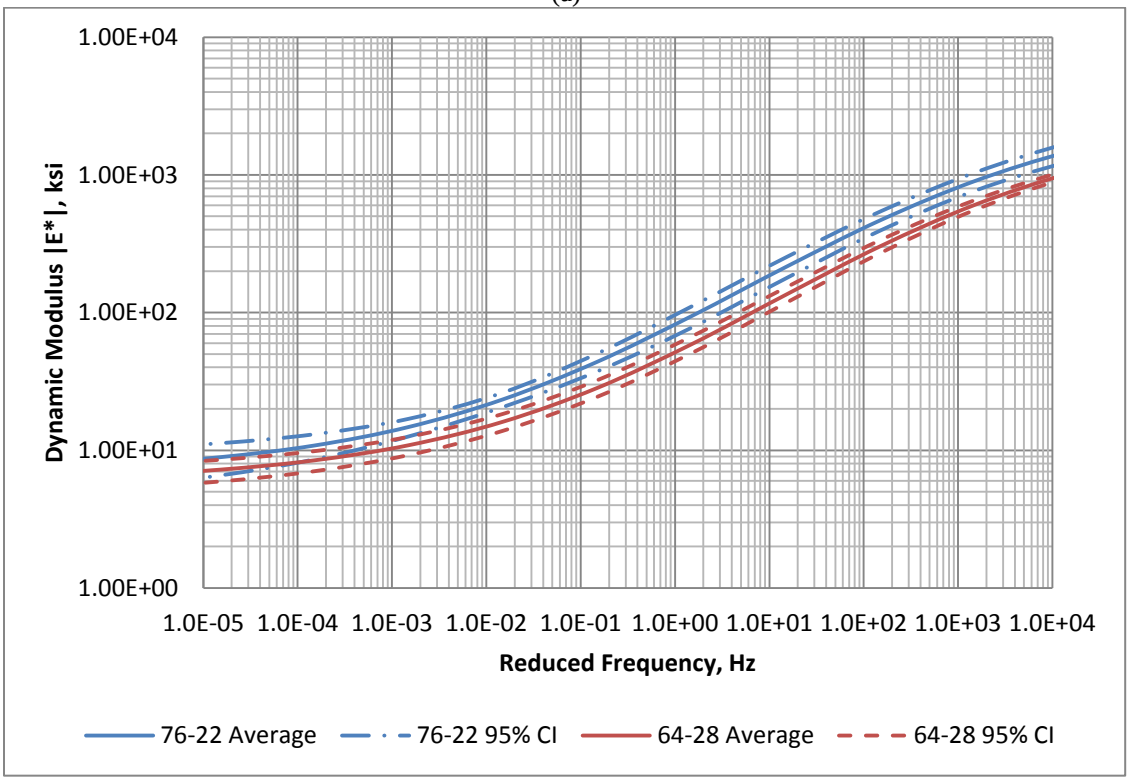

(b)

Figure 19. Dynamic Modulus Results for the Averages of PG64-28NV and PG76-22NV Mixtures (a) 70°F (b) 104°F

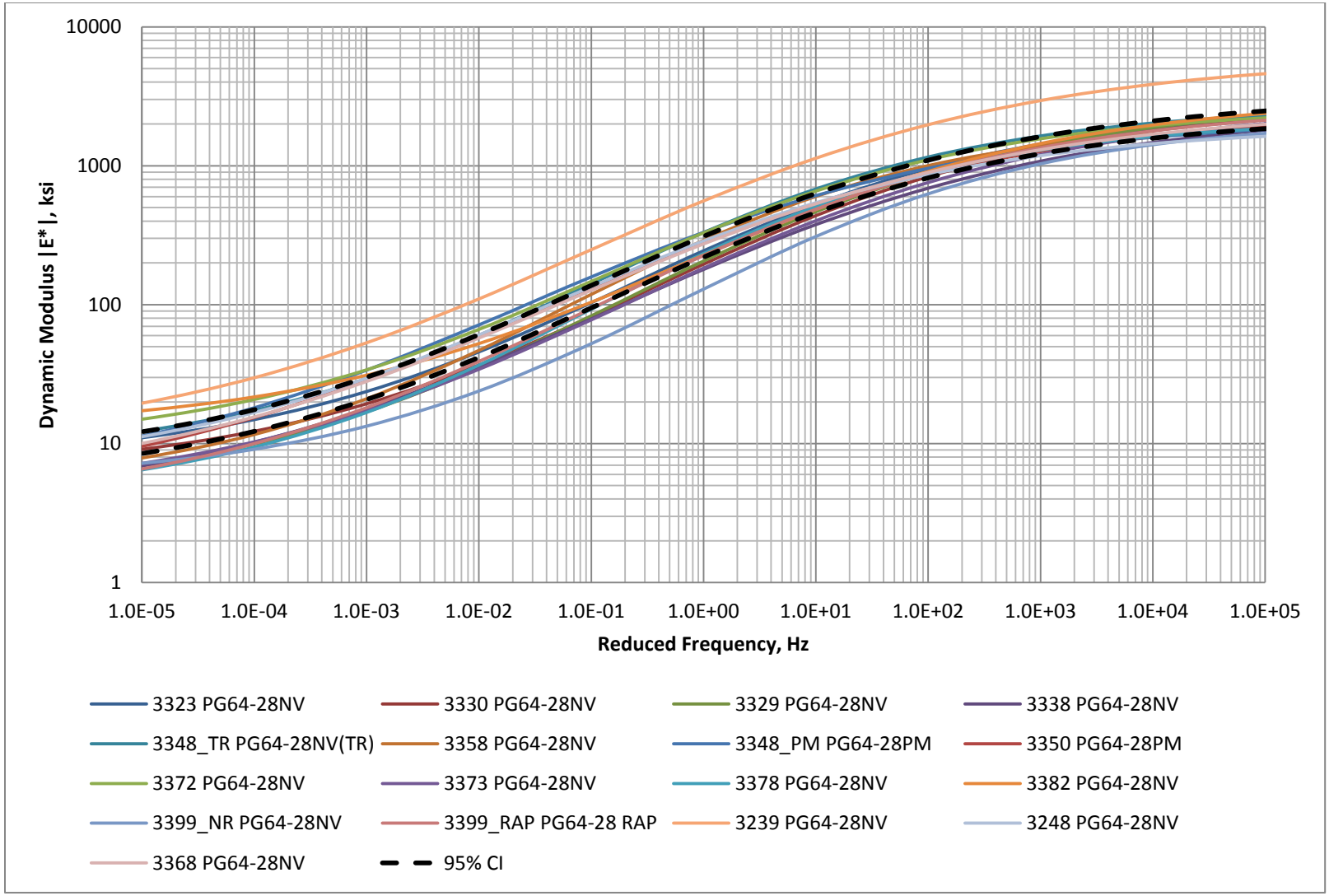

Figure 20. Dynamic Modulus Results for the PG64-28NV Mixtures at 70°F

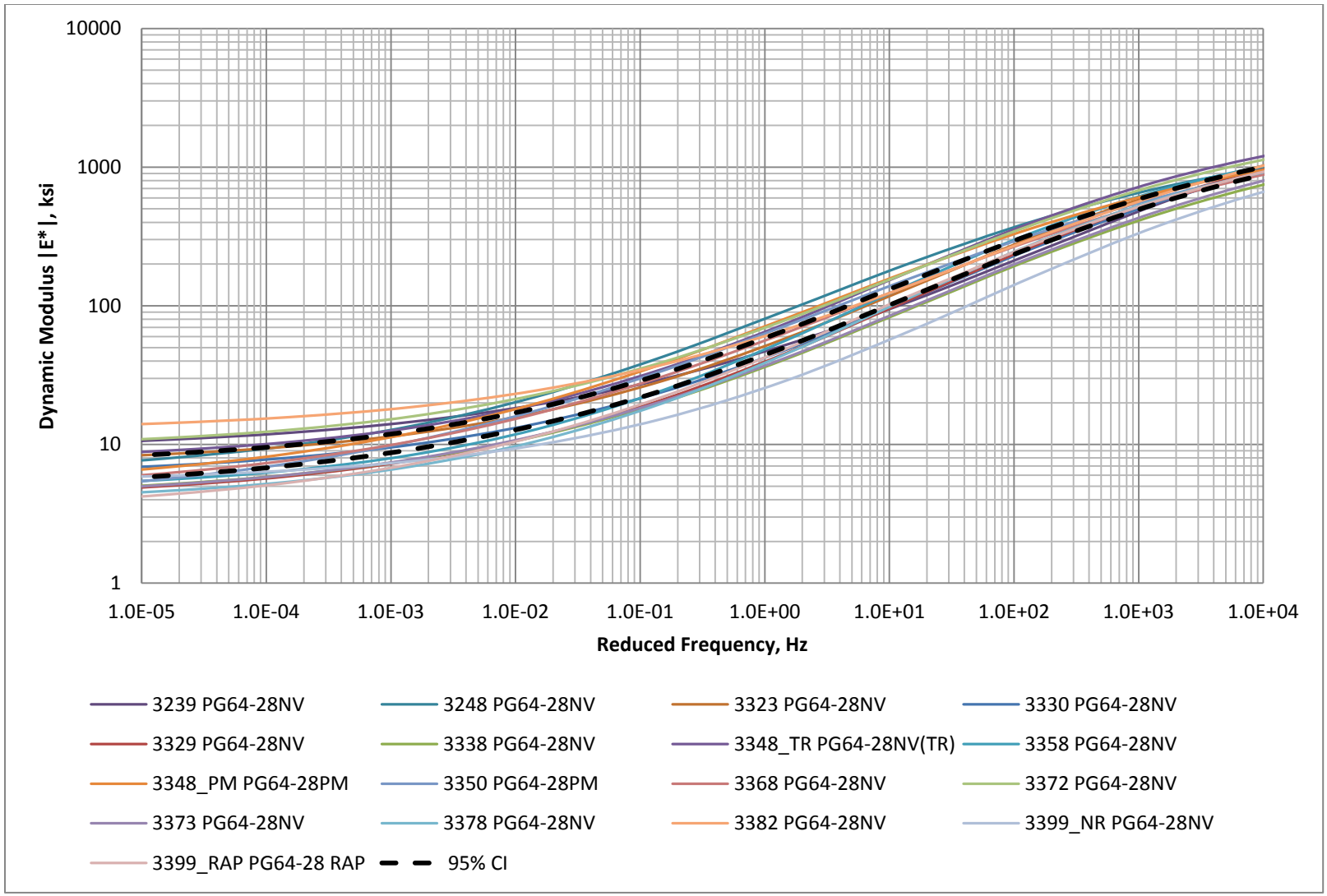

Figure 21. Dynamic Modulus Results for the PG64-28NV Mixtures at 104°F

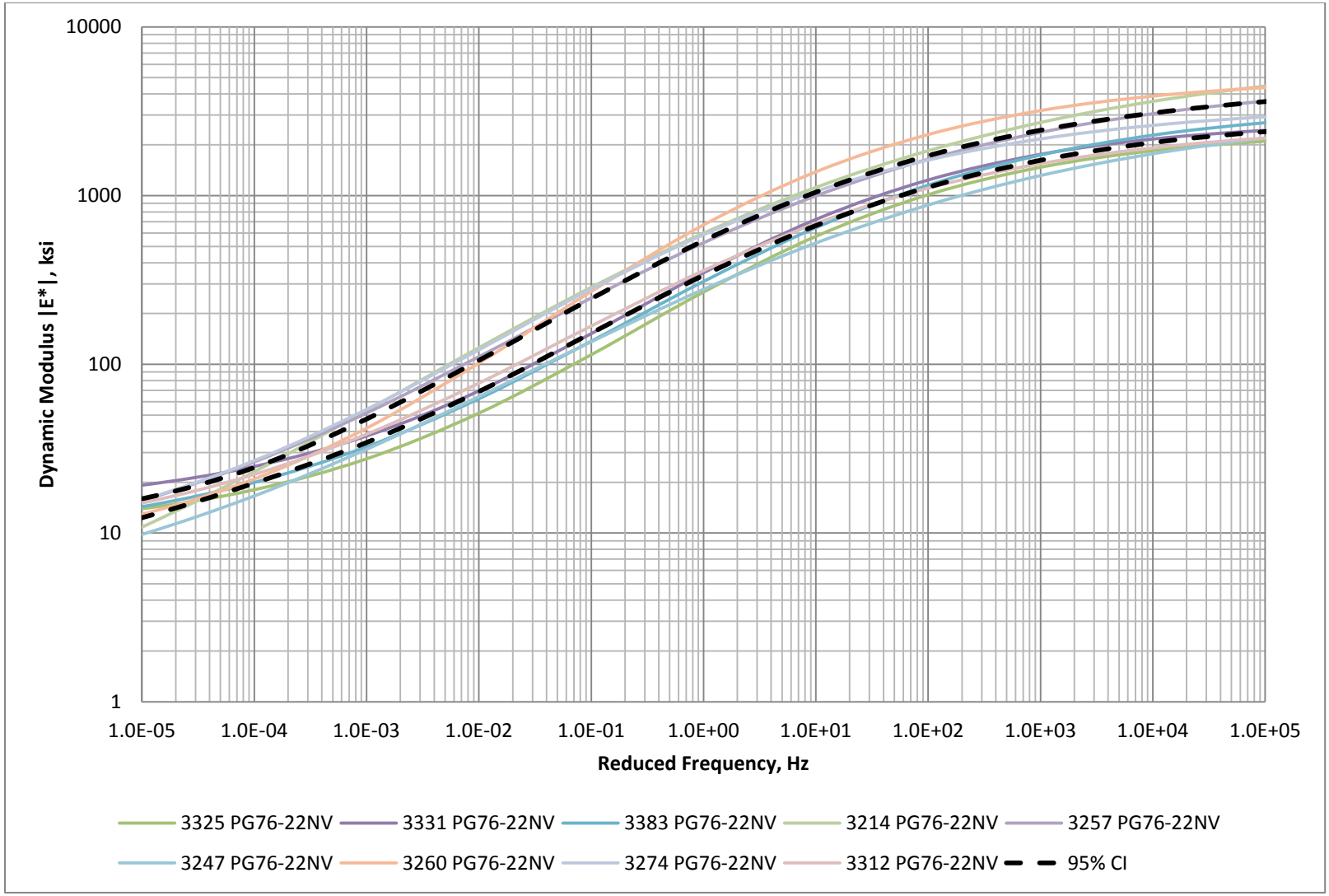

Figure 22. Dynamic Modulus Results for the PG76-22NV Mixtures at 70°F

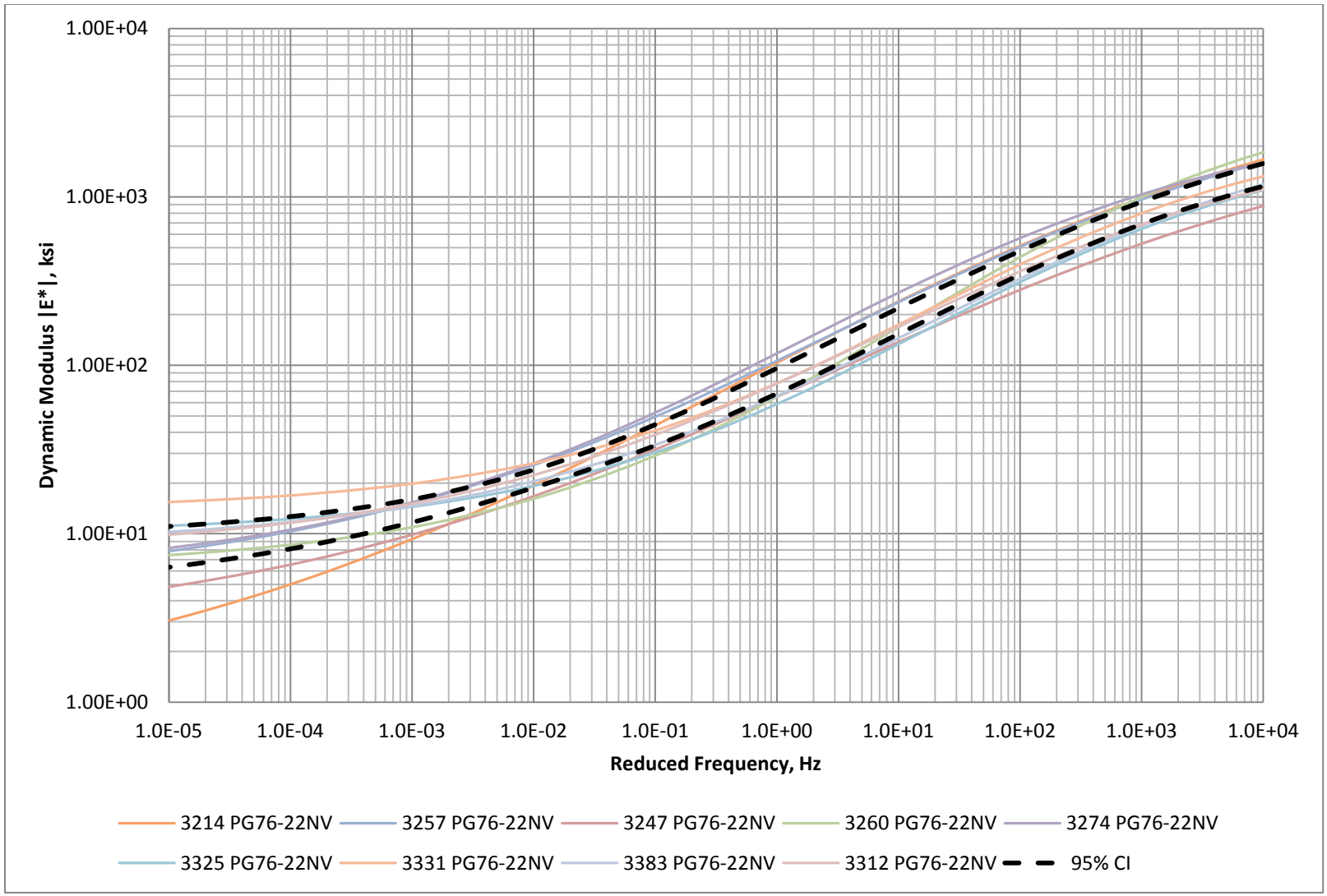

Figure 23. Dynamic Modulus Results for the PG76-22NV Mixtures at 104°F

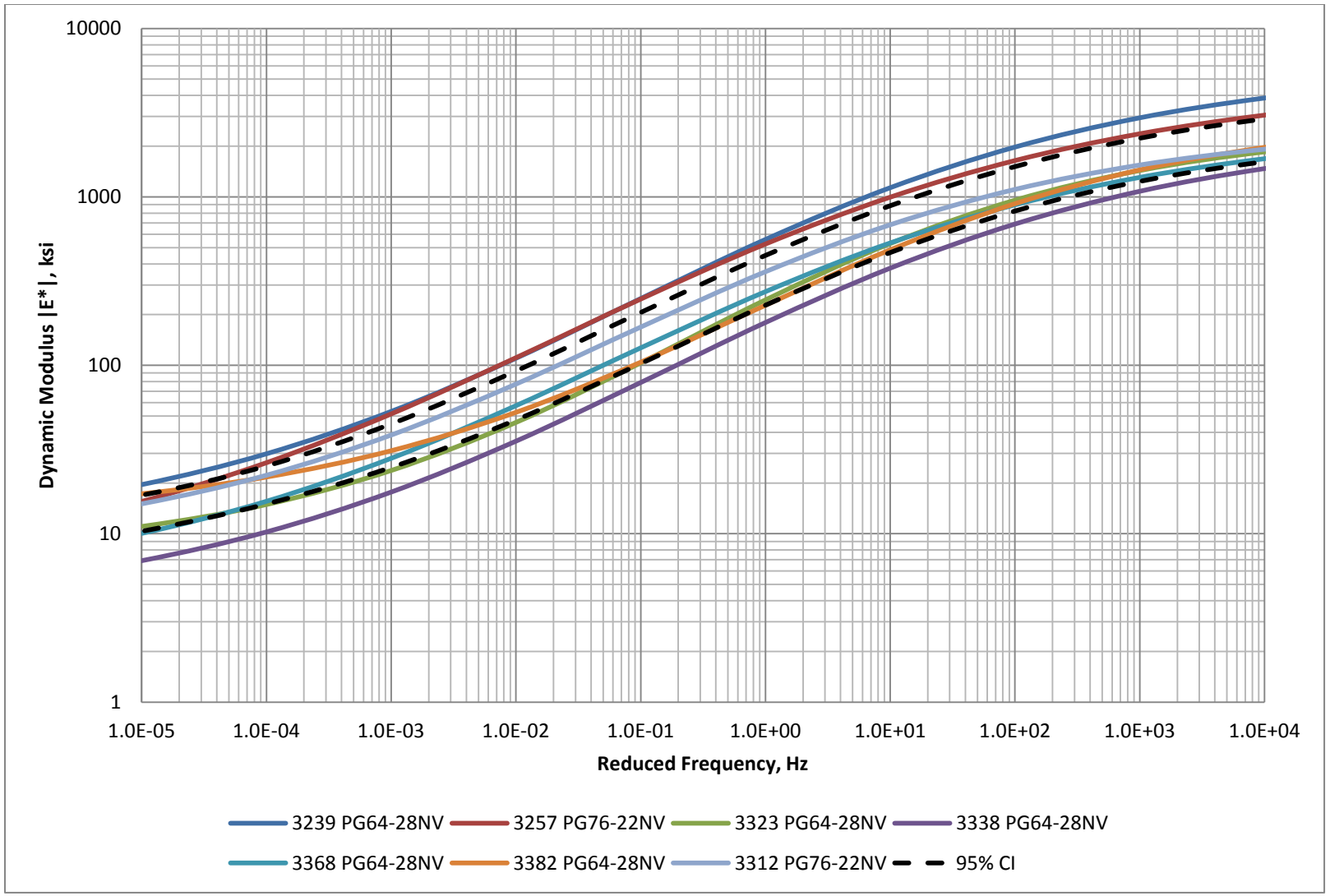

Figure 24. Dynamic Modulus Results for Type 2 Mixtures at 70°F

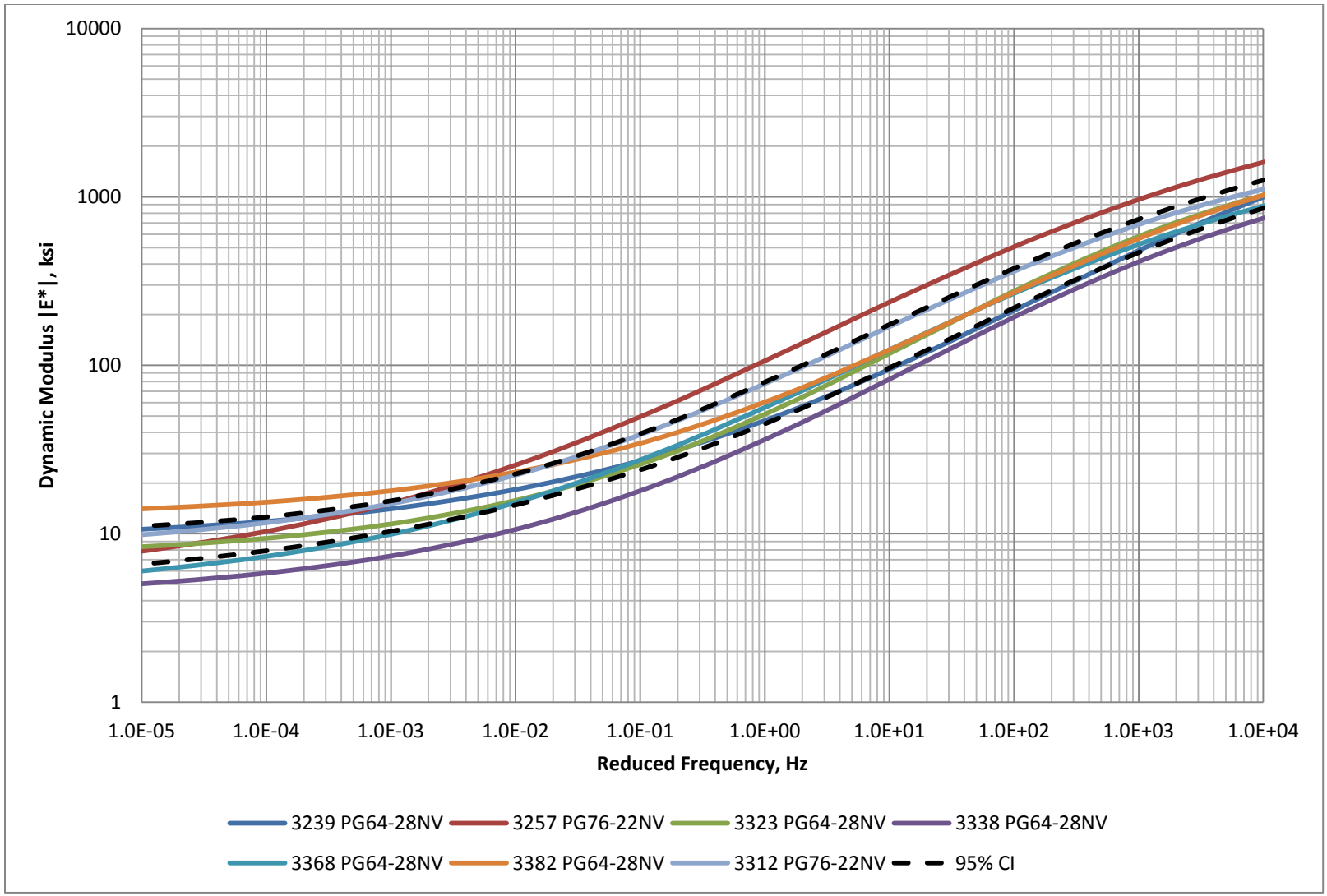

Figure 25. Dynamic Modulus Results for Type 2 Mixtures at 104°F

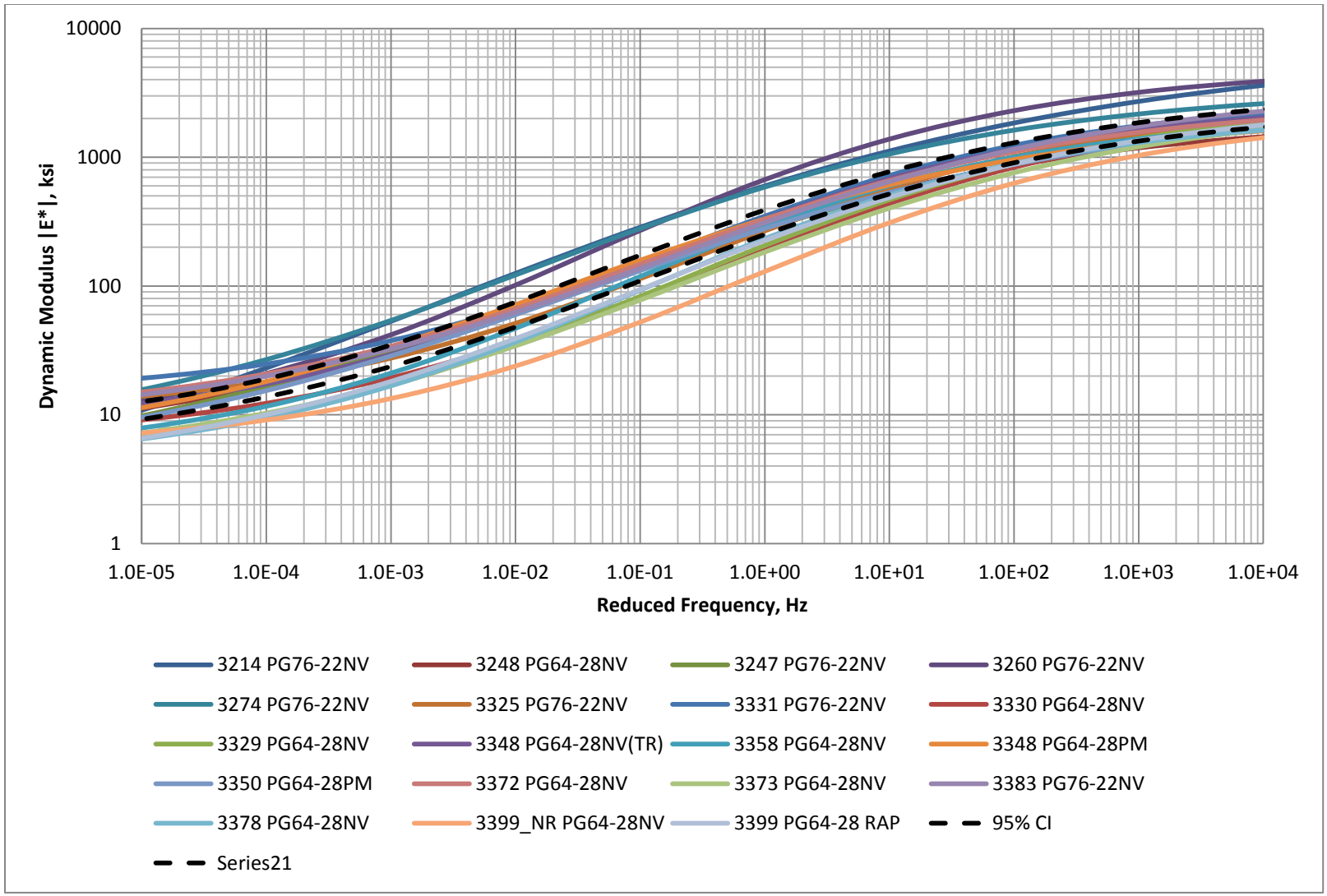

Figure 26. Dynamic Modulus Results for Type 2C Mixtures at 70°F

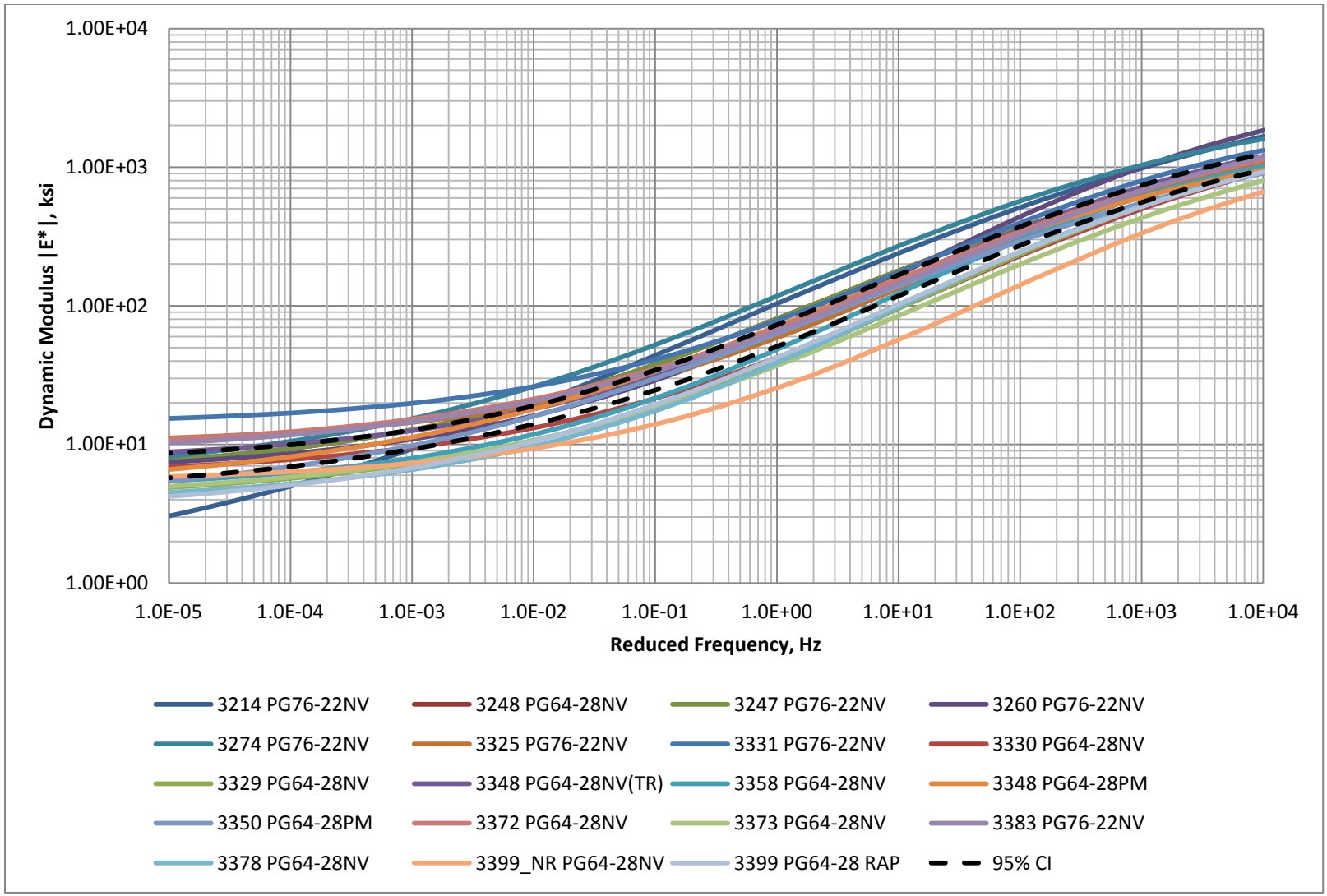

Figure 27. Dynamic Modulus Results for Type 2C Mixtures at 104°F

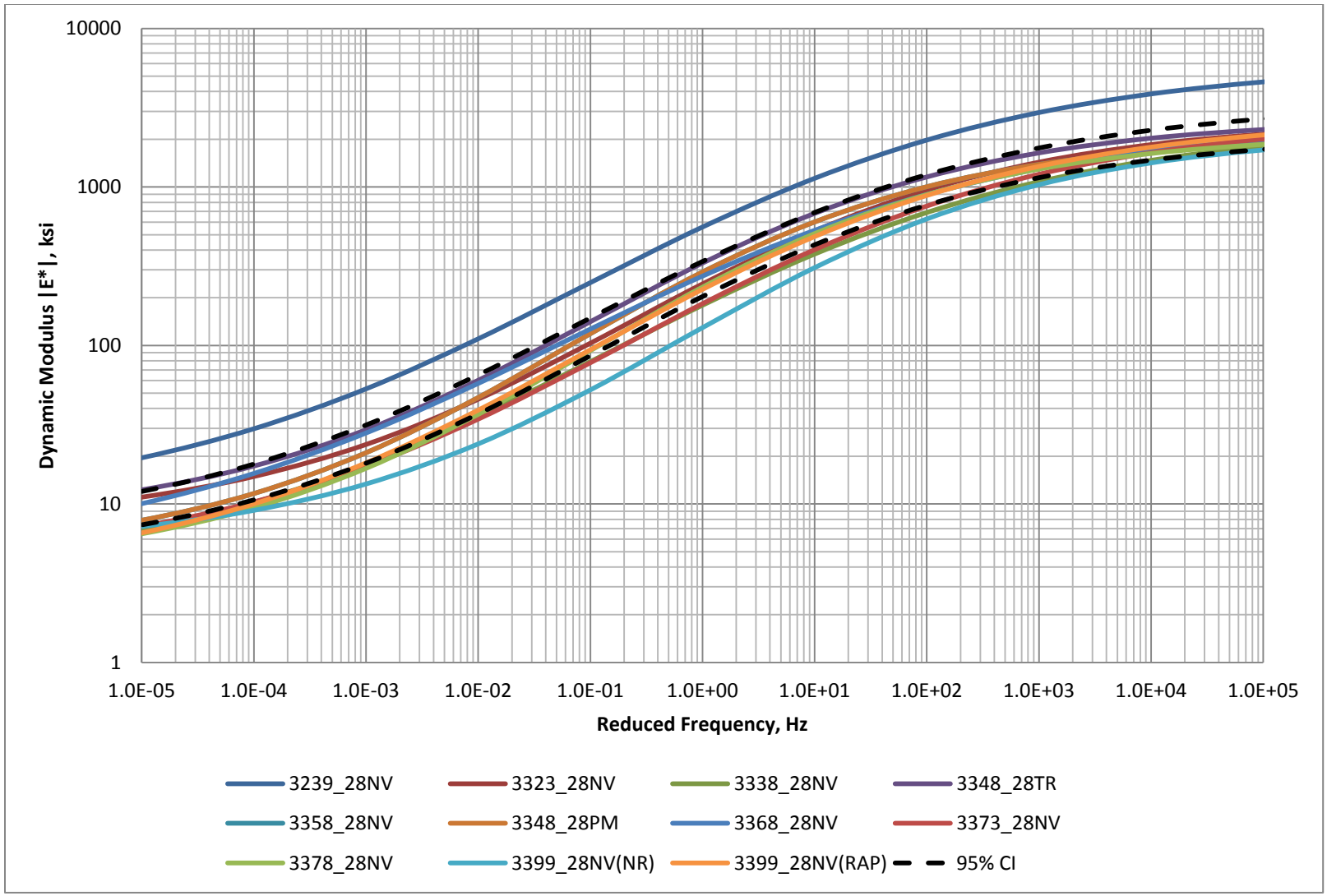

Figure 28. Dynamic Modulus Results for District 2 Mixtures at 70°F

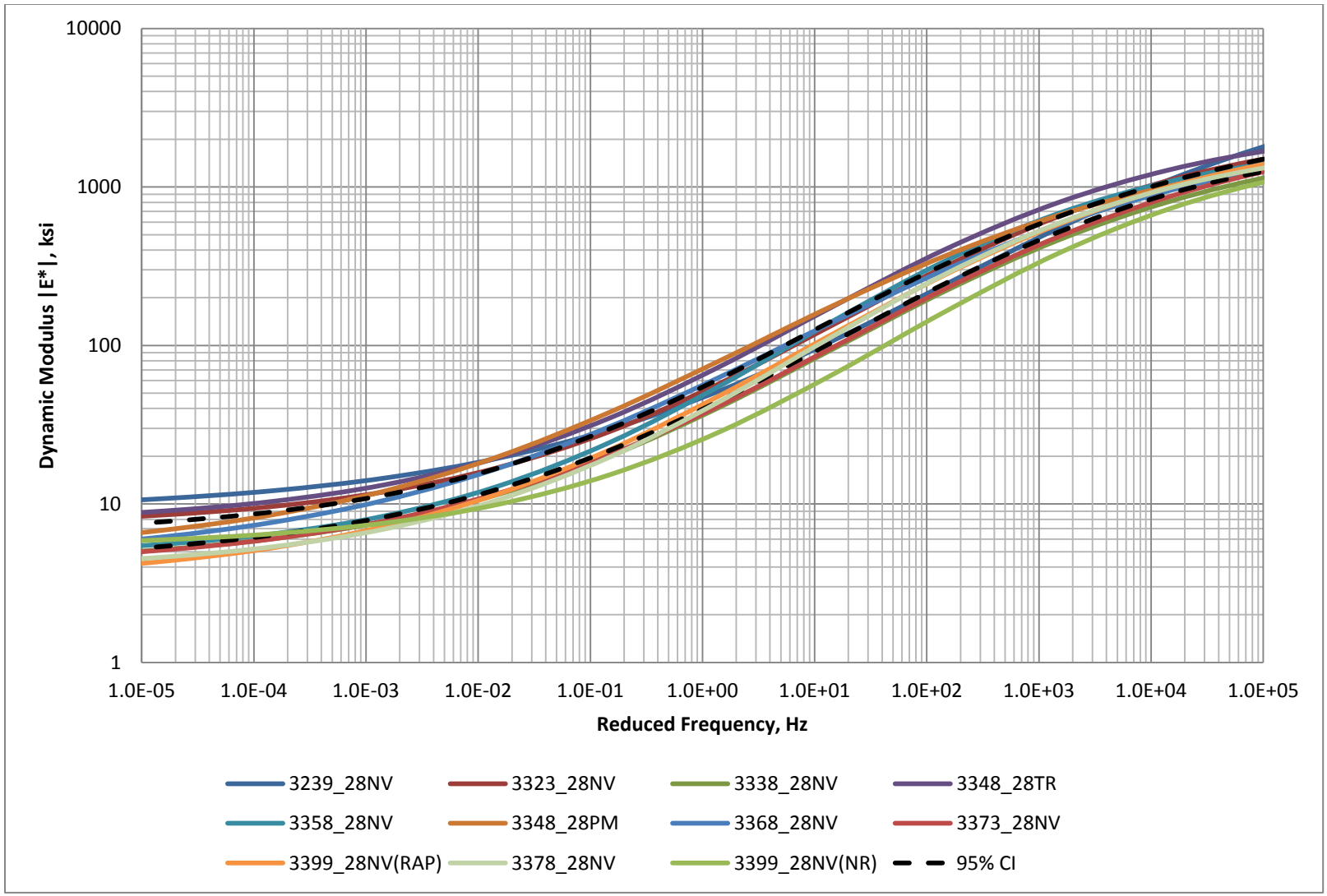

Figure 29. Dynamic Modulus Results for District 2 Mixtures at 104°F

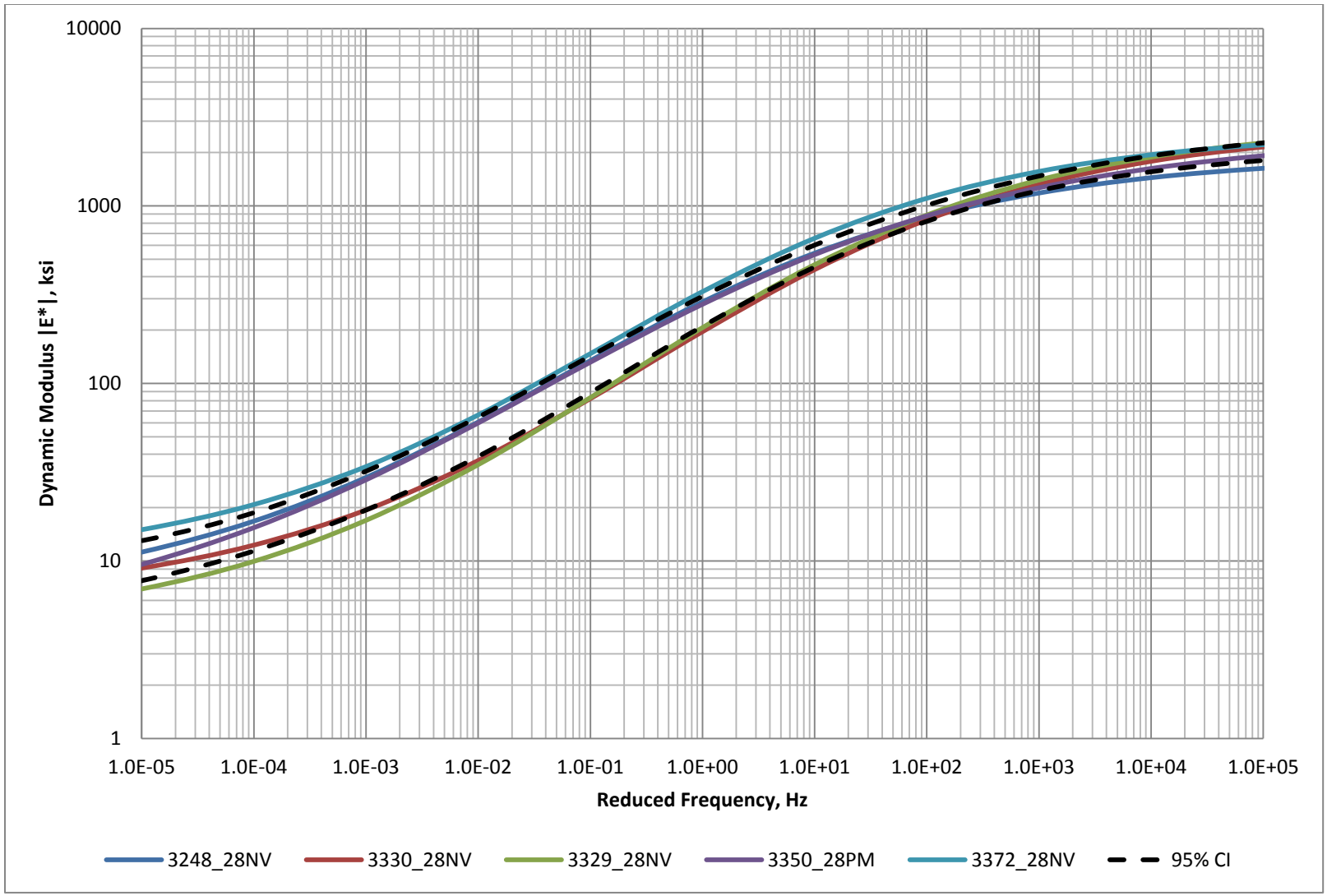

Figure 30. Dynamic Modulus Results for District 3 Mixtures at 70°F

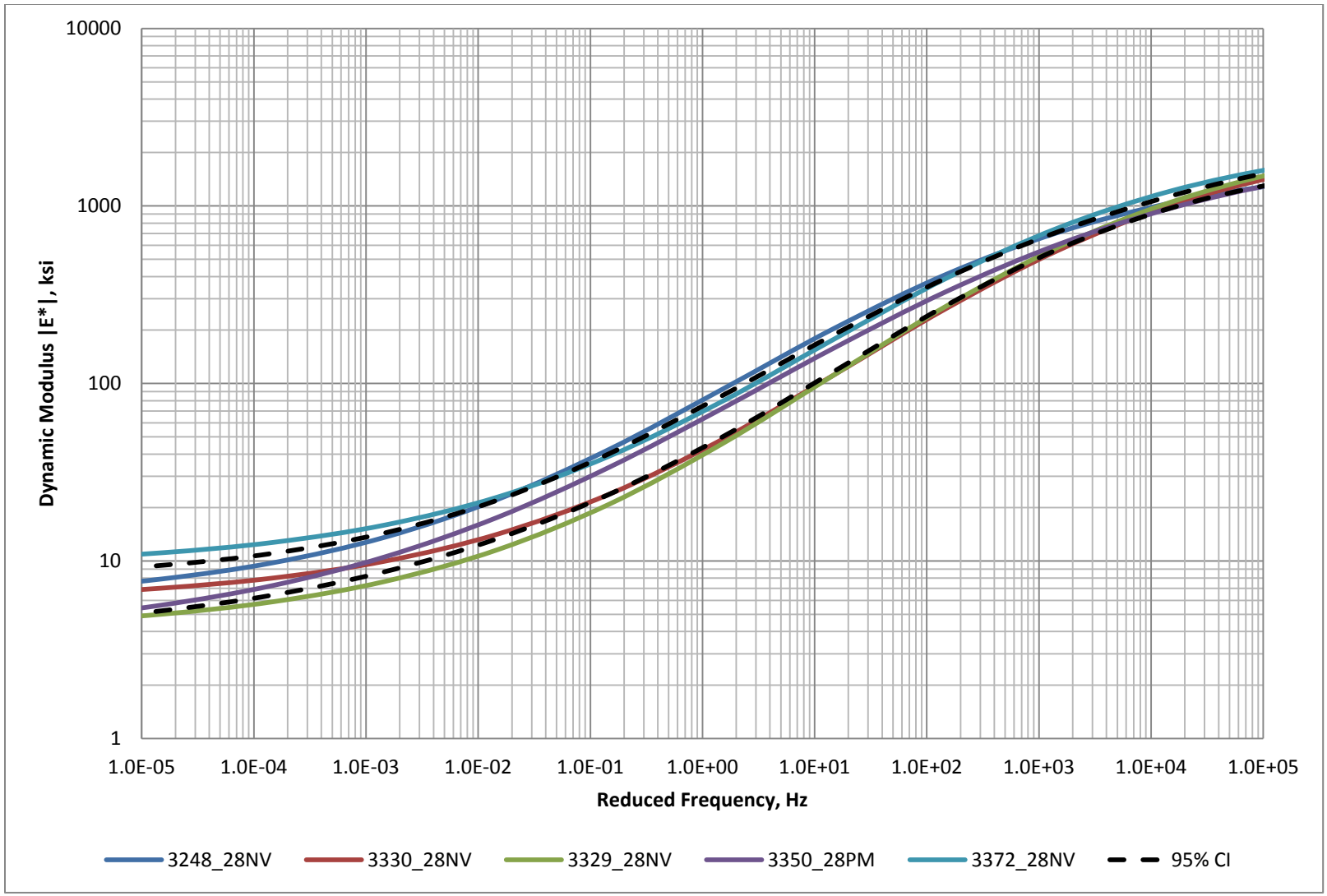

Figure 31. Dynamic Modulus Results for District 3 Mixtures at 104°F

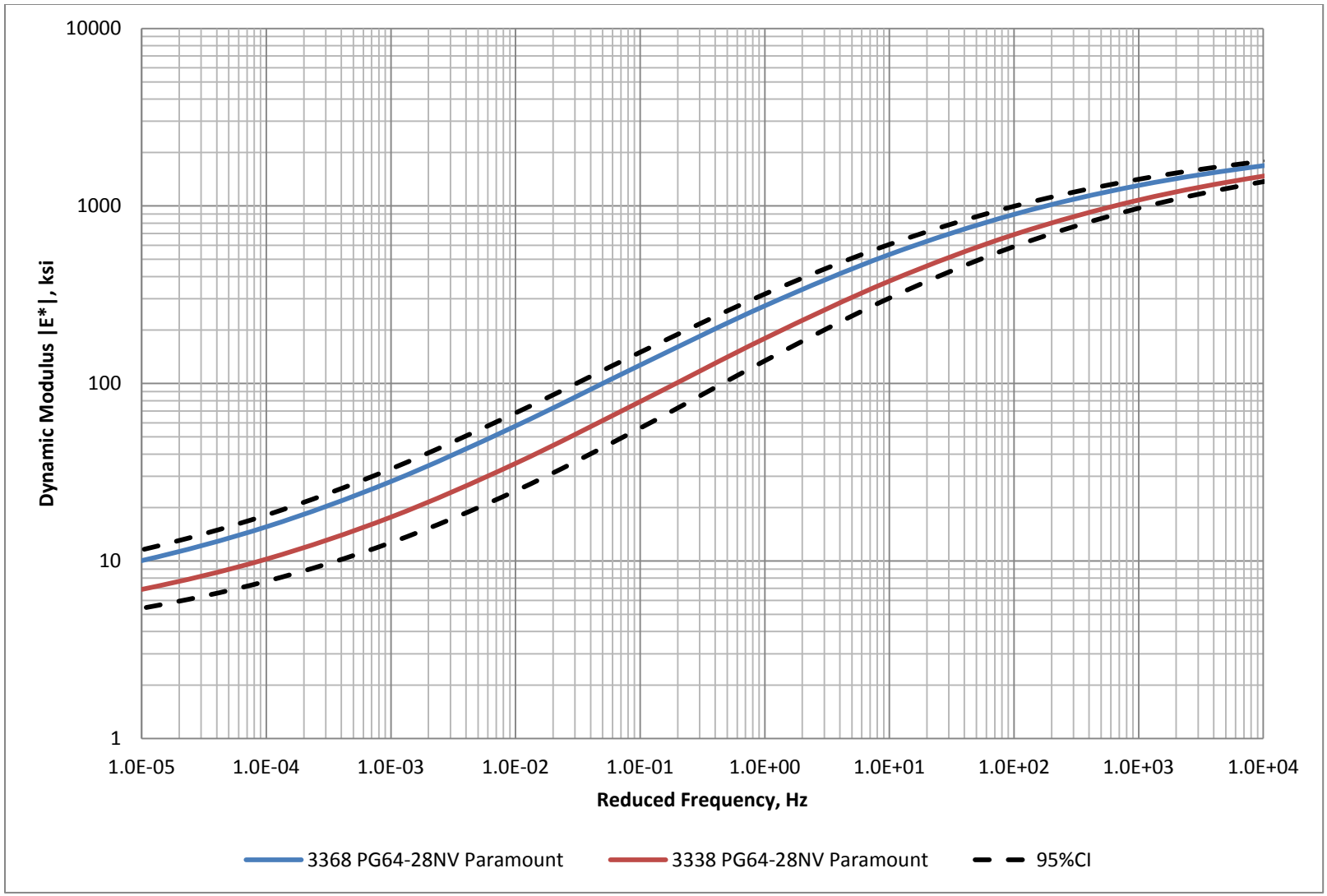

Figure 32. Dynamic Modulus Results for Aggregate Source Bertagnolli Mixtures at 70°F

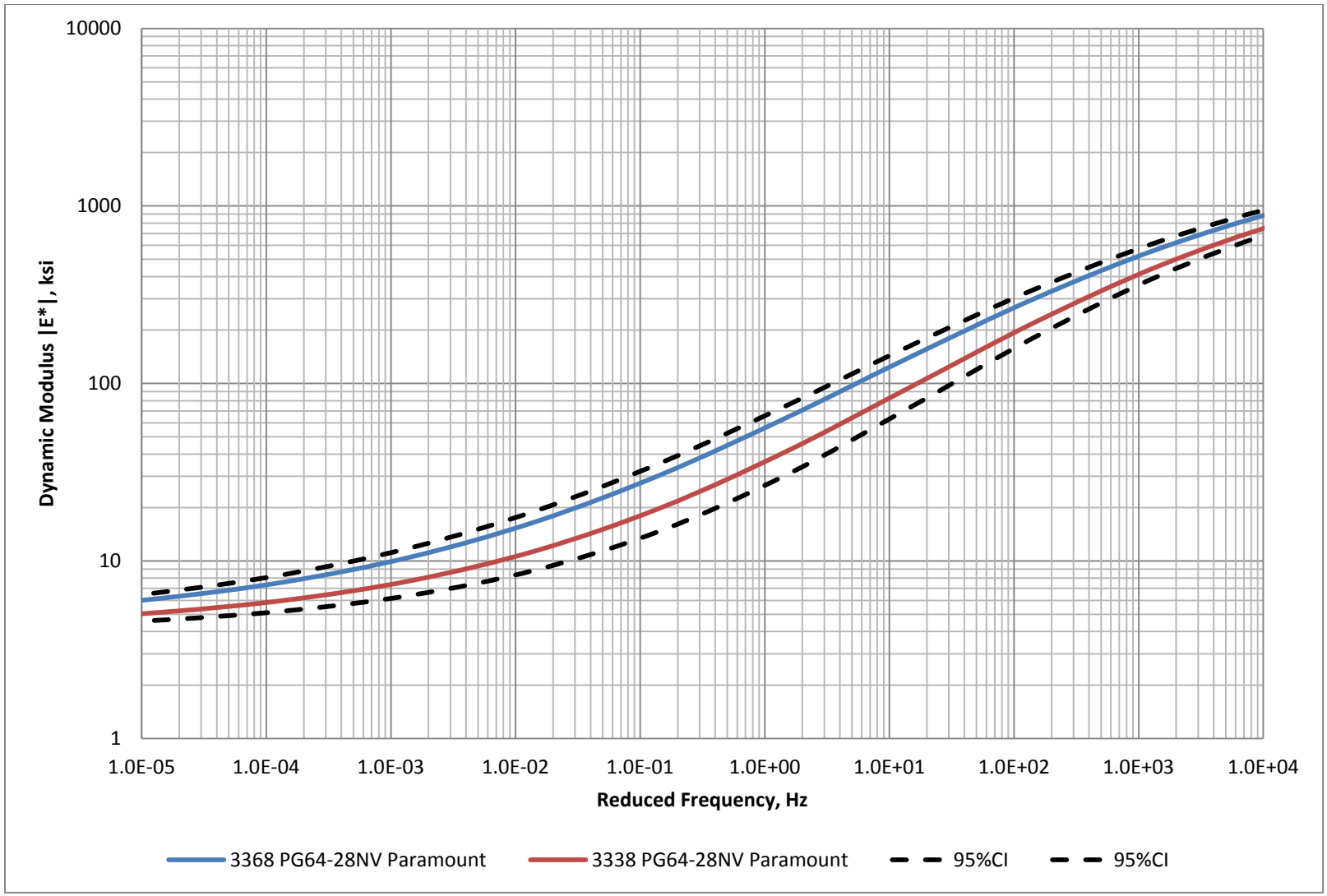

Figure 33. Dynamic Modulus Results for Aggregate Source Bertagnolli Mixtures at 104°F

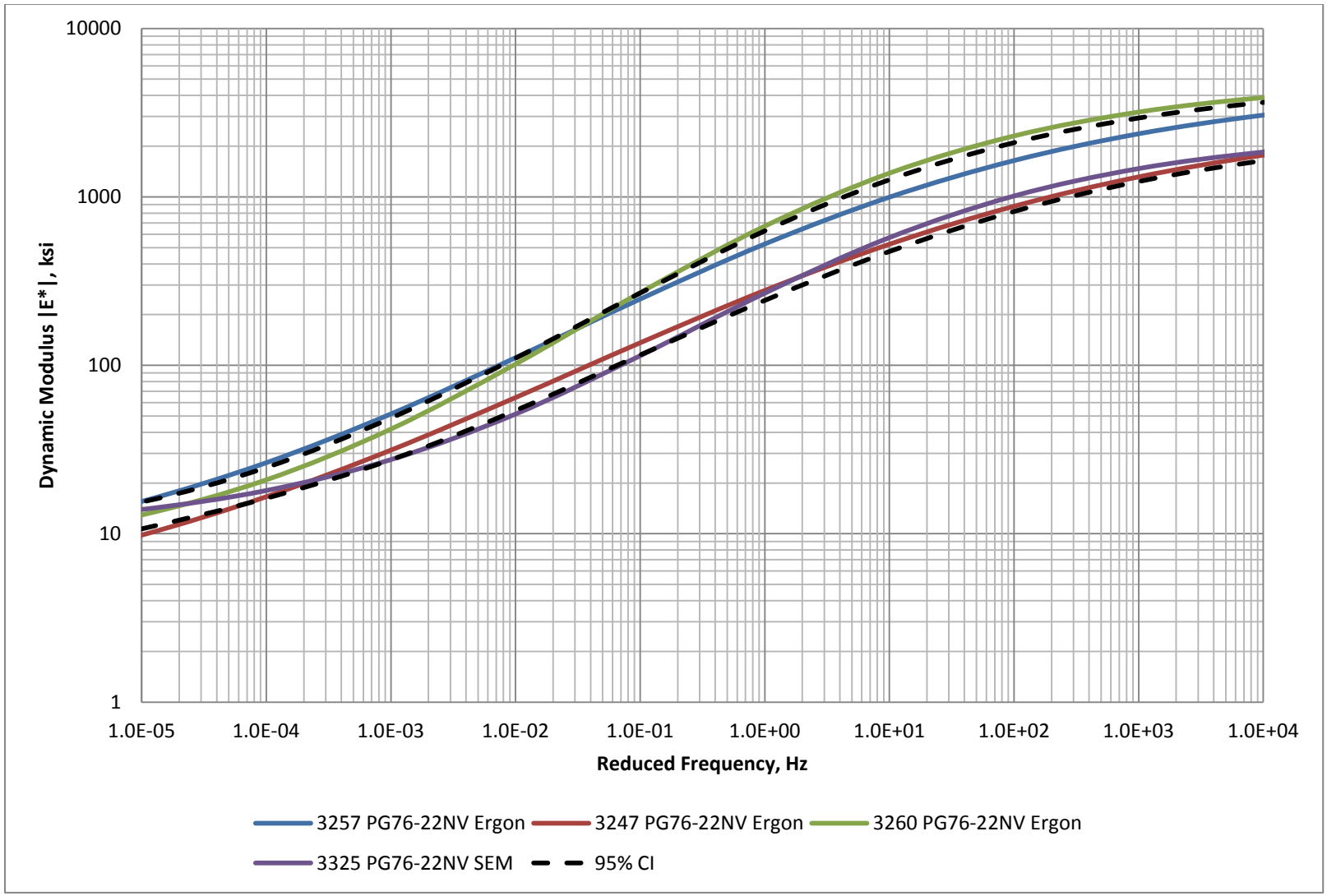

Figure 34. Dynamic Modulus Results for Aggregate Source Blue Diamond Mixtures at 70°F

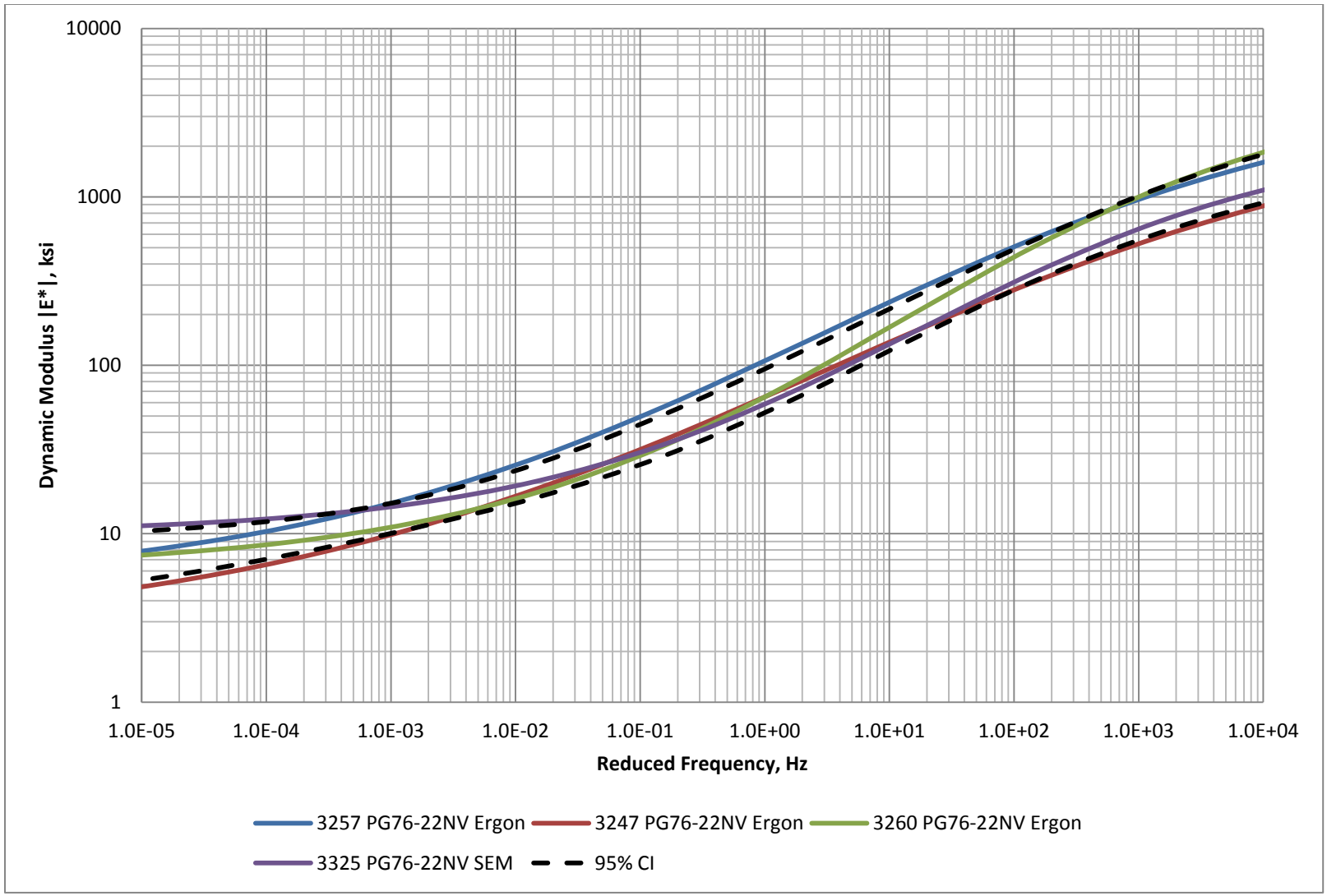

Figure 35. Dynamic Modulus Results for Aggregate Source Blue Diamond Mixtures at 104°F

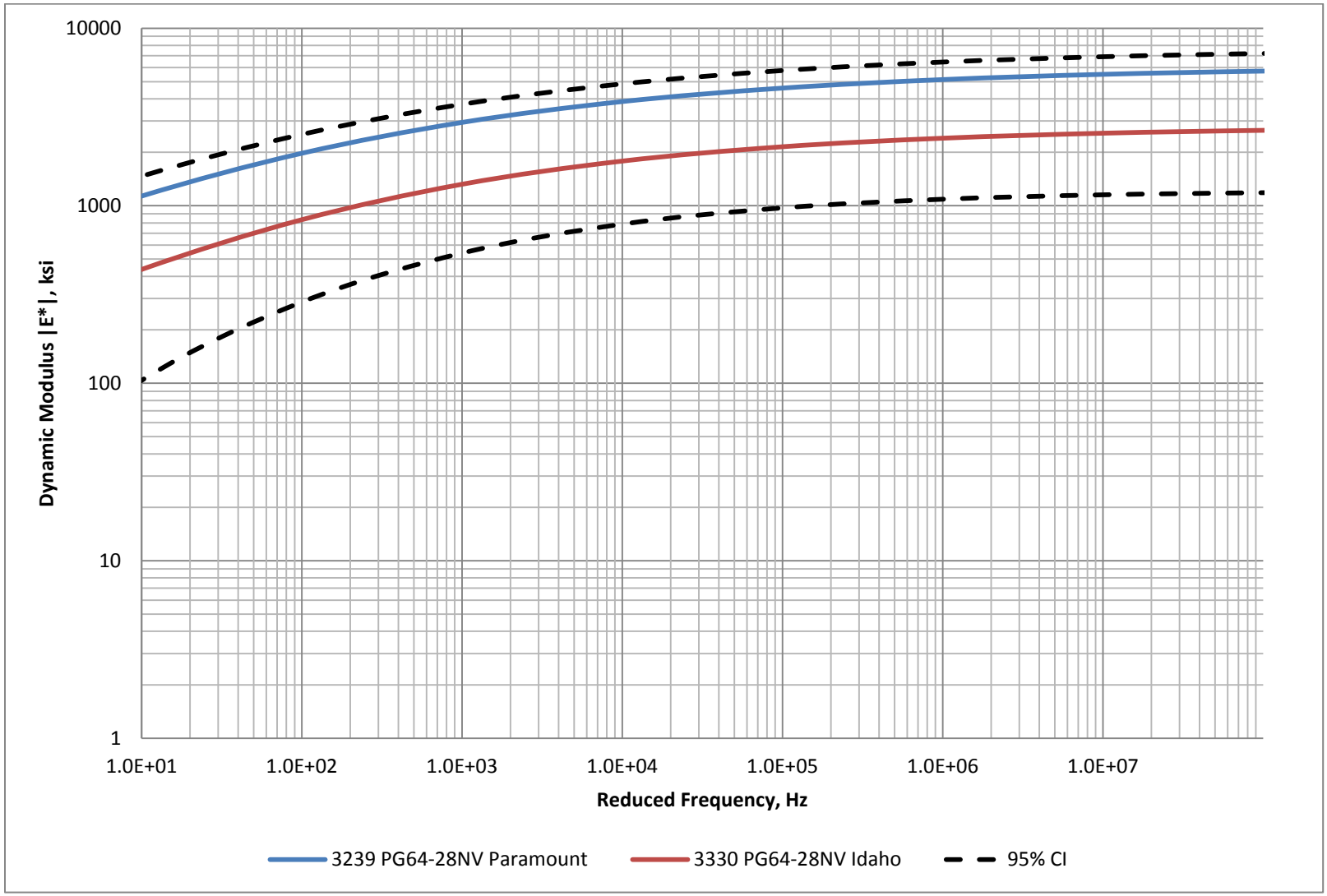

Figure 36. Dynamic Modulus Results for Aggregate Source Hunewill Mixtures at 70°F

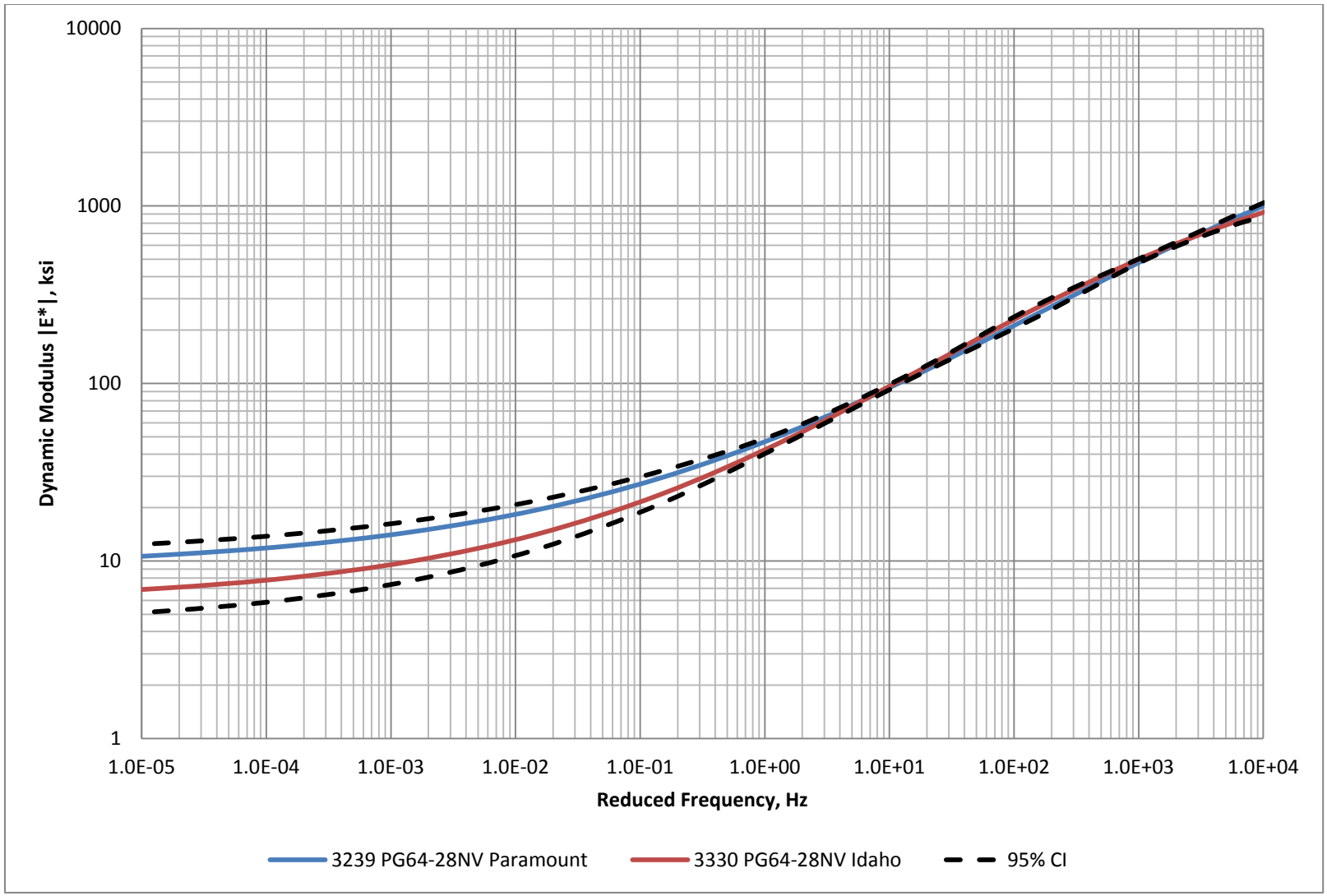

Figure 37. Dynamic Modulus Results for Aggregate Source Hunewill Mixtures at 104°F

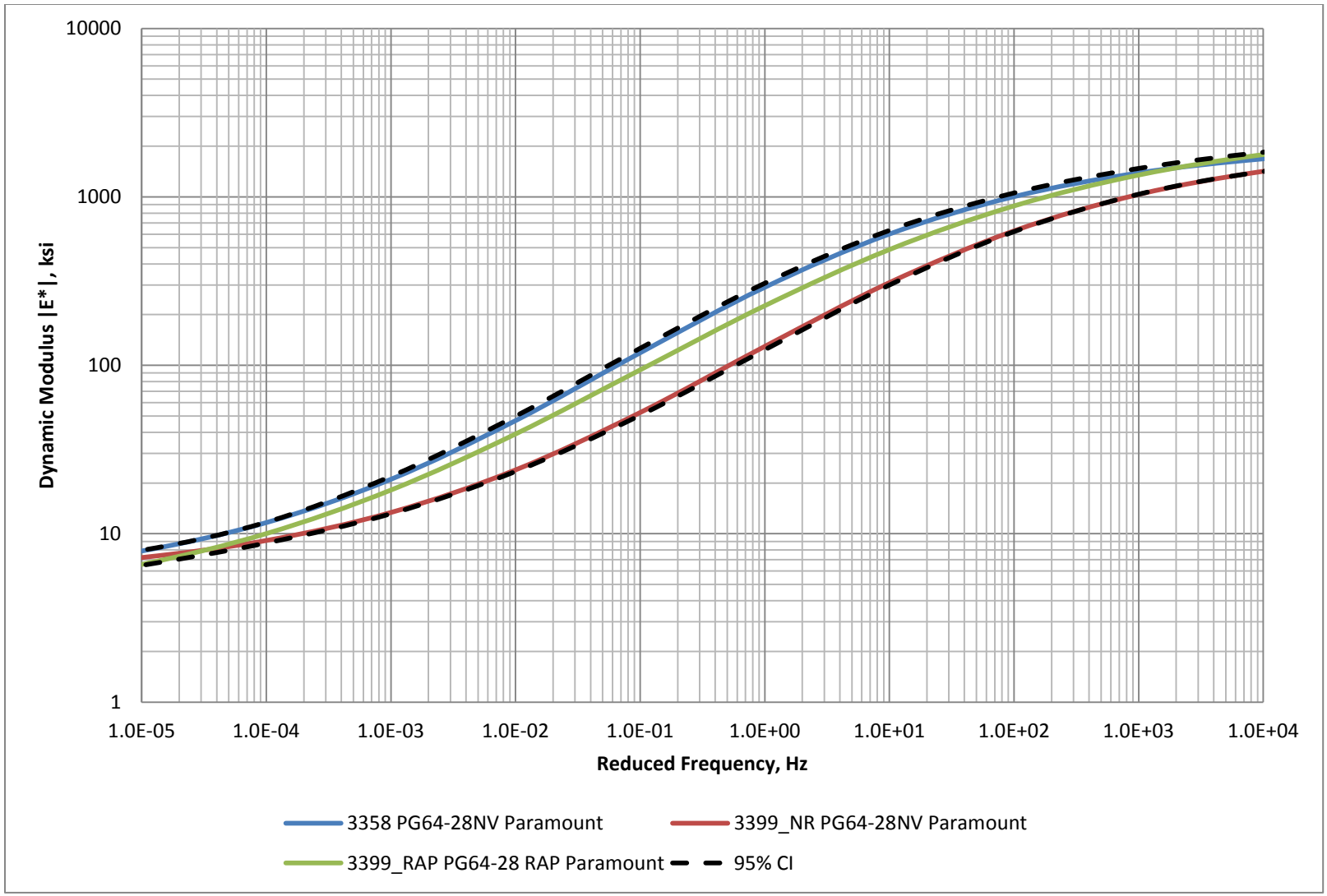

Figure 38. Dynamic Modulus Results for Aggregate Source Lockwood Mixtures at 70°F

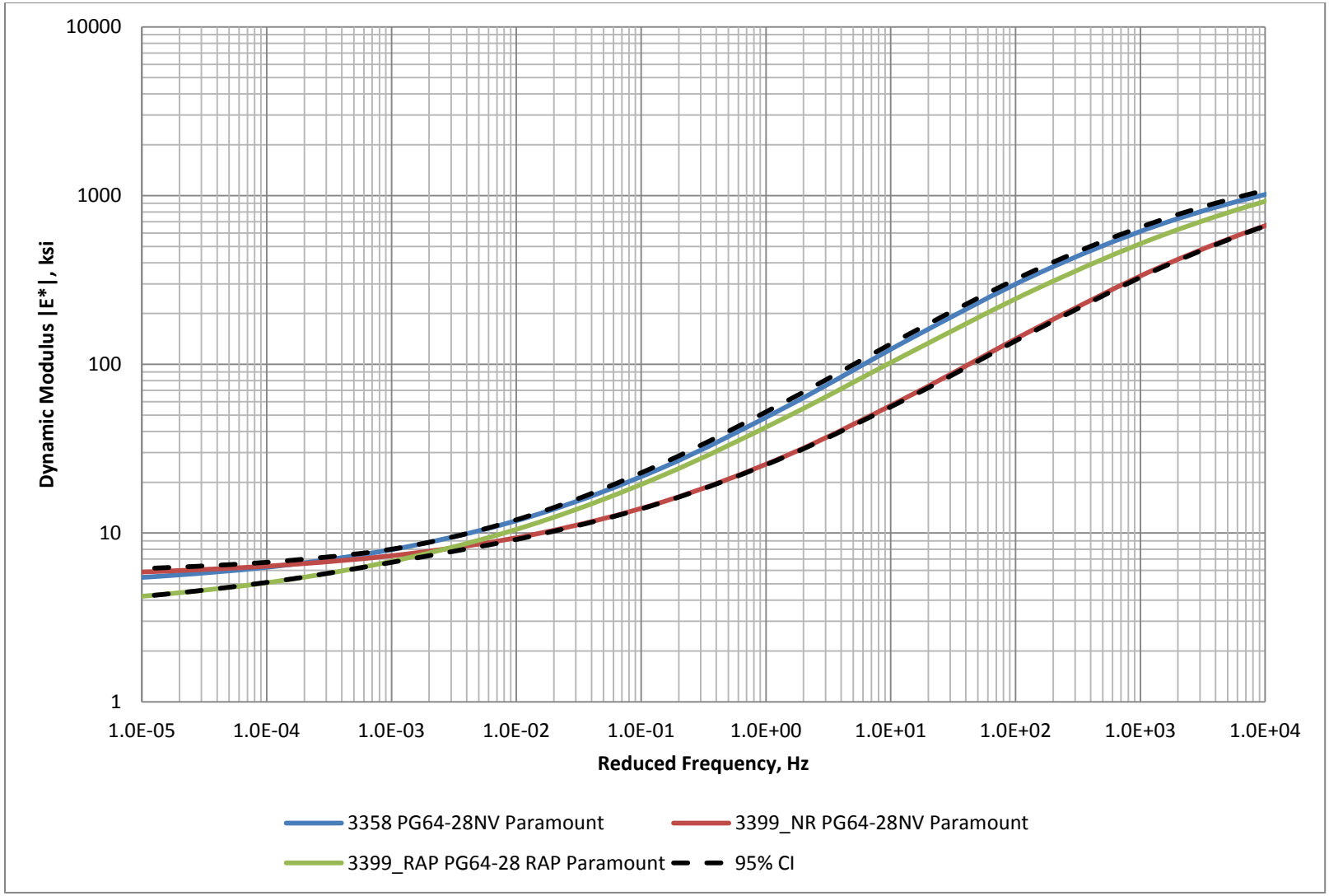

Figure 39. Dynamic Modulus Results for Aggregate Source Lockwood Mixtures at 104°F

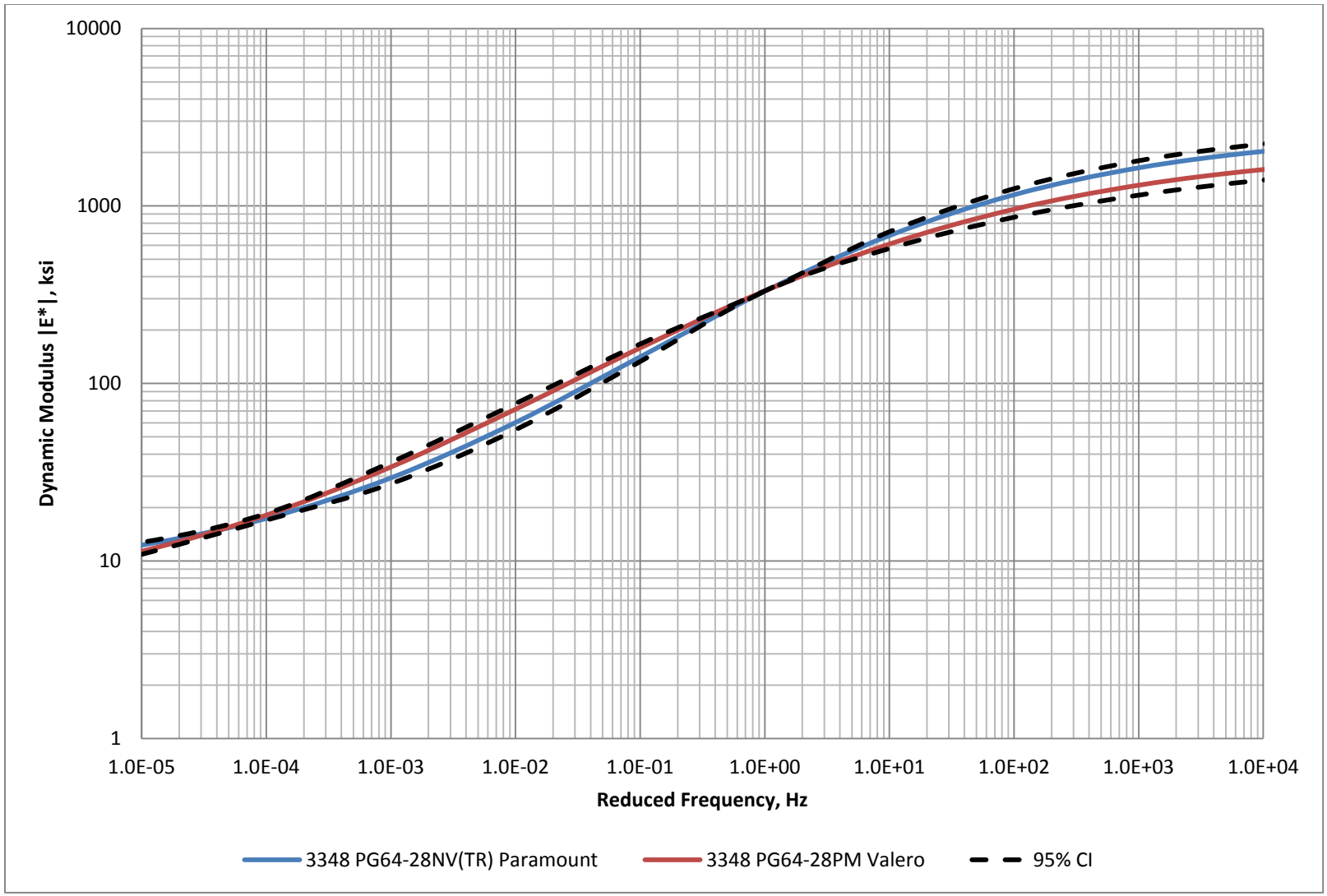

Figure 40. Dynamic Modulus Results for Aggregate Source PE 83-02 Mixtures at 70°F

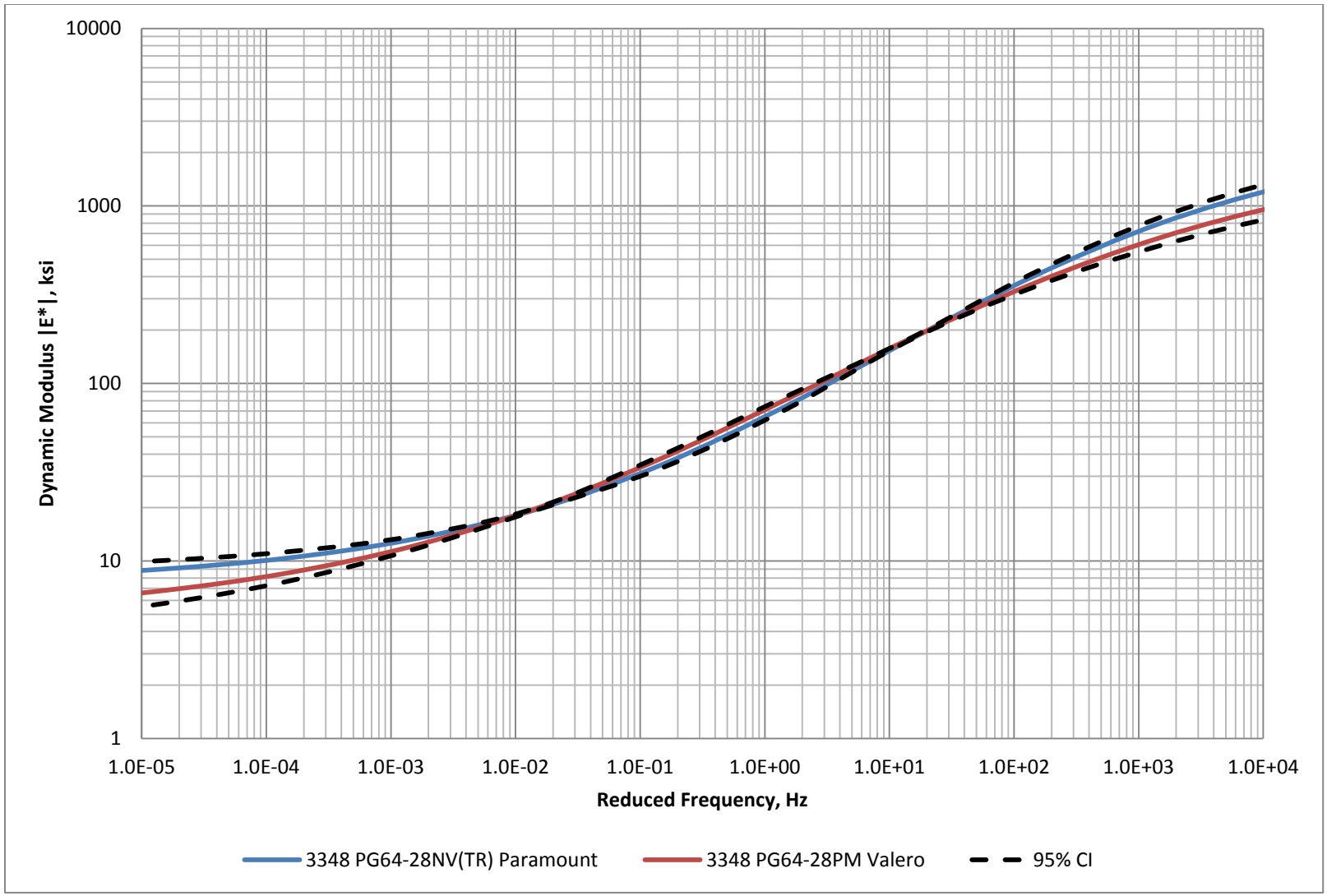

Figure 41. Dynamic Modulus Results for Aggregate Source PE 83-02 Mixtures at 104°F

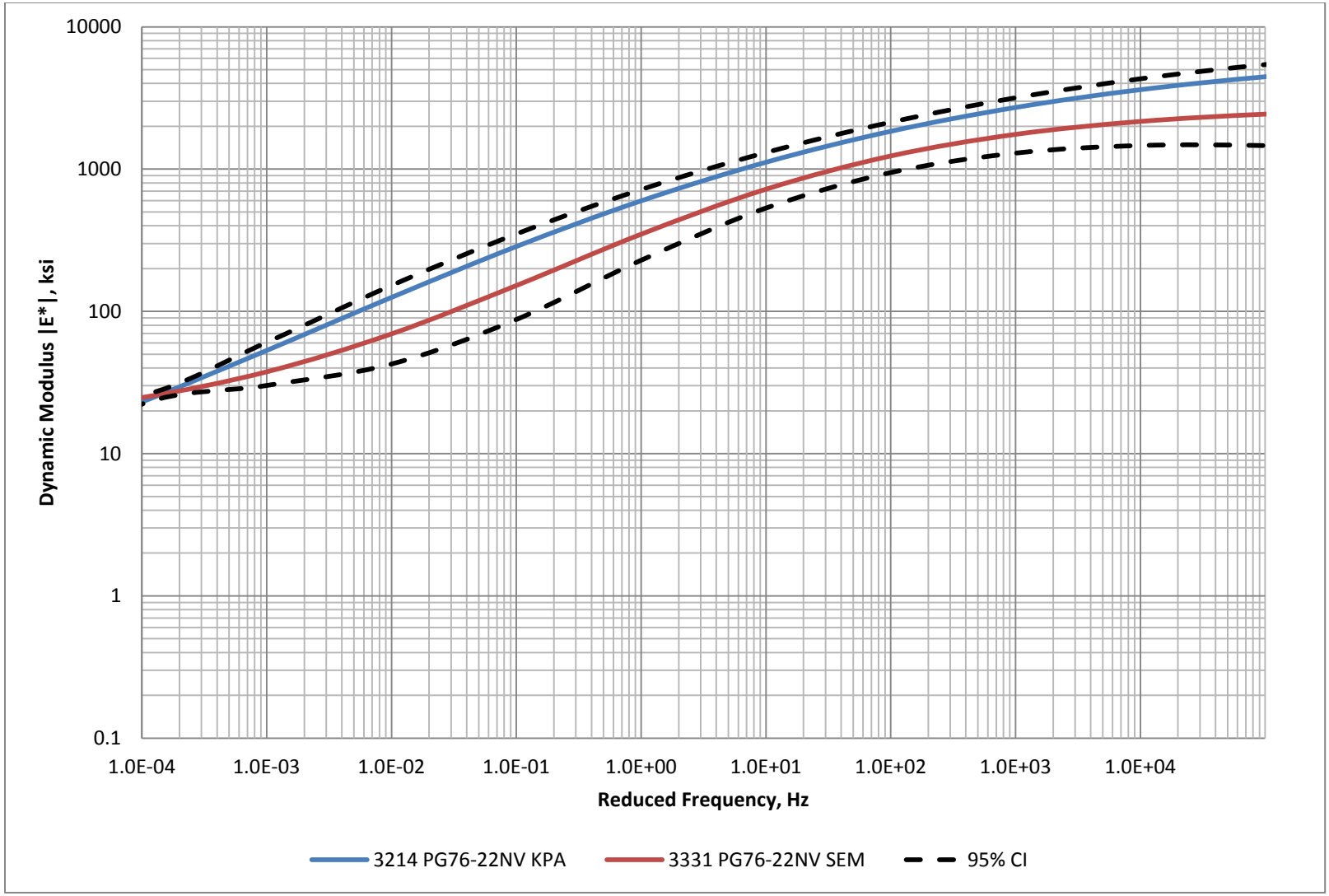

Figure 42. Dynamic Modulus Results for Aggregate Source Sloan Mixtures at 70°F

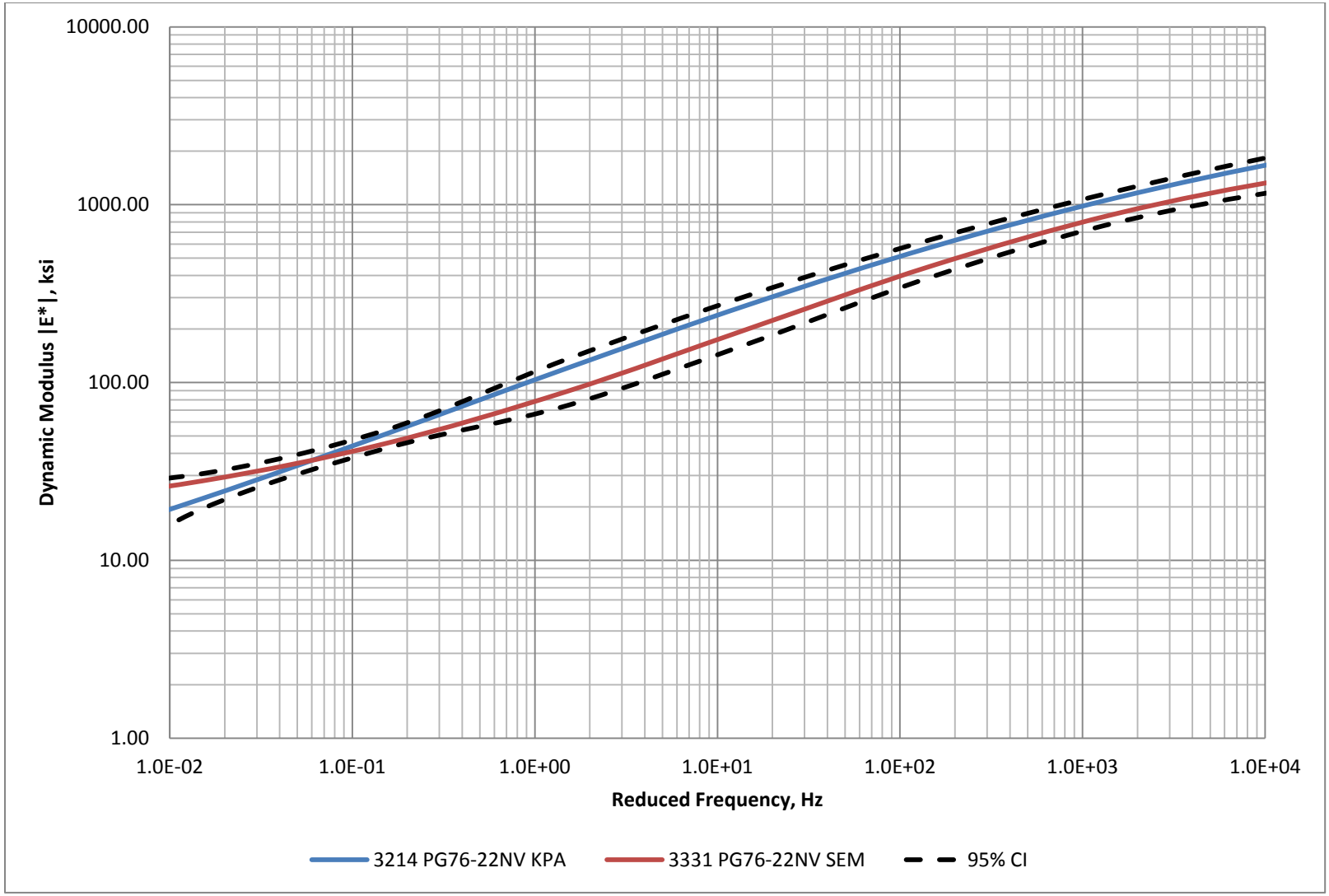

Figure 43. Dynamic Modulus Results for Aggregate Source Sloan Mixtures at 104°F

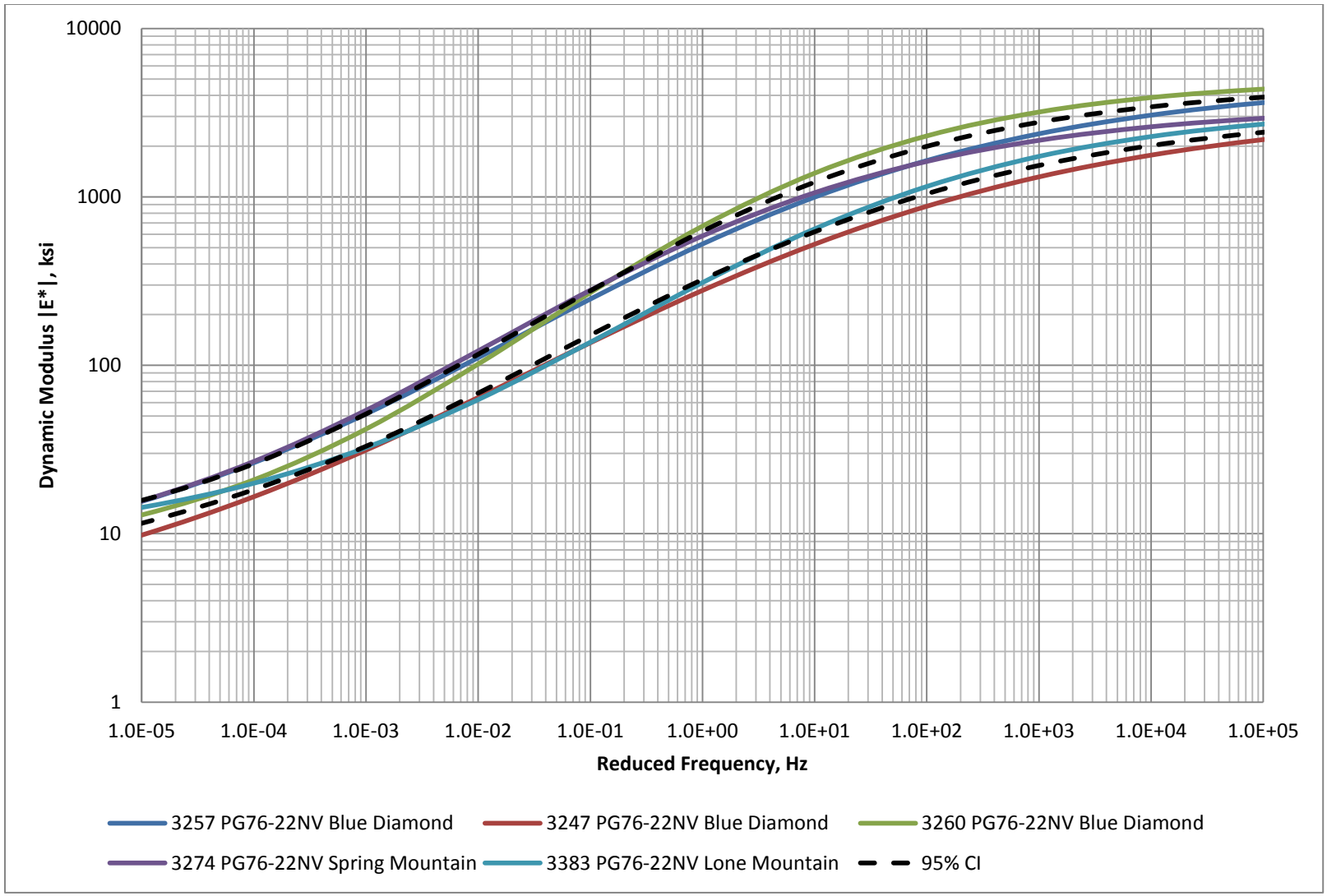

Figure 44. Dynamic Modulus Results for Binder Source Ergon Mixtures at 70°F

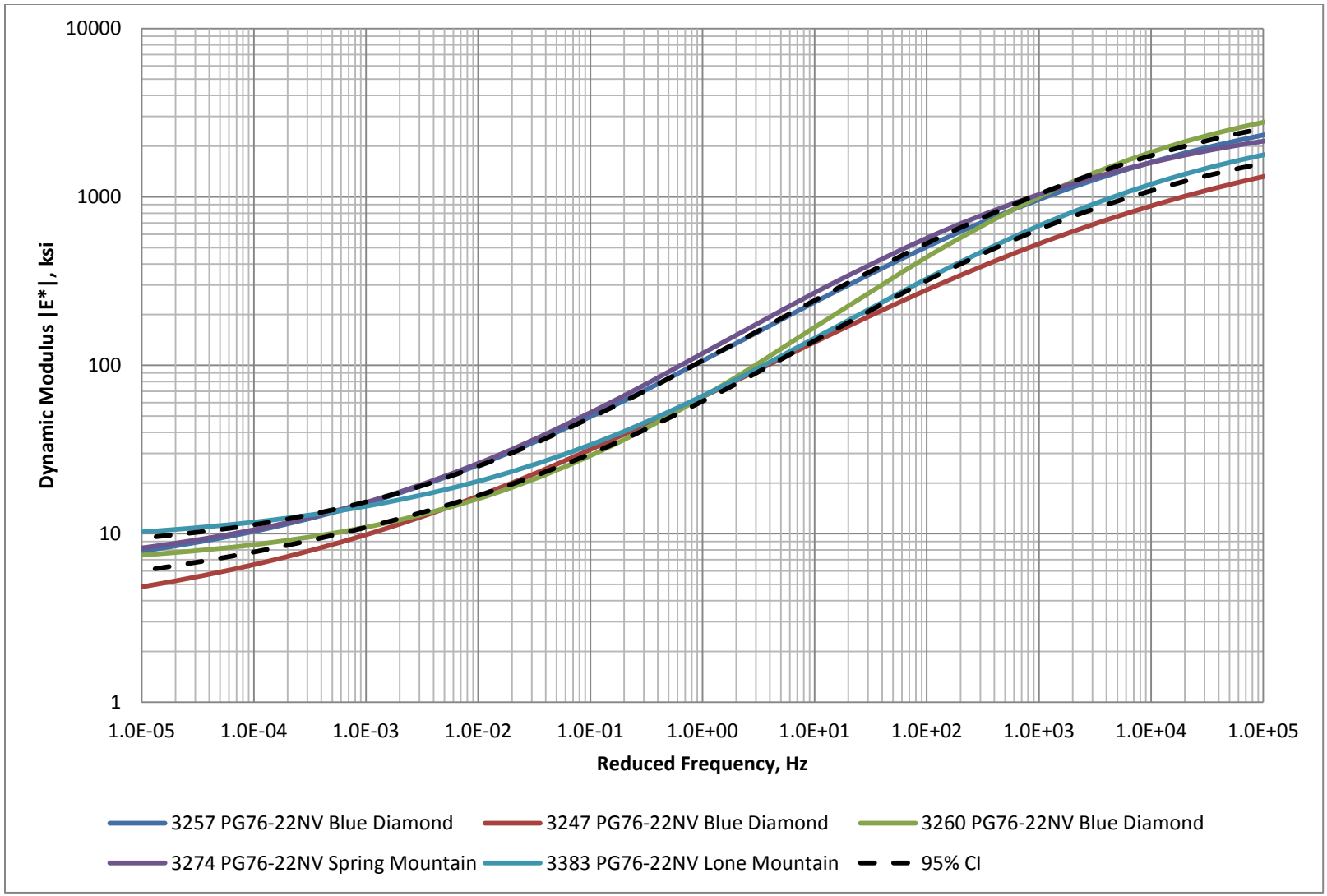

Figure 45. Dynamic Modulus Results for Binder Source Ergon Mixtures at 104°F

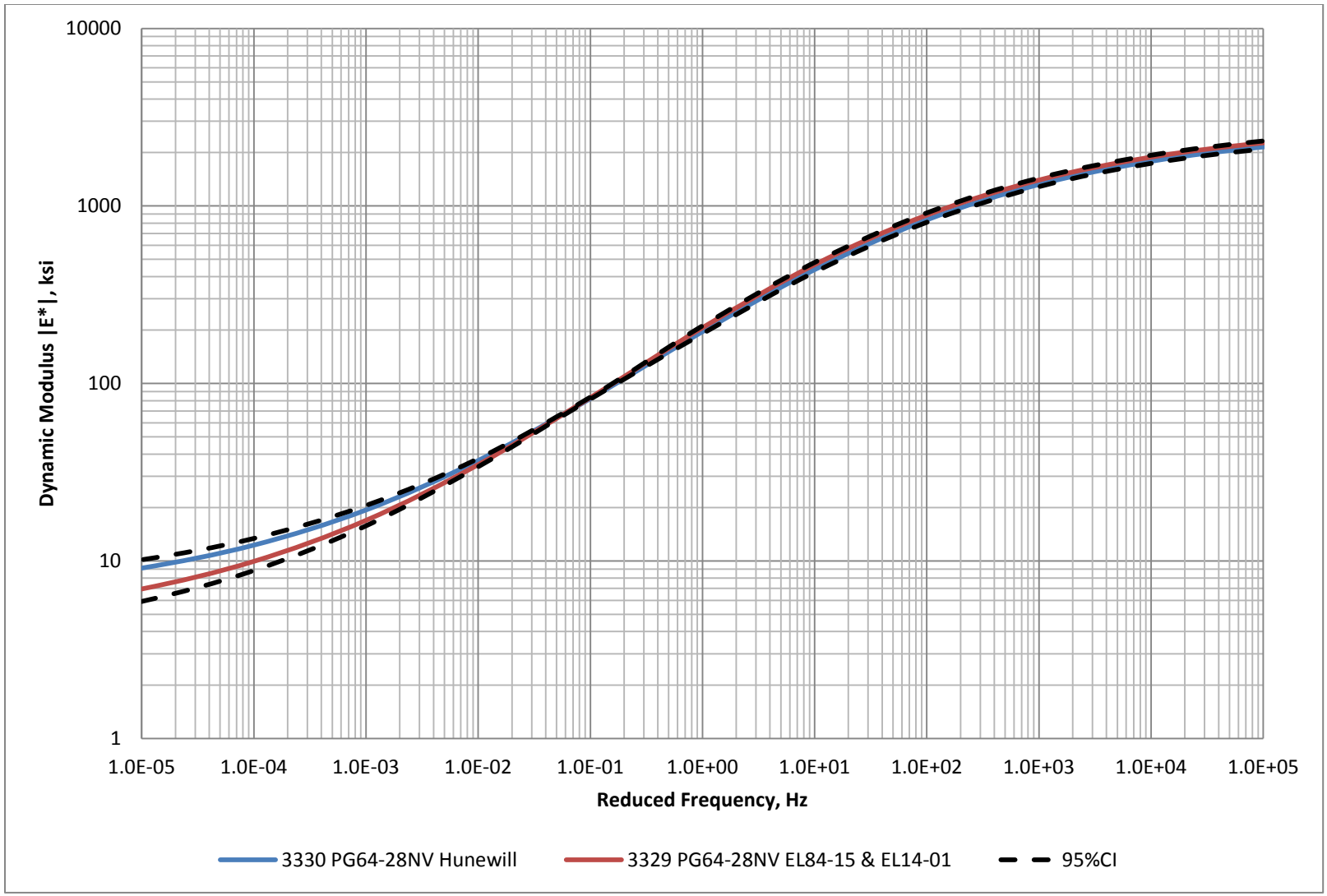

Figure 46. Dynamic Modulus Results for Binder Source Idaho Mixtures at 70°F

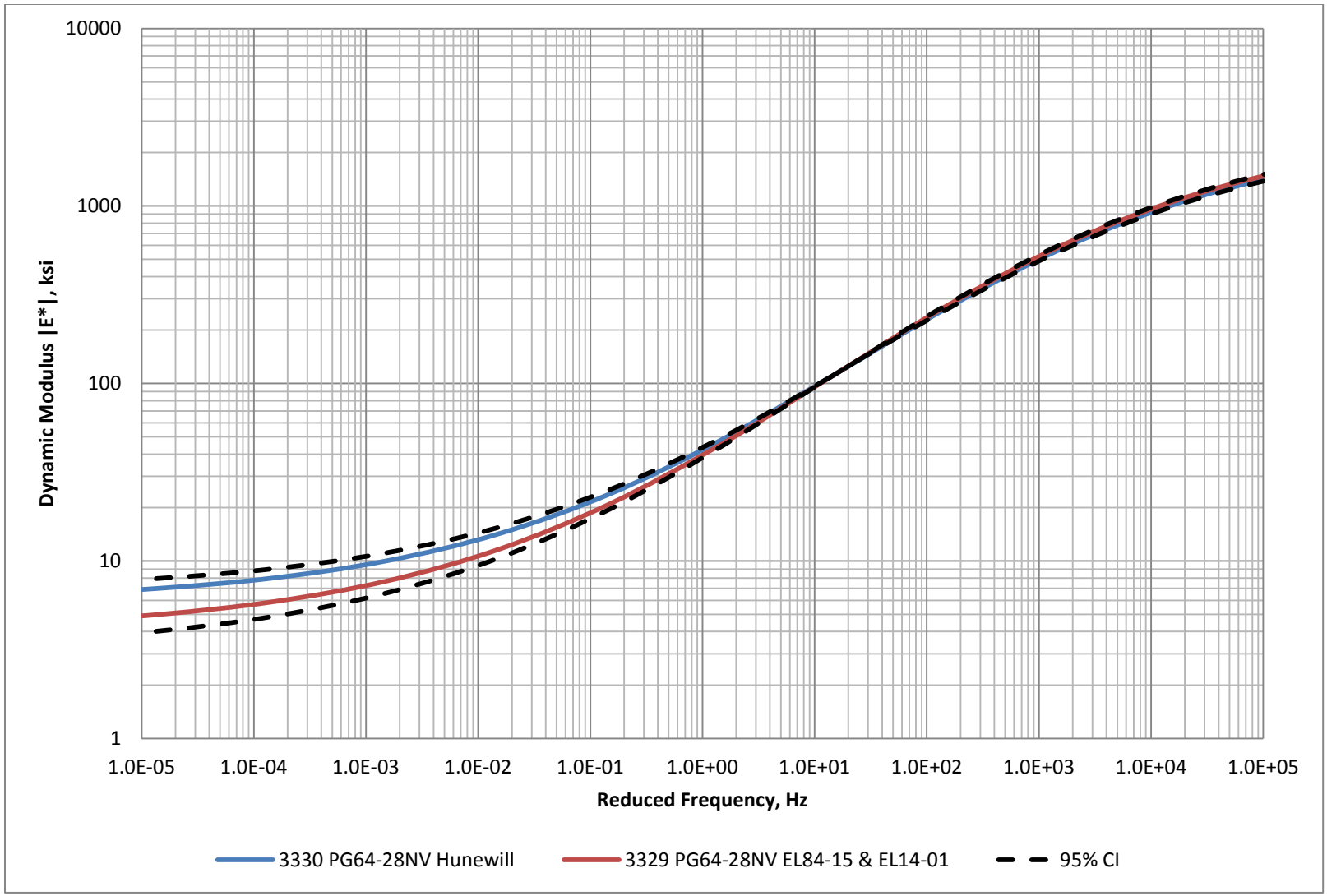

Figure 47. Dynamic Modulus Results for Binder Source Idaho Mixtures at 104°F

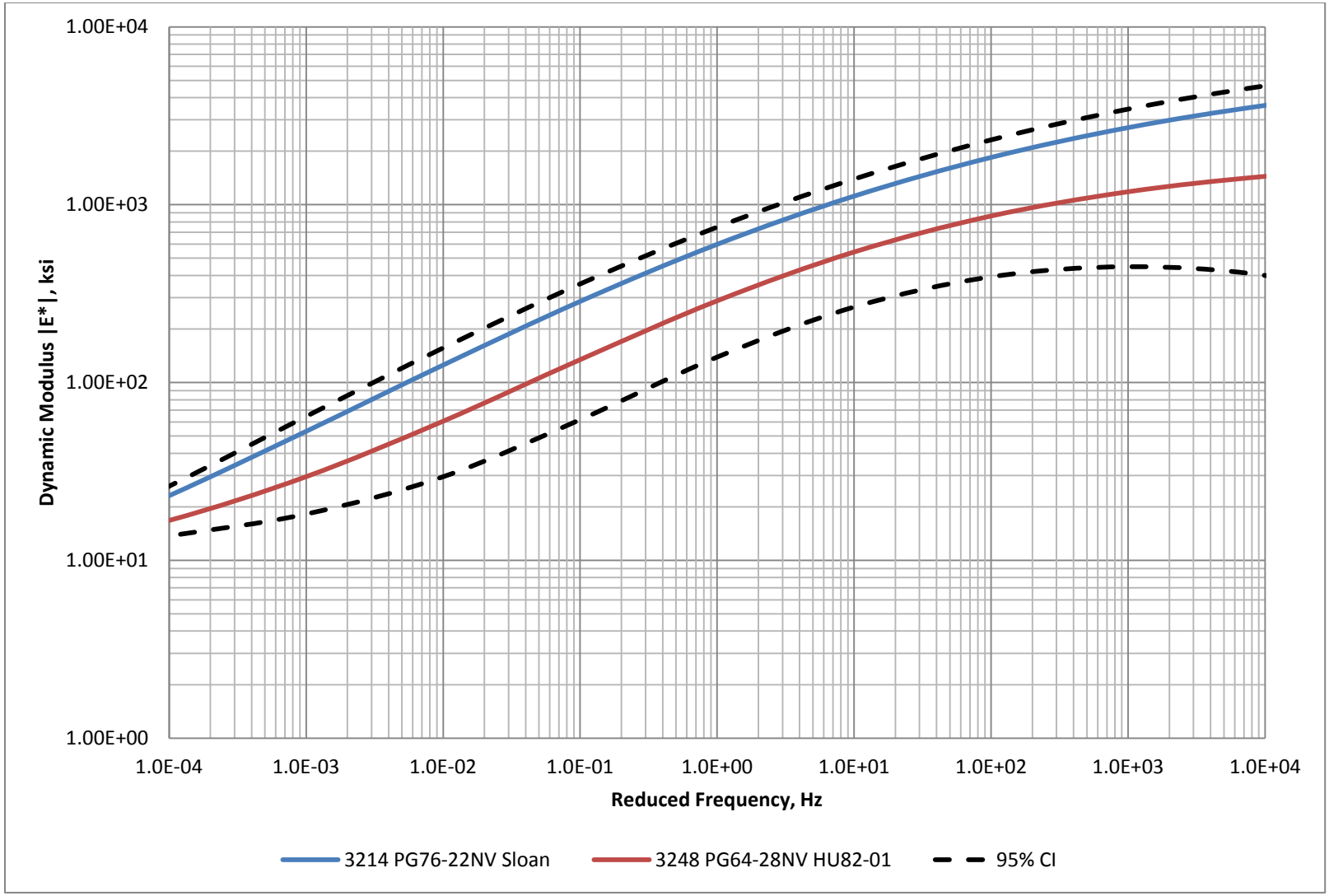

Figure 48. Dynamic Modulus Results for Binder Source KPA Mixtures at 70°F

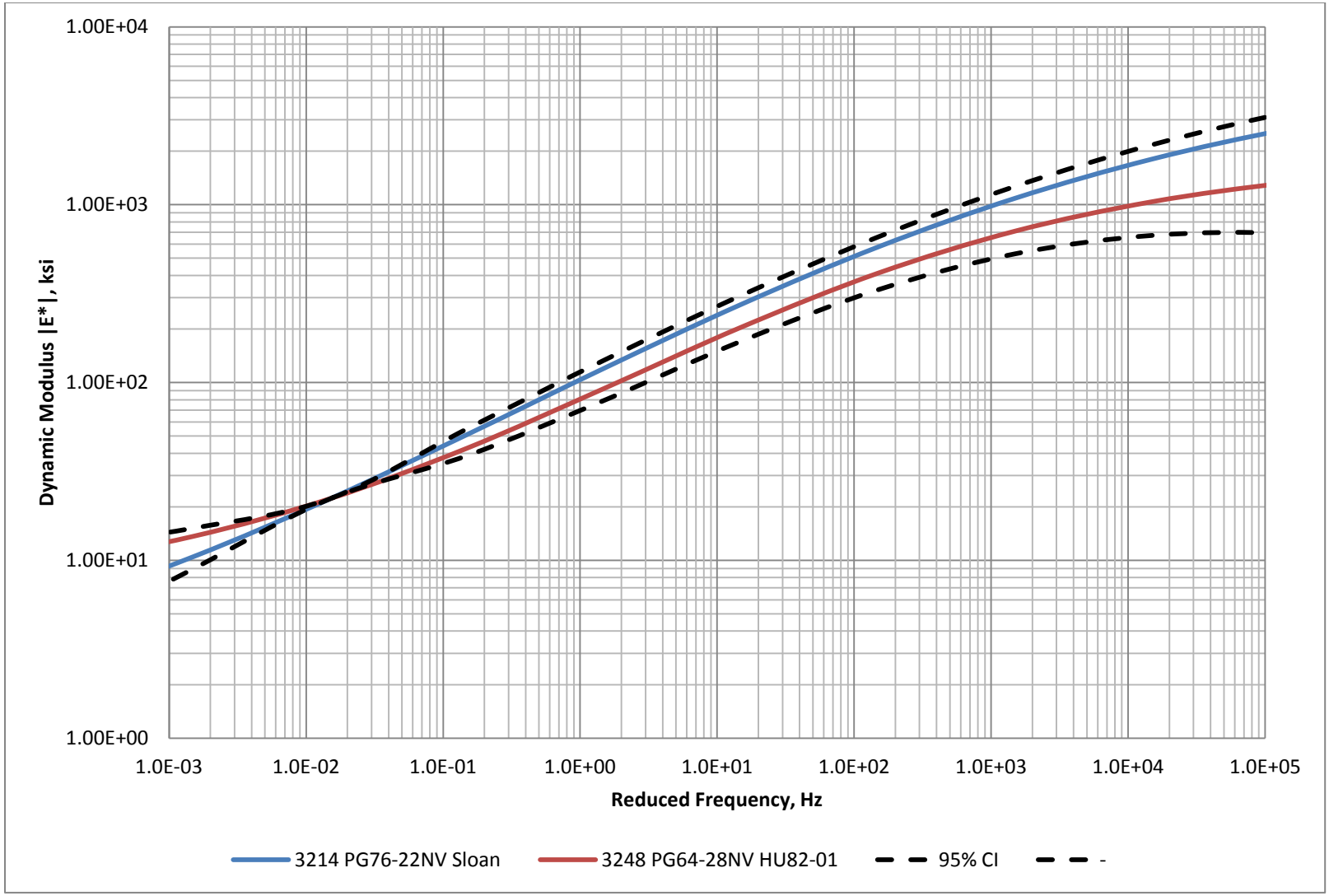

Figure 49. Dynamic Modulus Results for Binder Source KPA Mixtures at 104°F

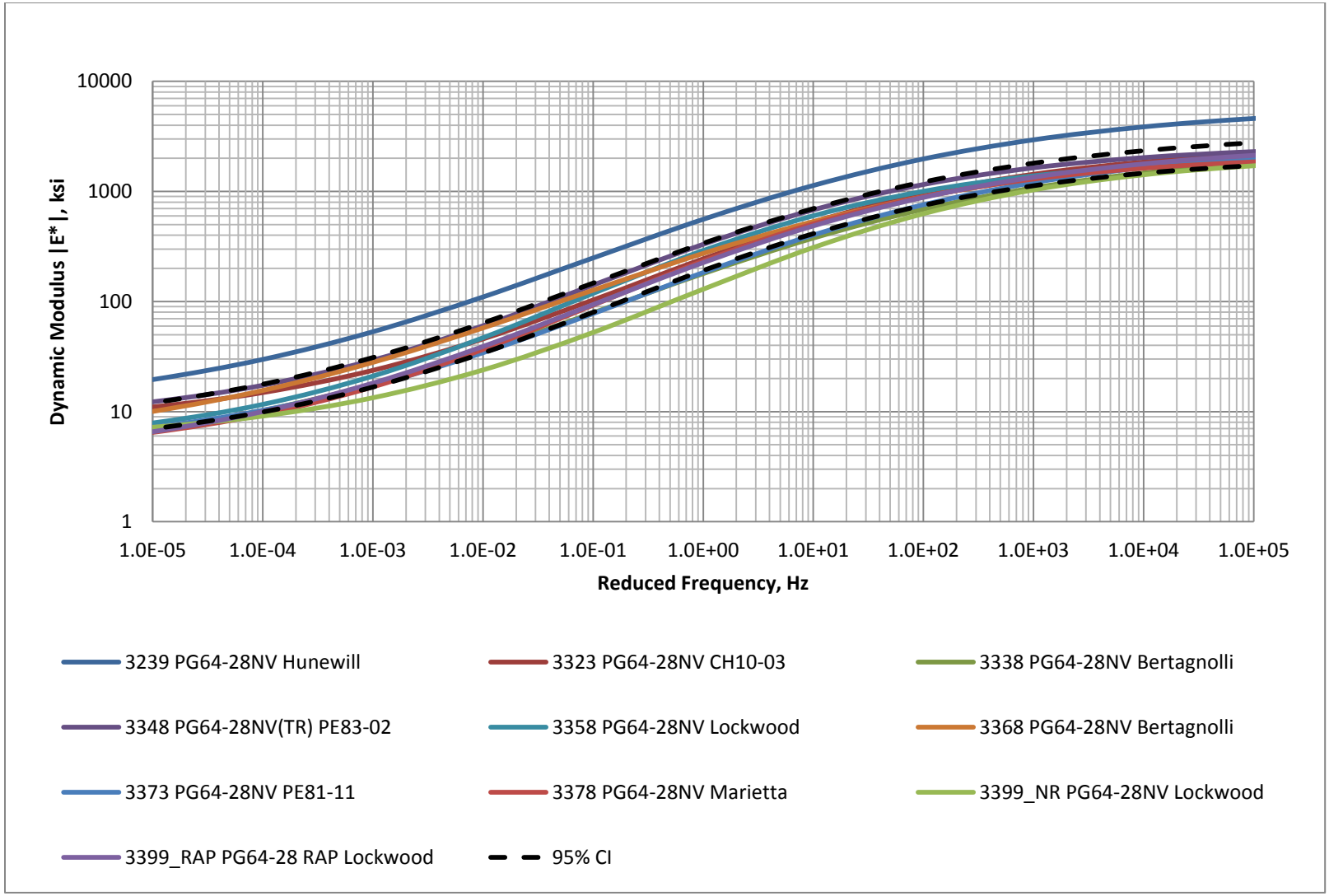

Figure 50. Dynamic Modulus Results for Binder Source Paramount Mixtures at 70°F

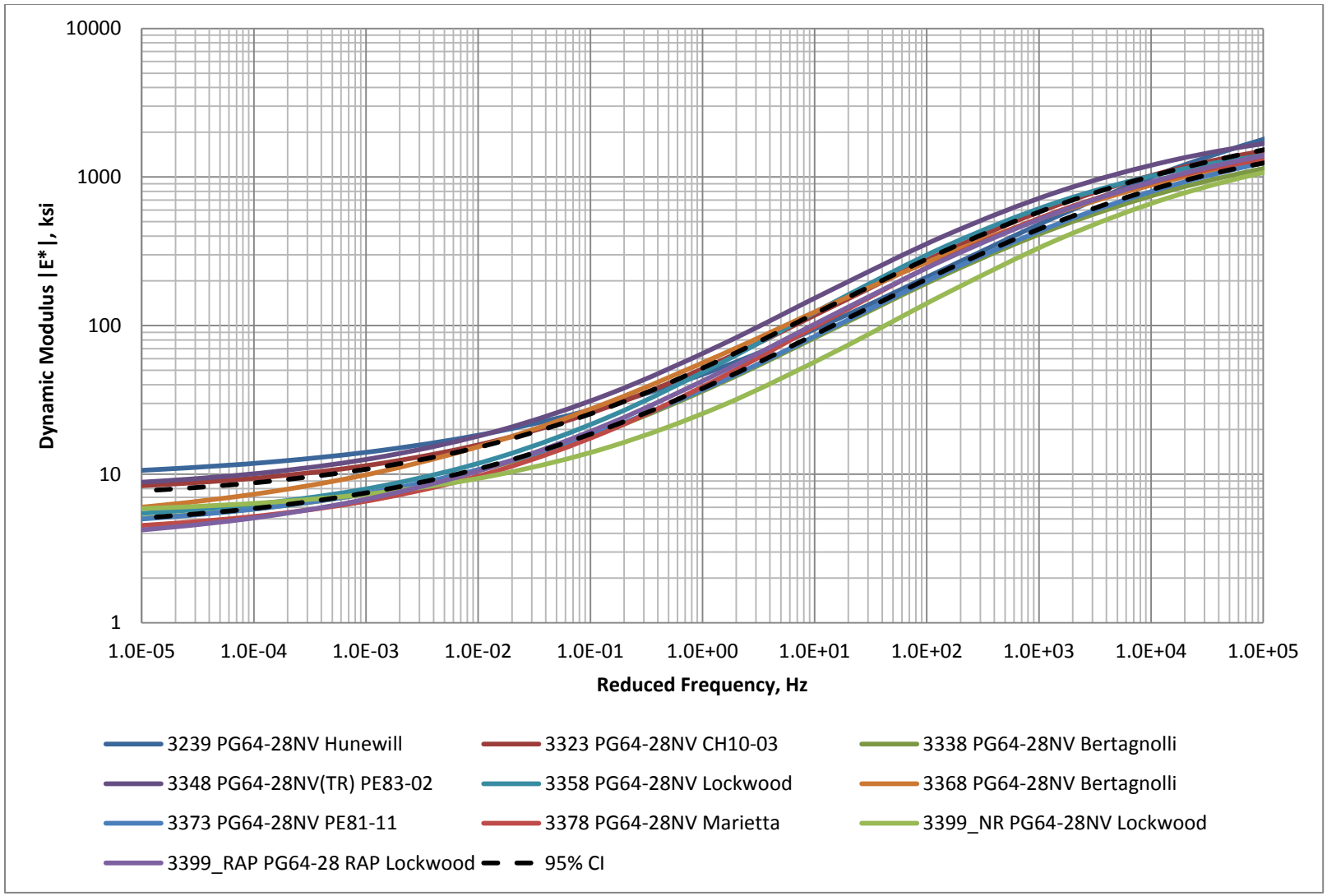

Figure 51. Dynamic Modulus Results for Binder Source Paramount Mixtures at 104°F

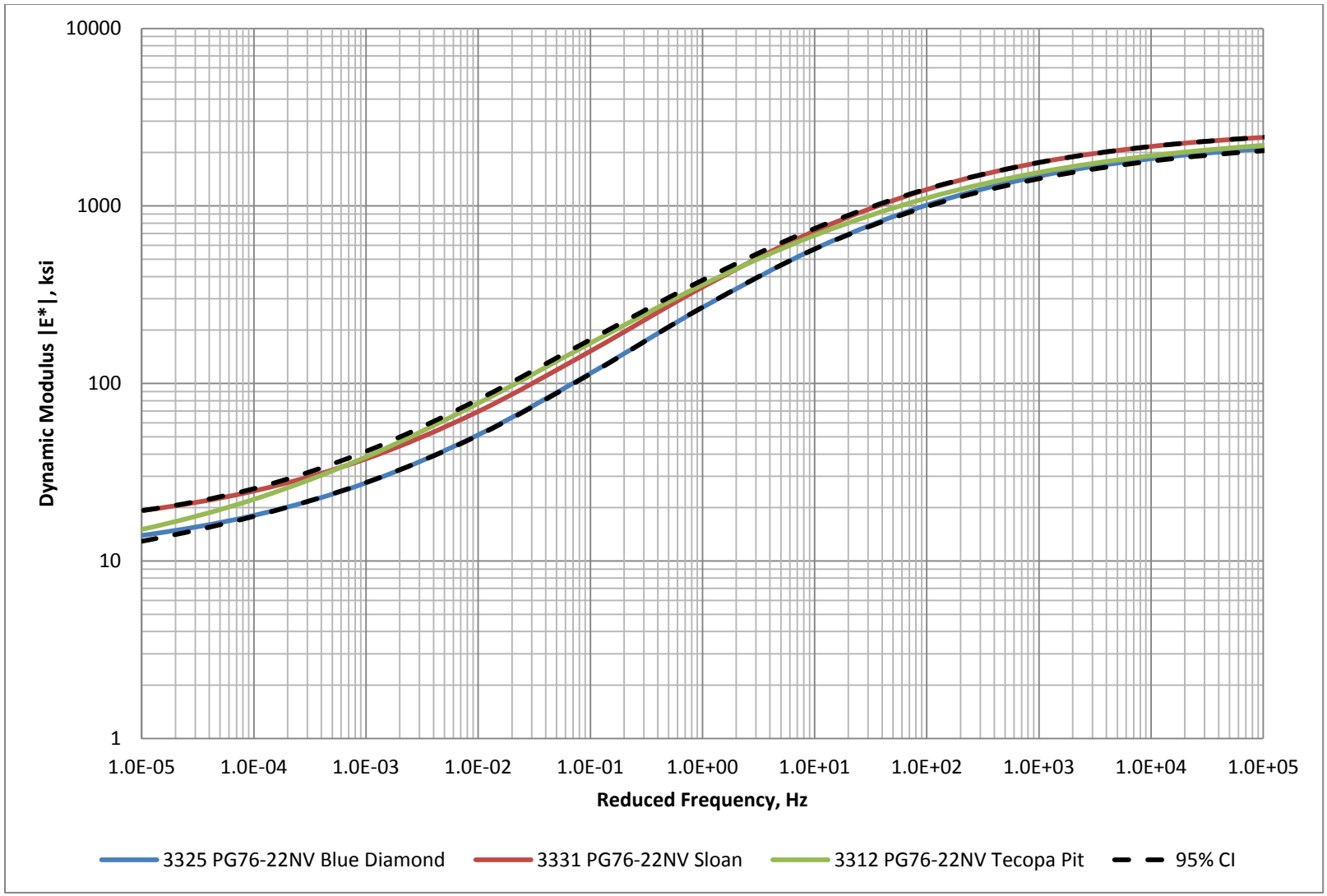

Figure 52. Dynamic Modulus Results for Binder Source SEM Mixtures at 70°F

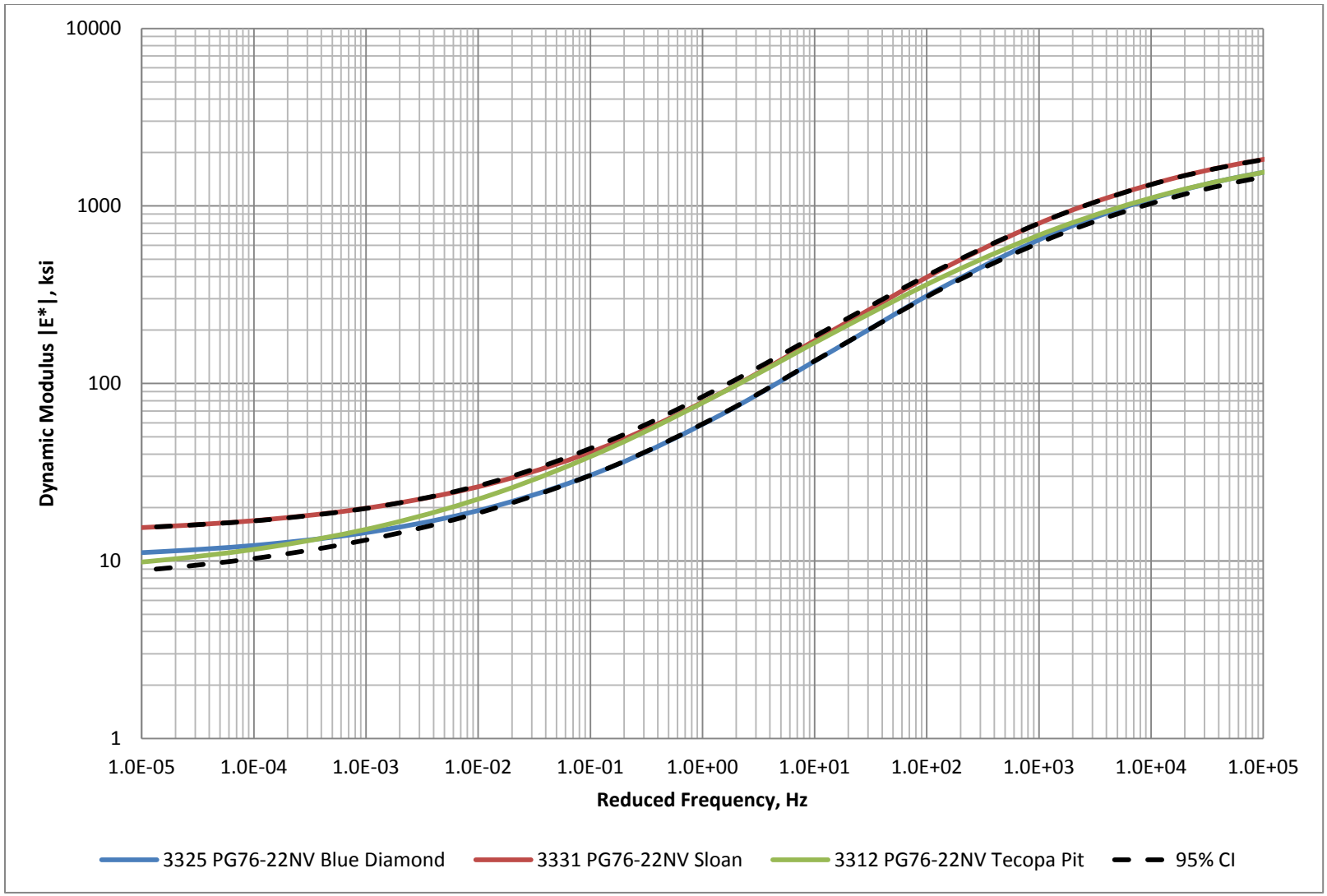

Figure 53. Dynamic Modulus Results for Binder Source SEM Mixtures at 104°F

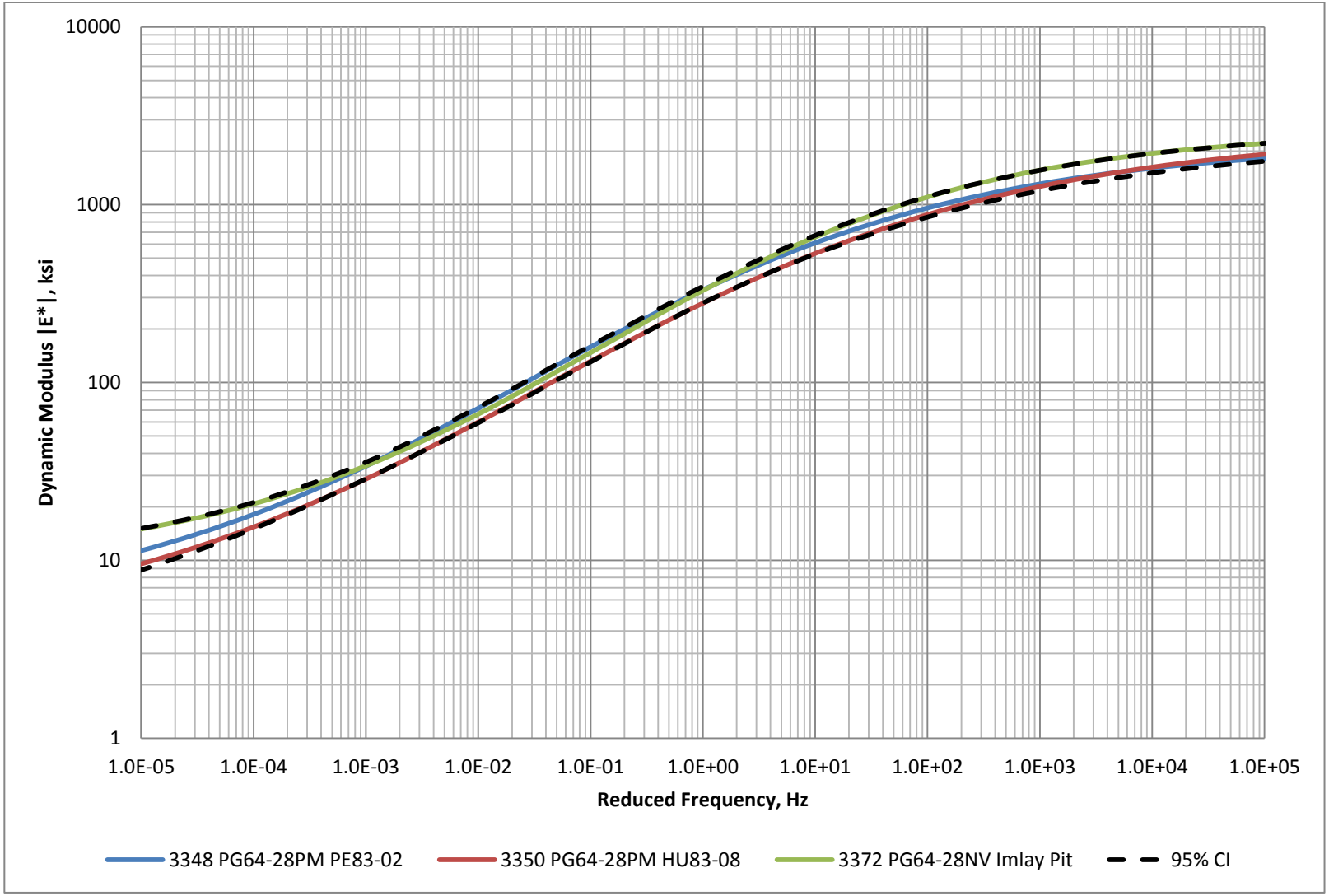

Figure 54. Dynamic Modulus Results for Binder Source Valero Mixtures at 70°F

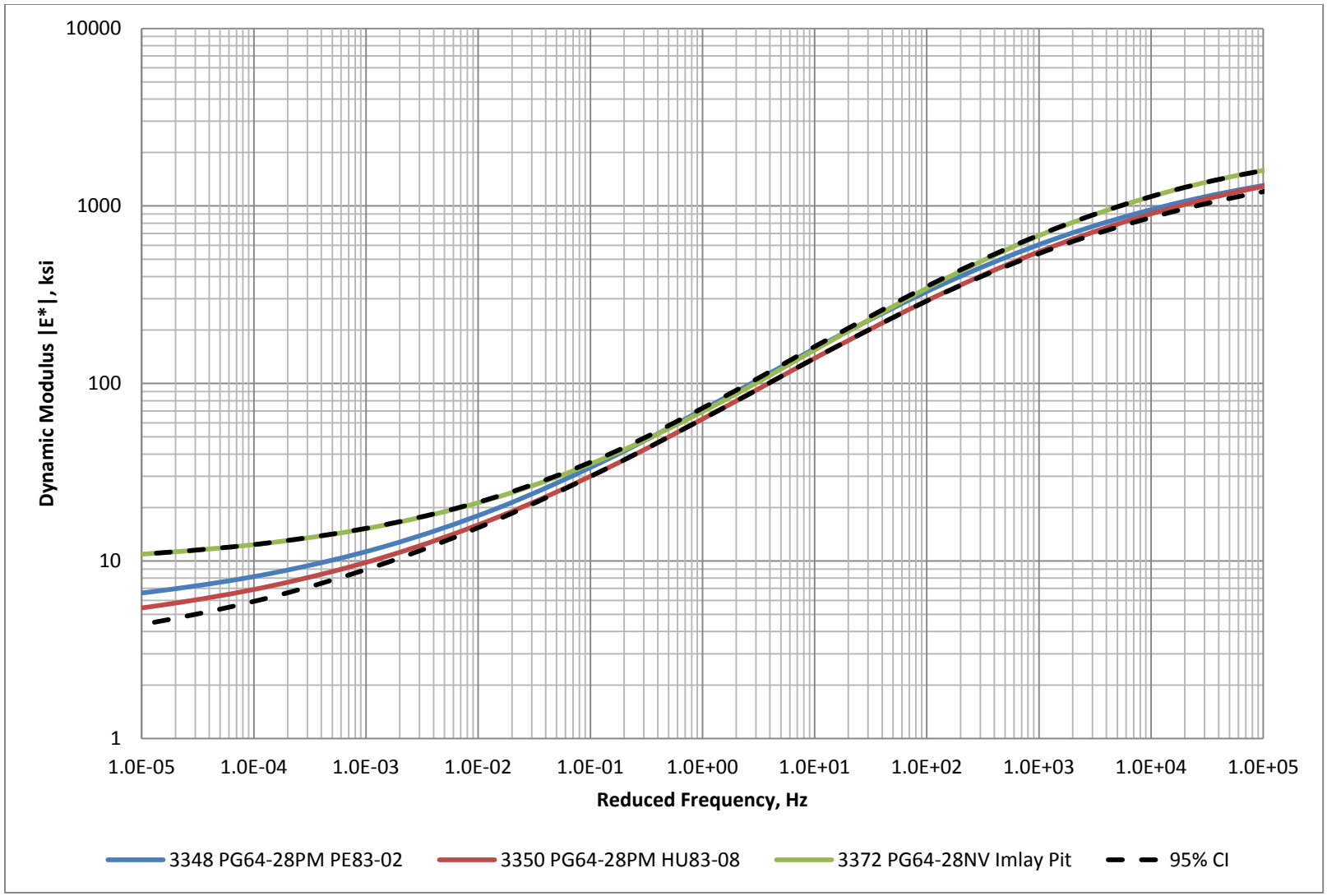

Figure 55. Dynamic Modulus Results for Binder Source Valero Mixtures at 104°F

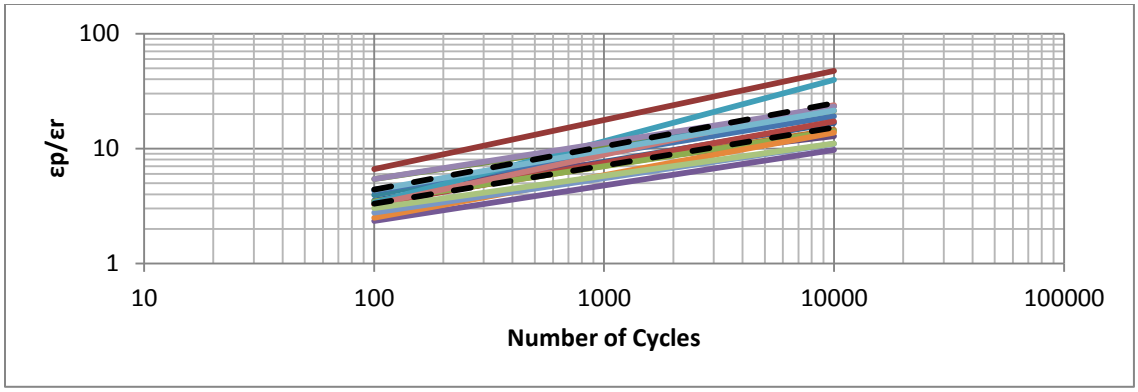

(a)

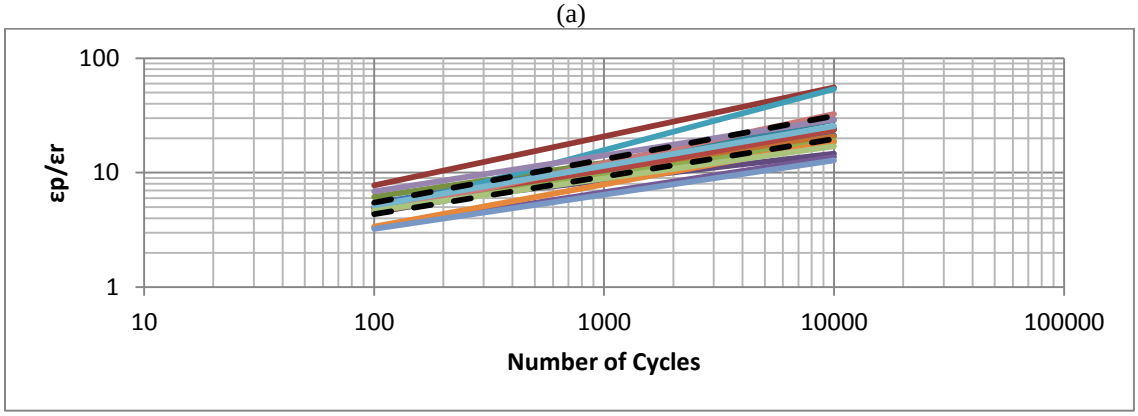

(b)

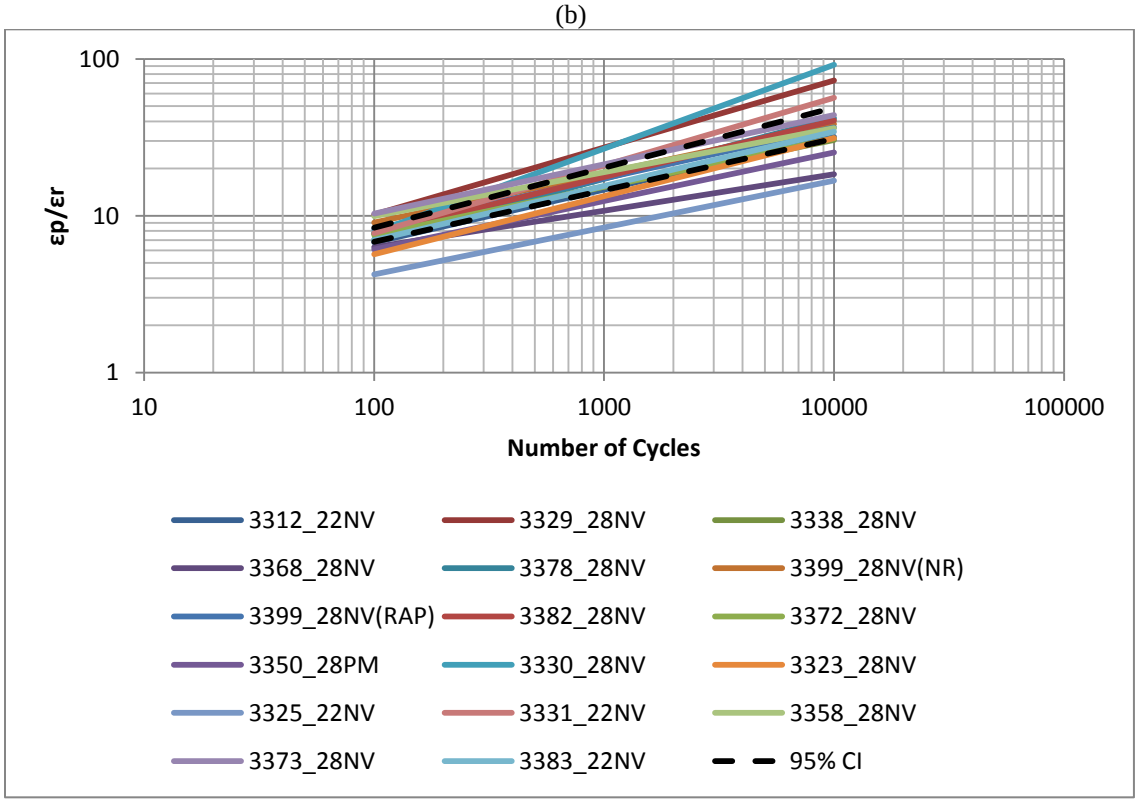

(c)

Figure 56. Rutting Results for all Sampled Nevada Mixtures (a)104°F (b) 114.8°F (c) 136.4°F

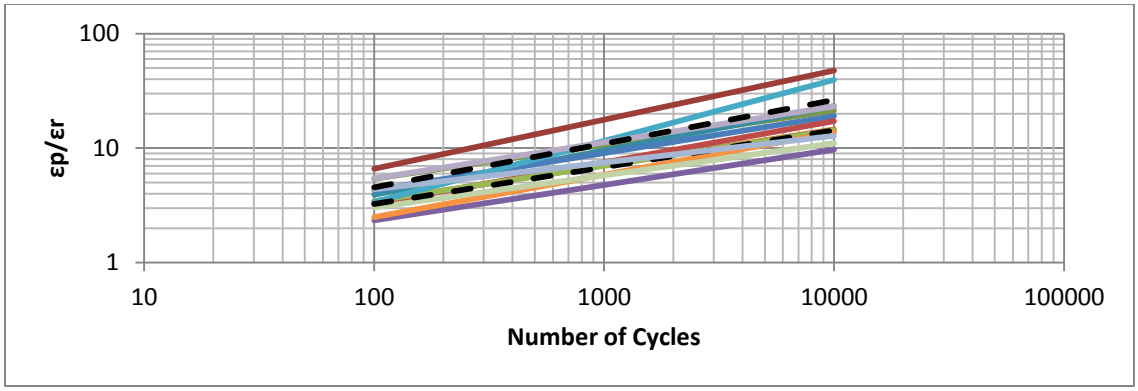

(a)

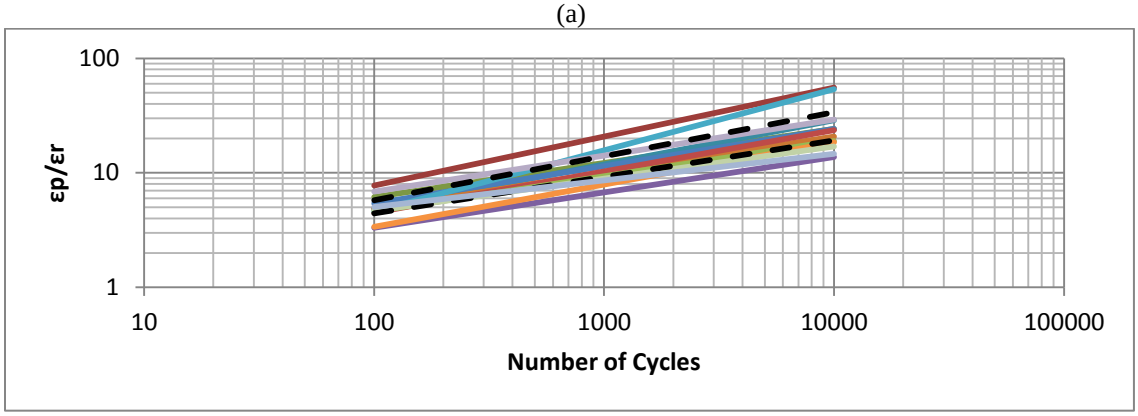

(b)

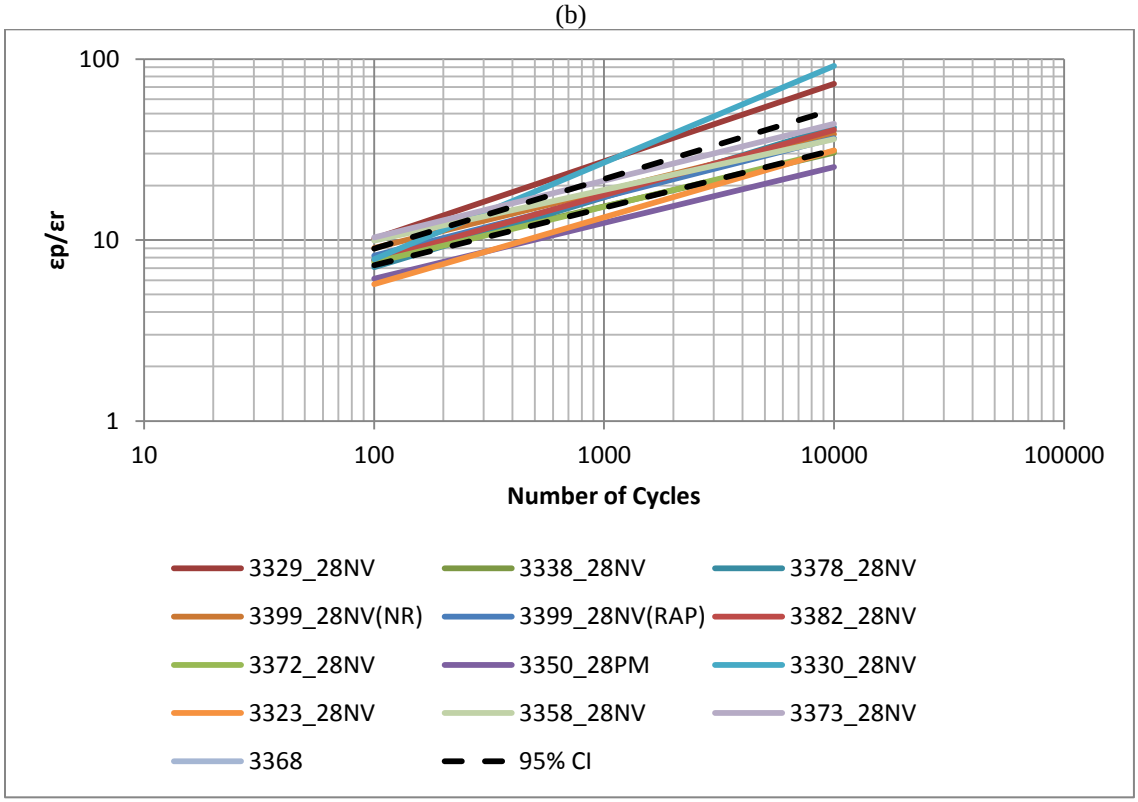

(c)

Figure 57. Rutting Results for all PG64-28NV Mixtures (a)104°F (b) 114.8°F (c) 136.4°F

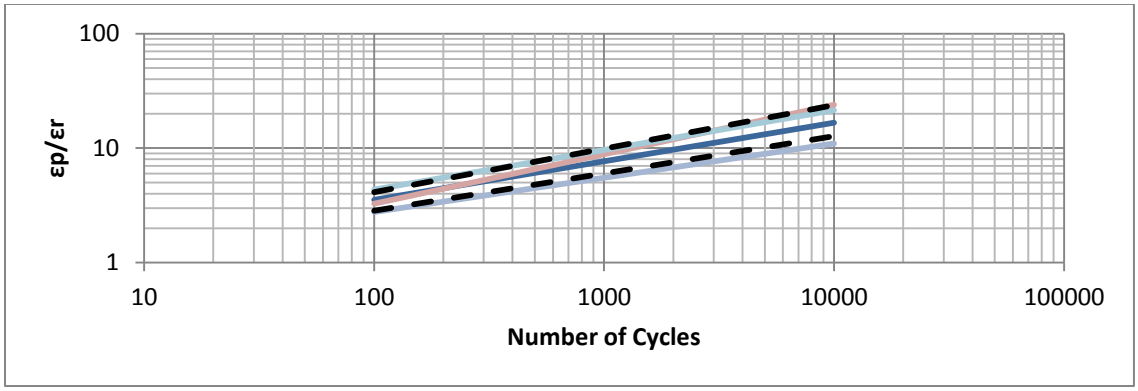

(a)

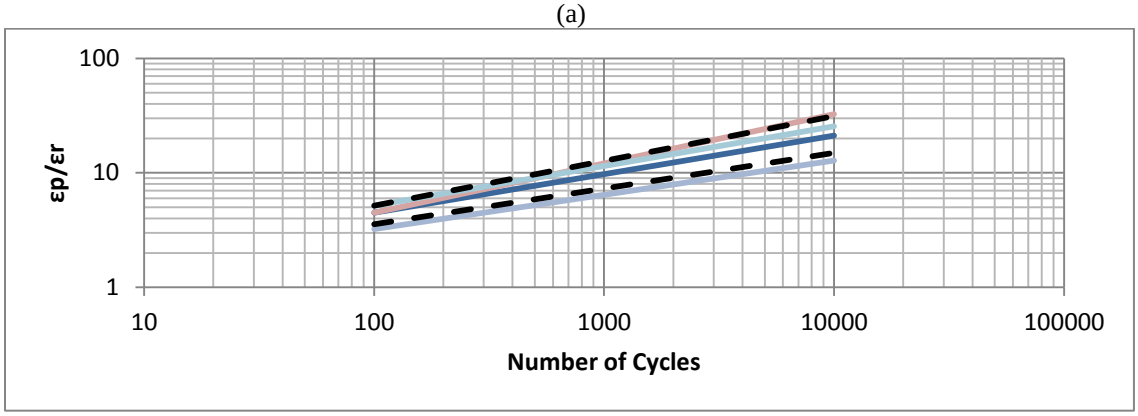

(b)

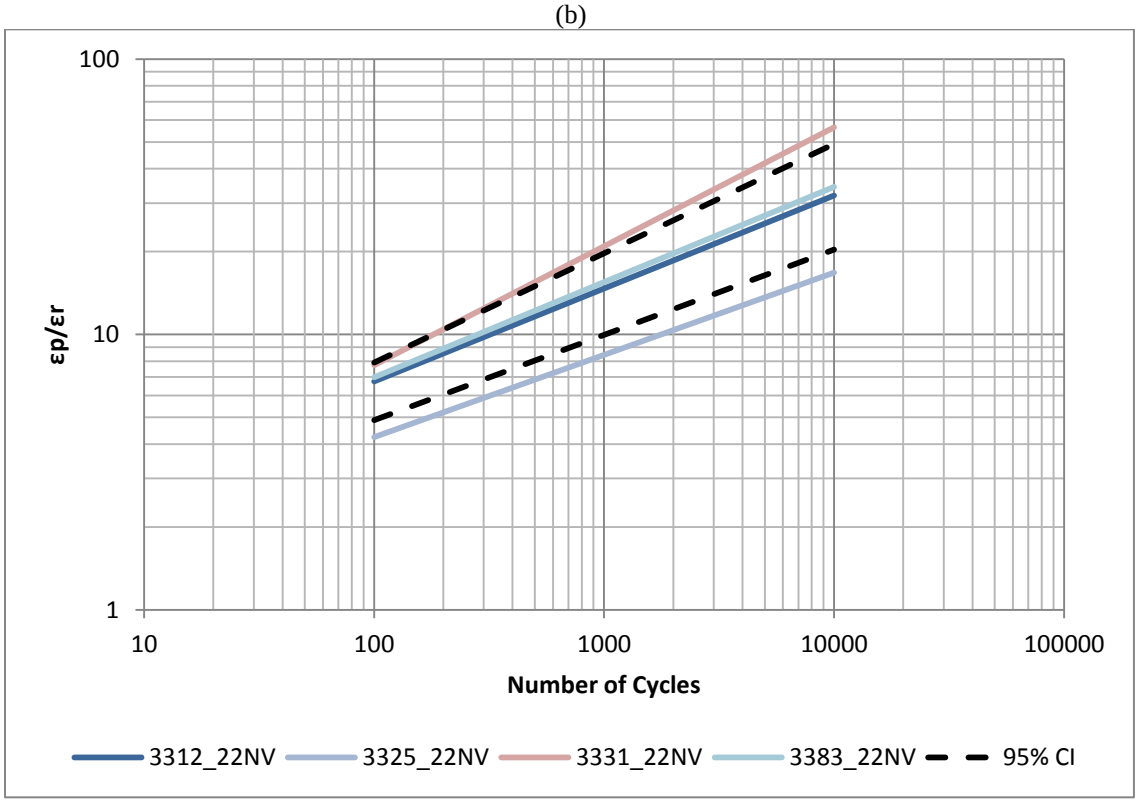

(c)

Figure 58. Rutting Results for all PG76-22NV Mixtures (a)104°F (b) 114.8°F (c) 136.4°F

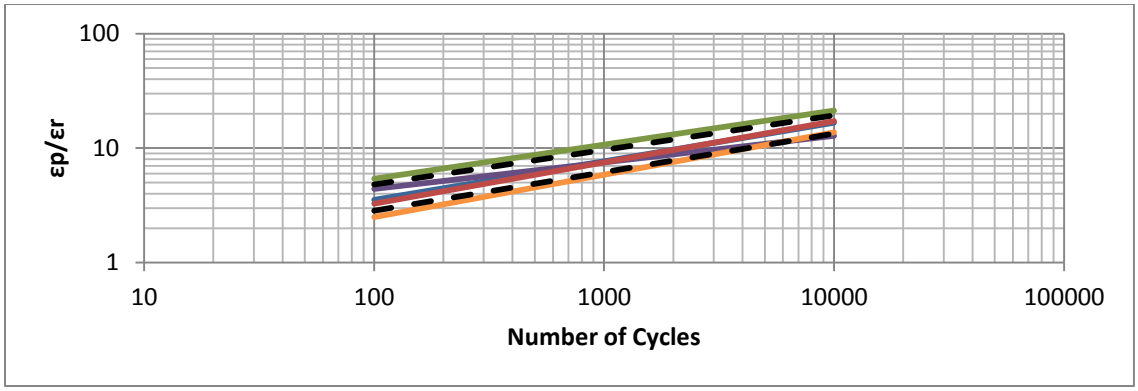

(a)

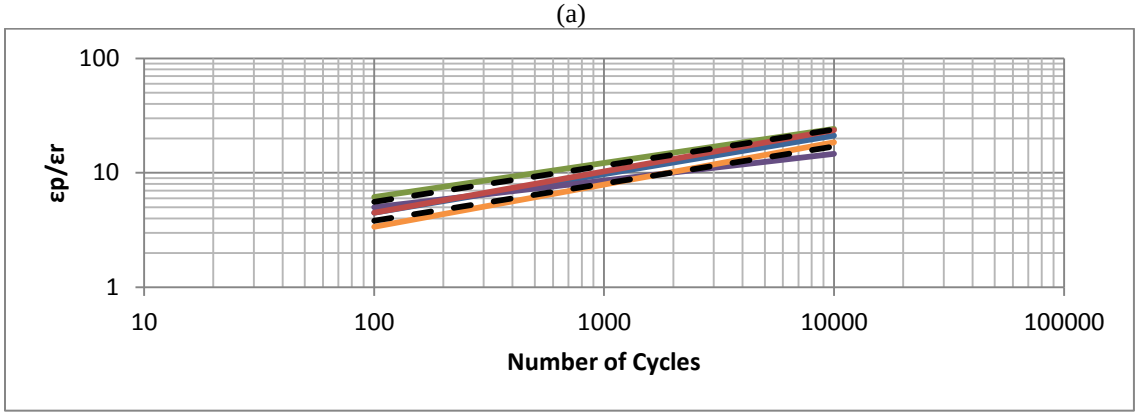

(b)

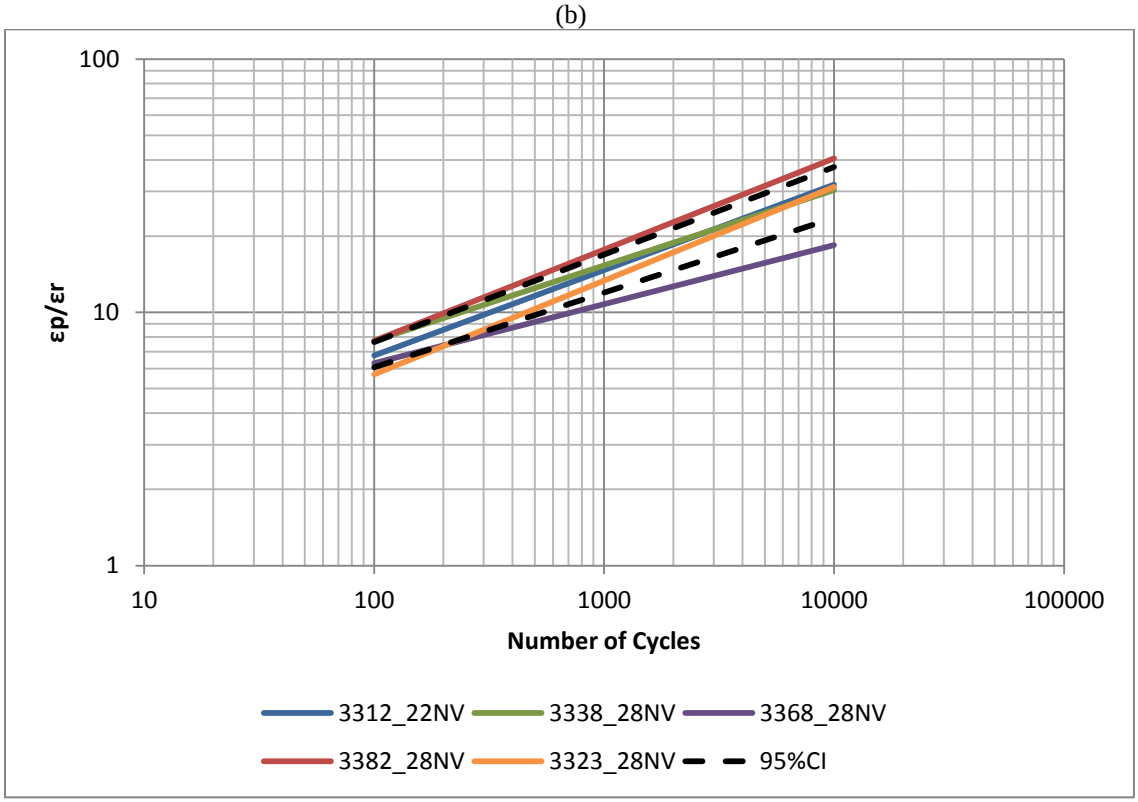

(c)

Figure 59. Rutting Results for all Type 2 Mixtures (a)104°F (b) 114.8°F (c) 136.4°F

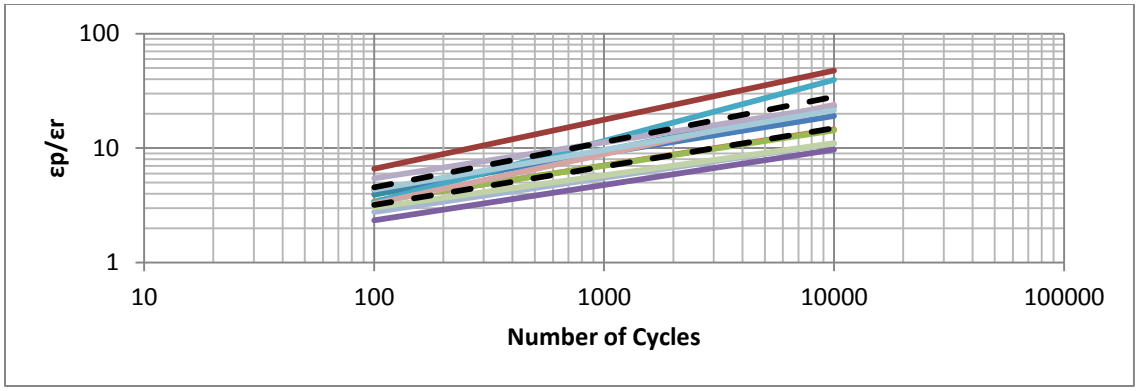

(a)

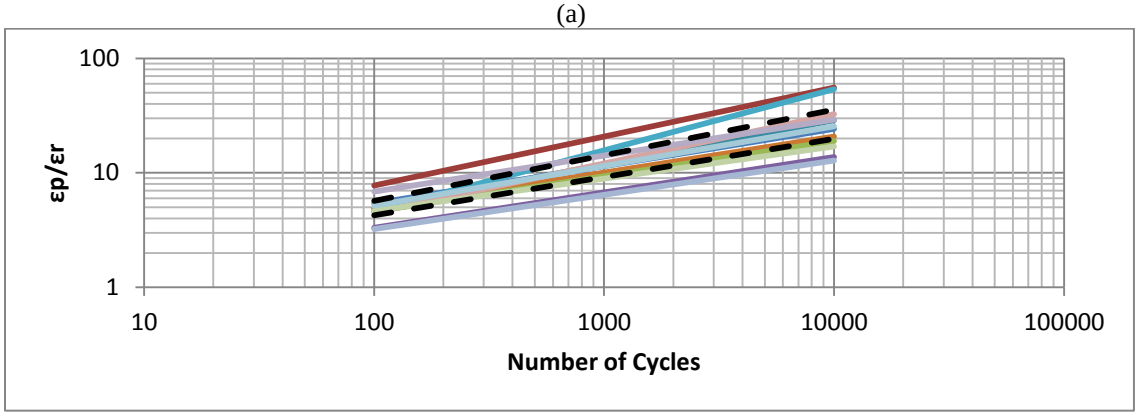

(b)

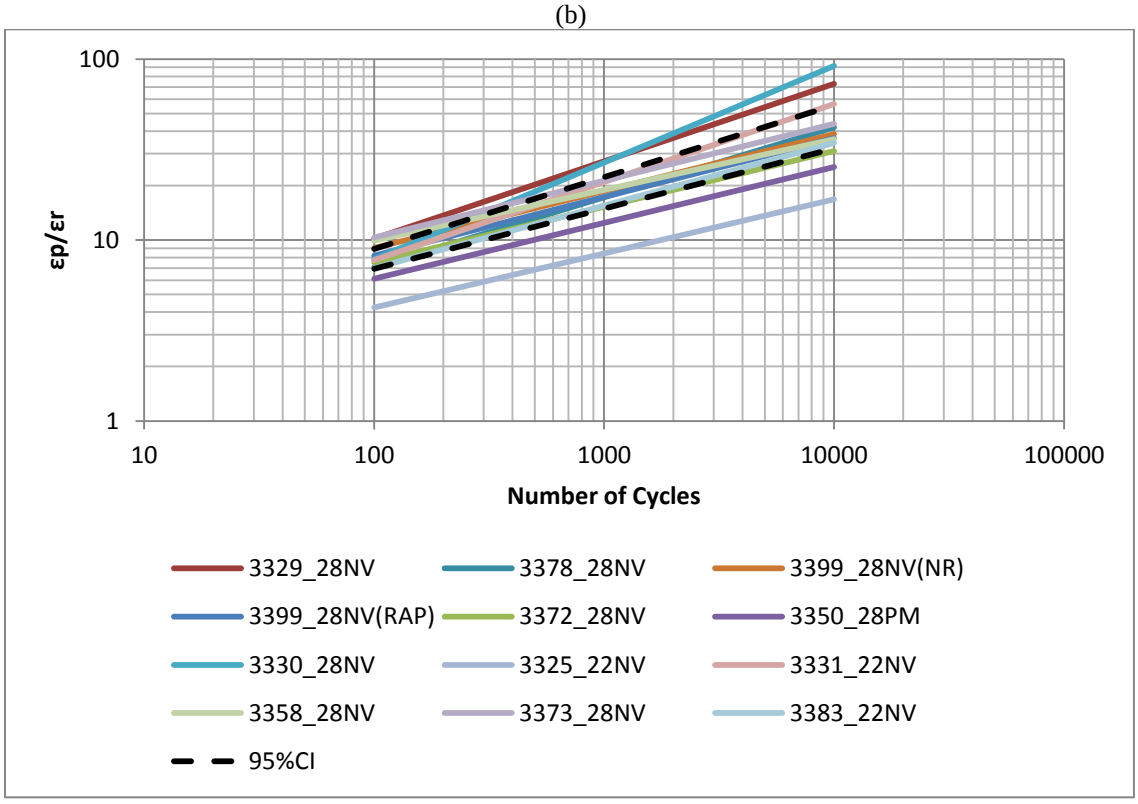

(c)

Figure 60. Rutting Results for all Type 2C Mixtures (a)104°F (b) 114.8°F (c) 136.4°F

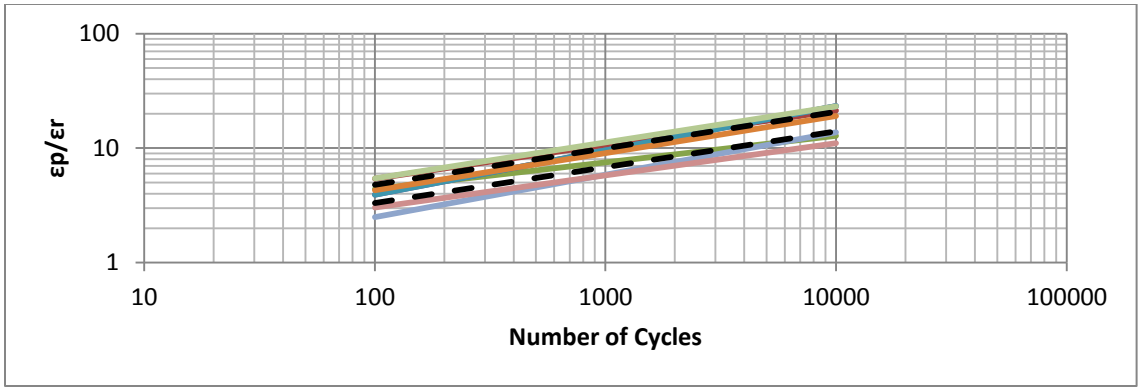

(a)

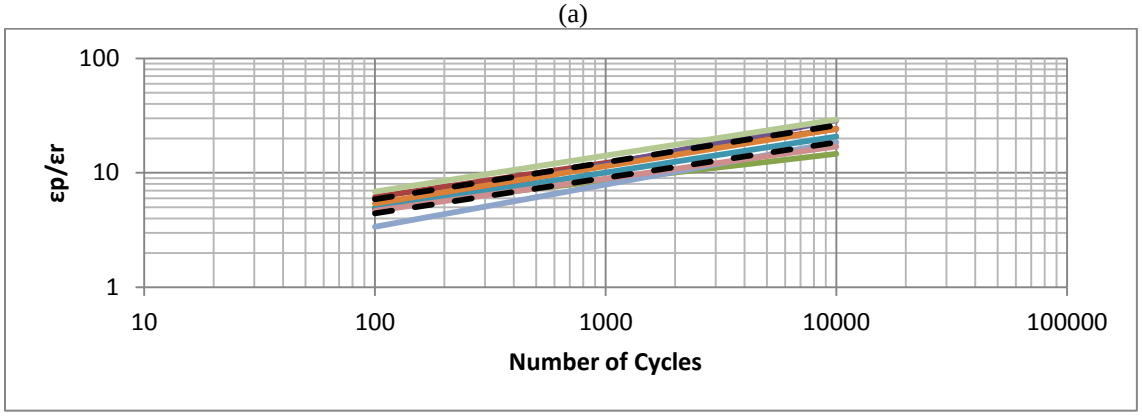

(b)

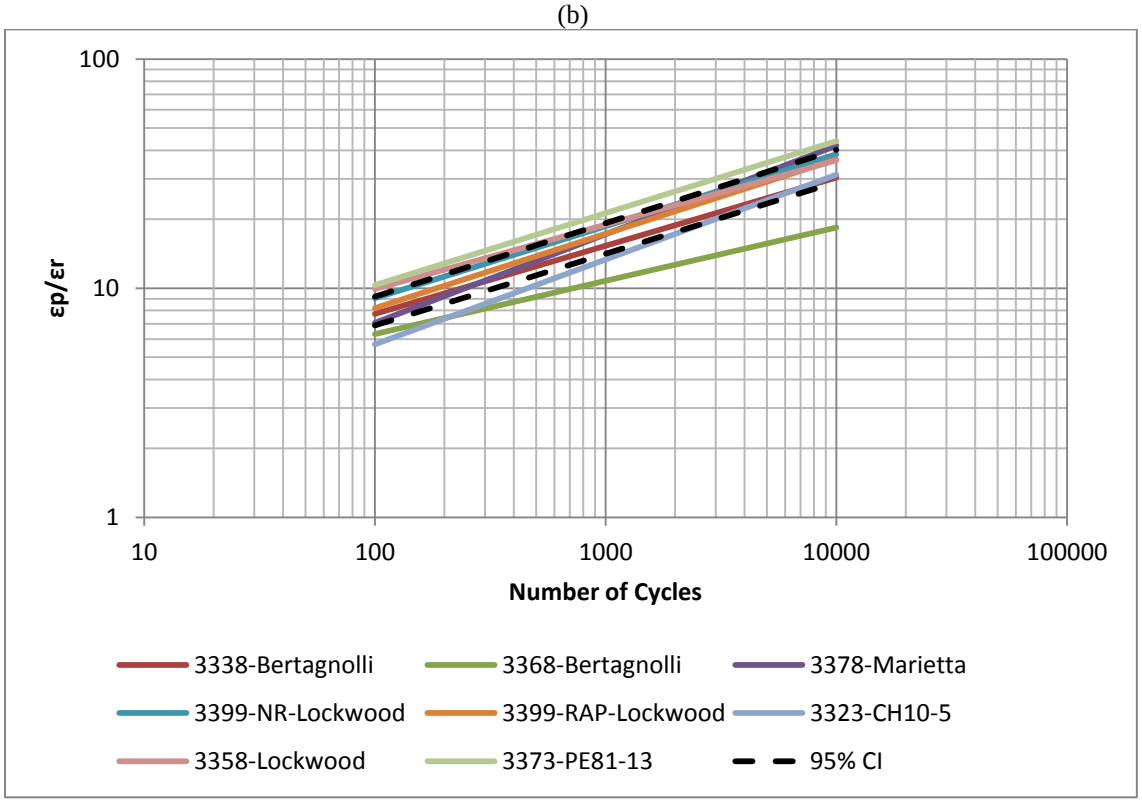

(c)

Figure 61. Rutting Results for District 2 Mixtures (a)104°F (b) 114.8°F (c) 136.4°F

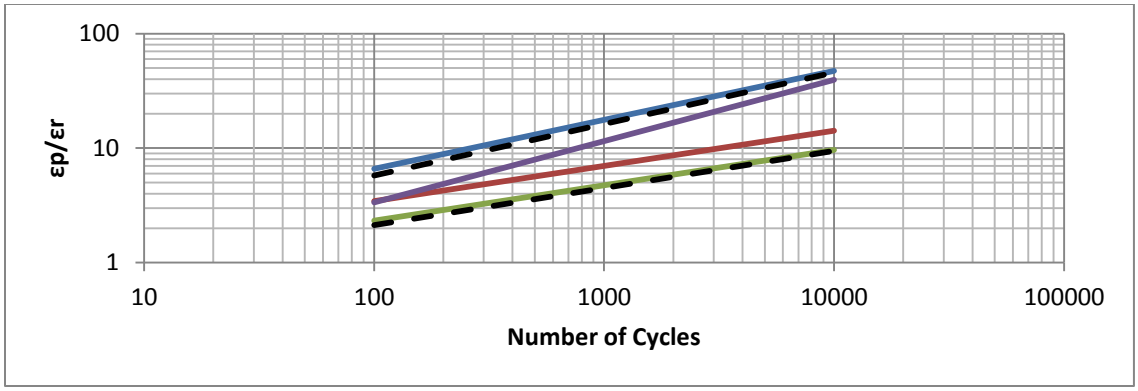

(a)

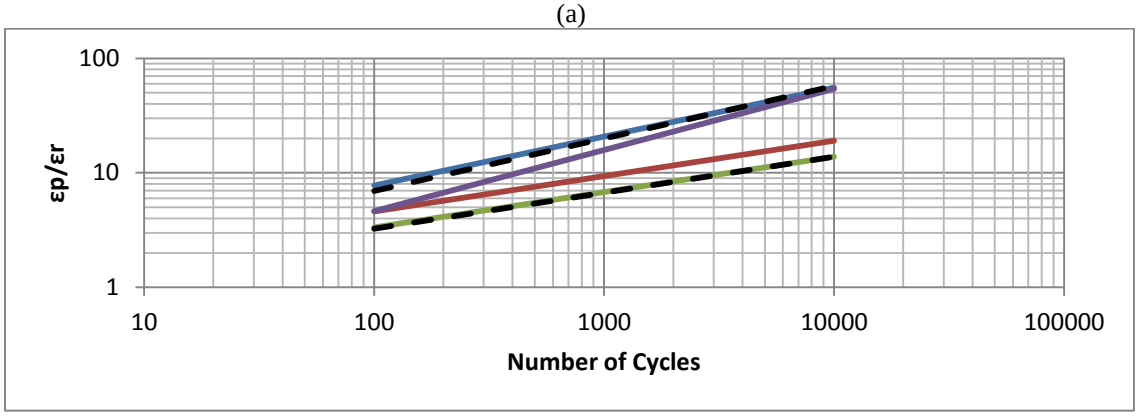

(b)

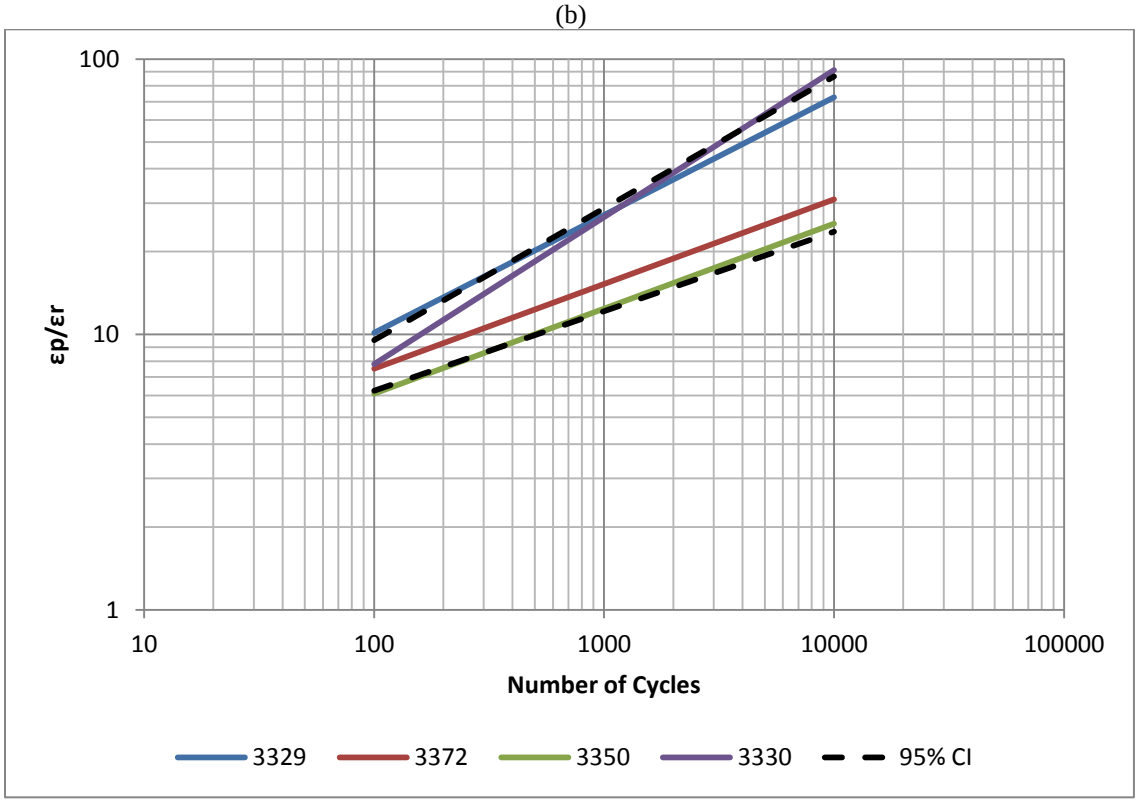

(c)

Figure 62. Rutting Results for District 3 Mixtures (a) 104°F (b) 114.8°F (c) 136.4°F

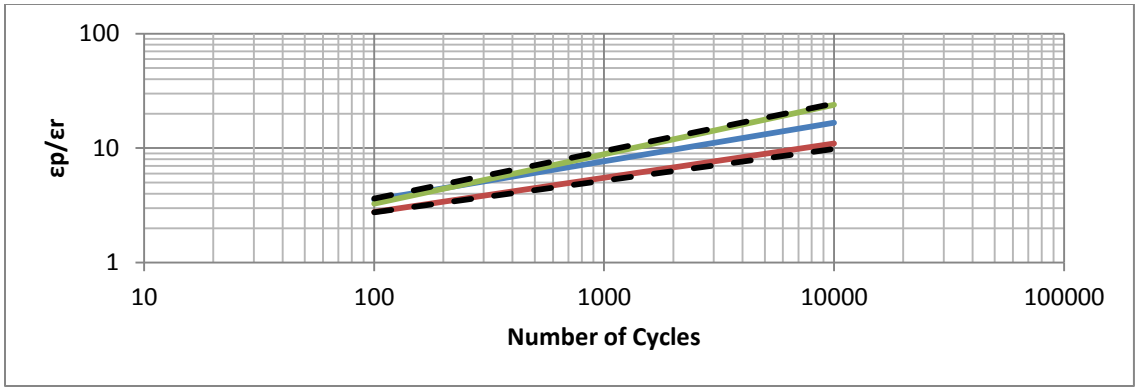

(a)

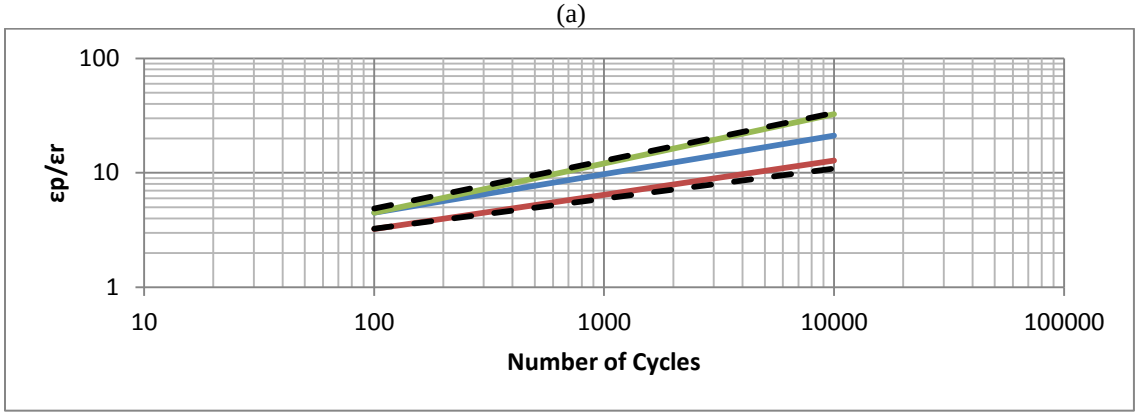

(b)

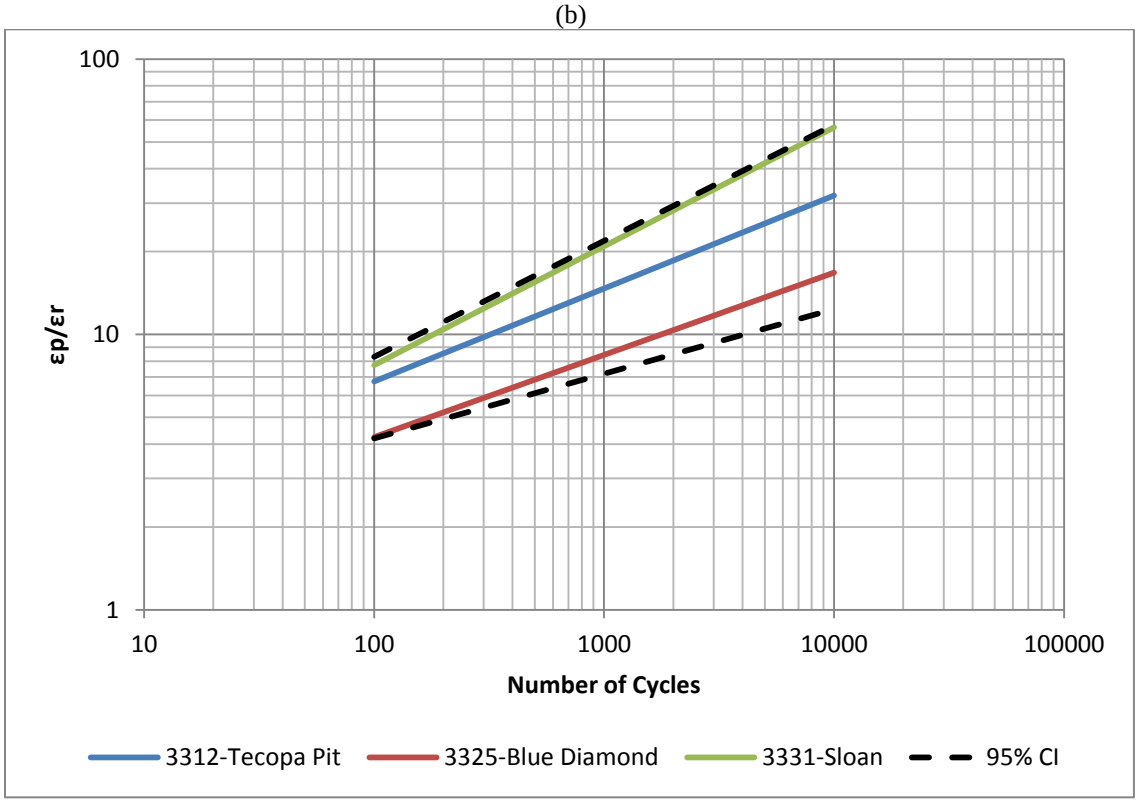

(c)

Figure 63. Rutting Results for Binder Source SEM Mixtures (a) 104°F (b) 114.8°F (c) 136.4°F

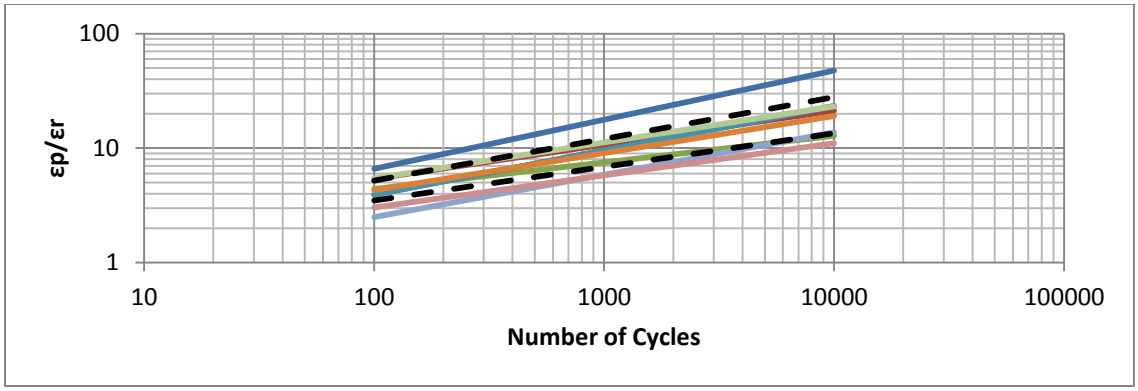

(a)

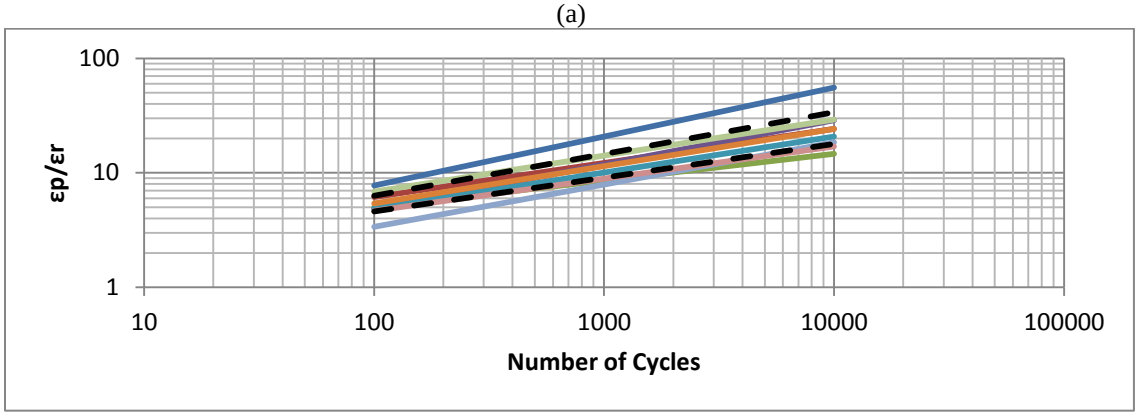

(b)

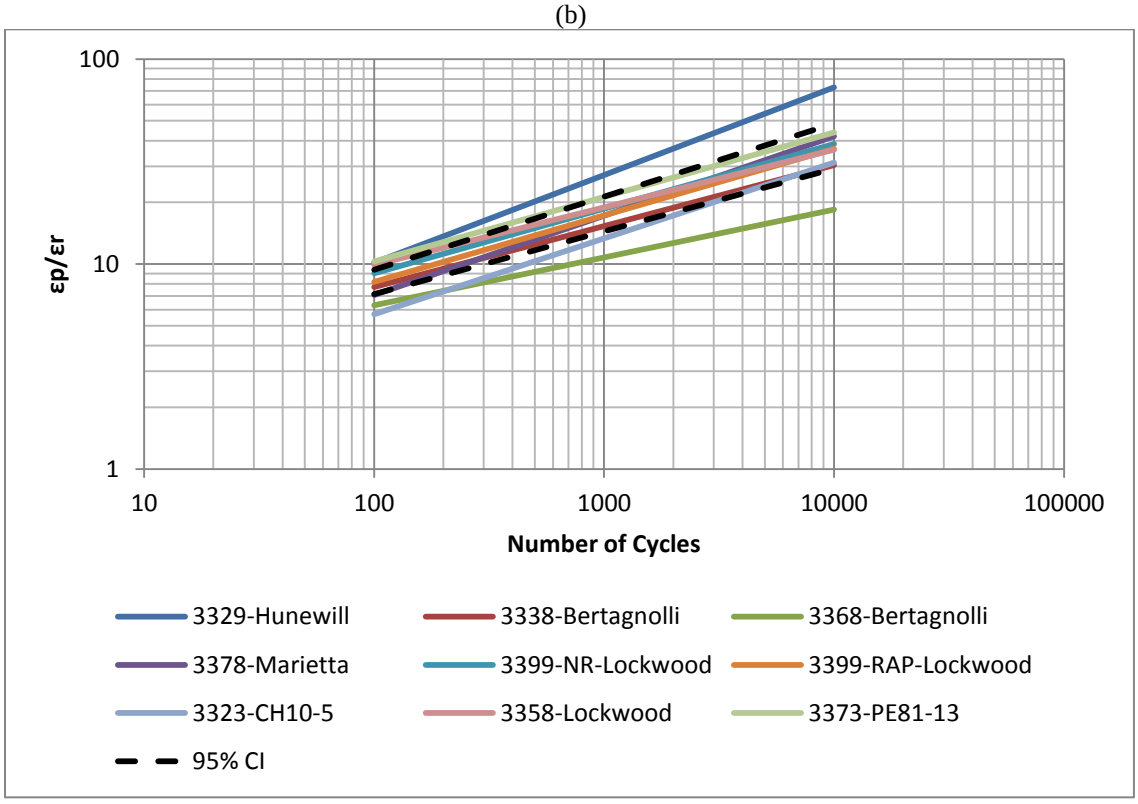

(c)

Figure 64. Rutting Results for Binder Source Paramount Mixtures (a) 104°F (b) 114.8°F (c) 136.4°F

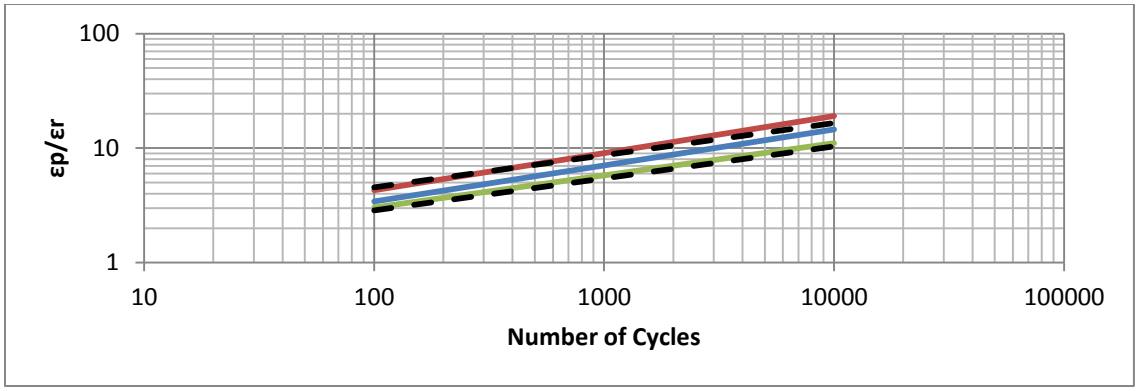

(a)

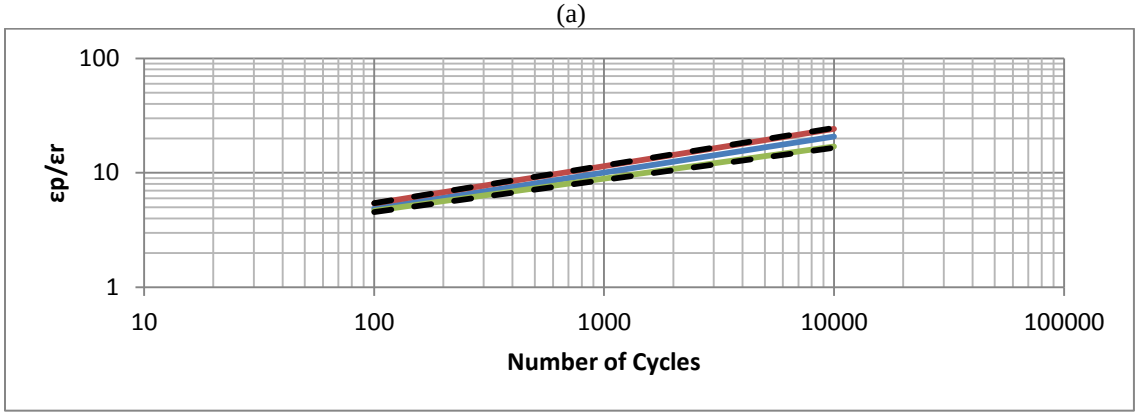

(b)

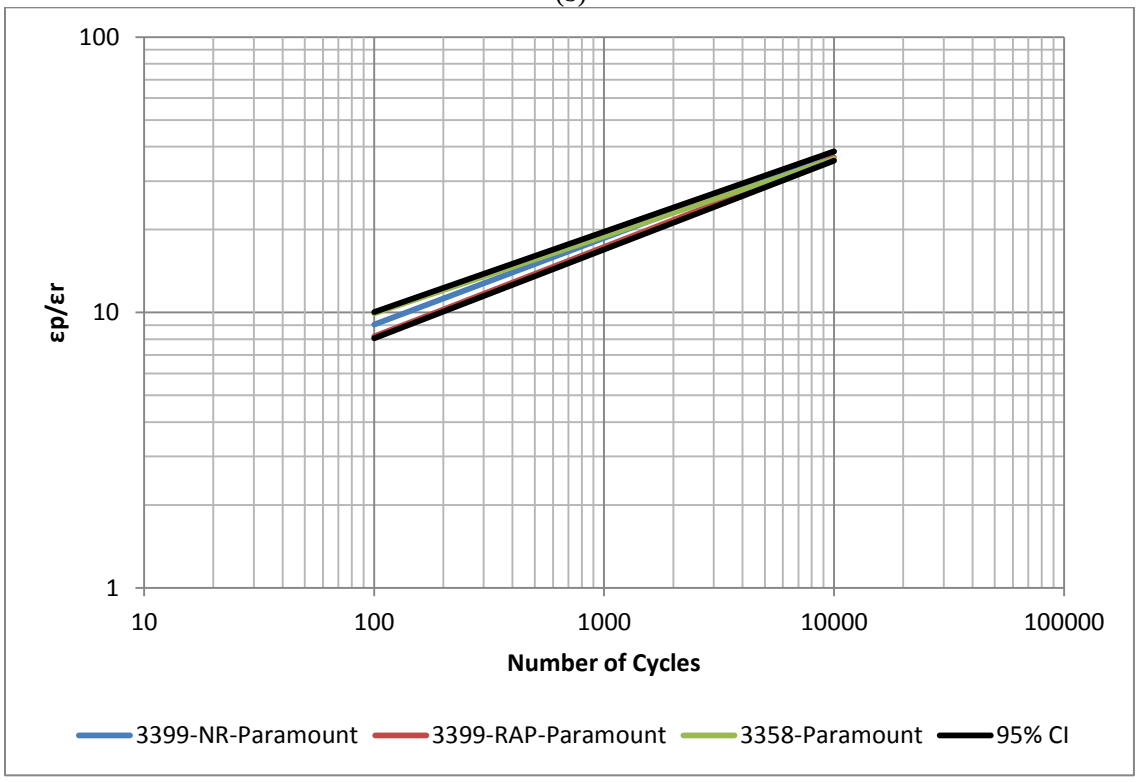

(c)

Figure 65. Rutting Results for Aggregate Source Lockwood Mixtures (a) 104°F (b) 114.8°F (c) 136.4°F

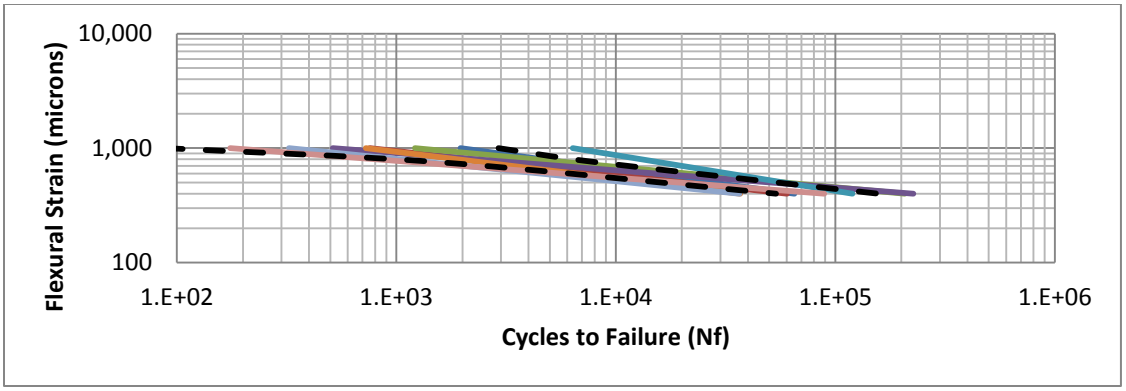

(a)

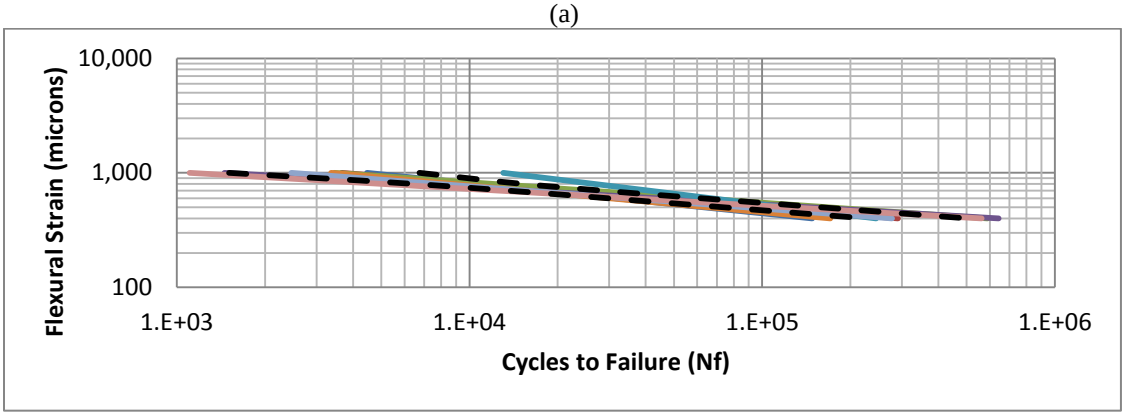

(b)

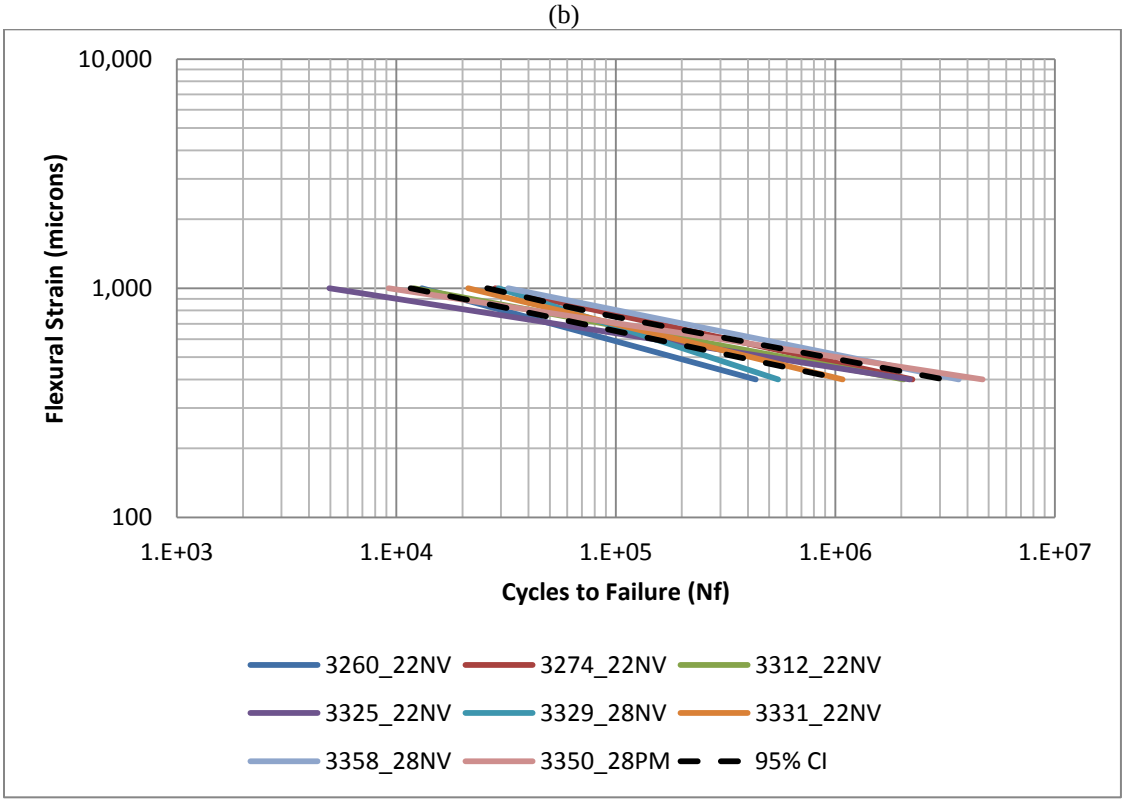

(c)

Figure 66. Fatigue Results for Sampled Mixtures in Nevada (a) 55°F (b) 70°F (c) 85°F

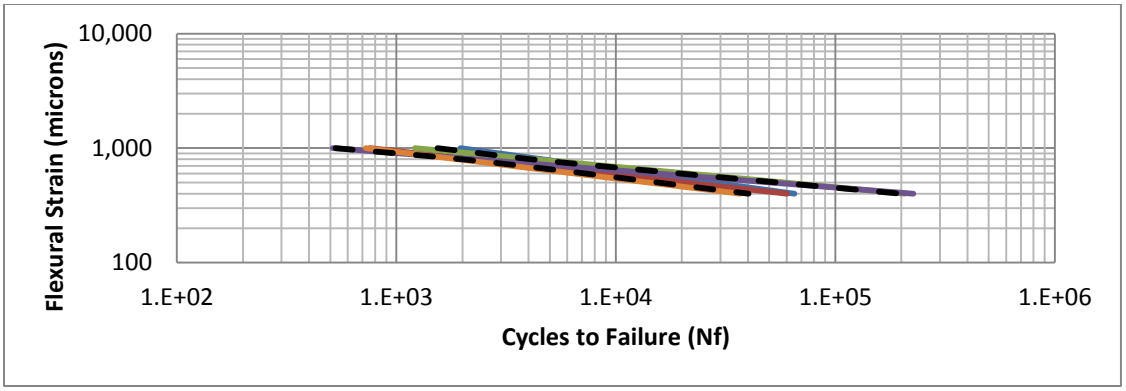

(a)

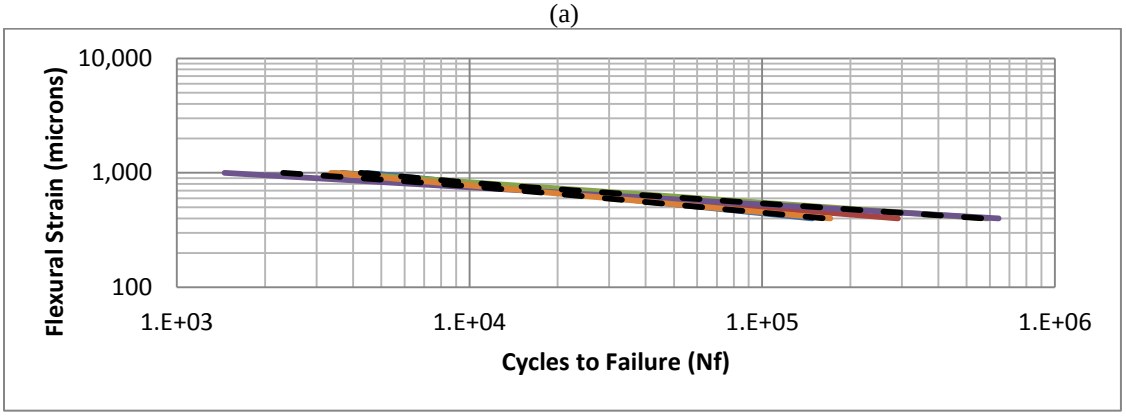

(b)

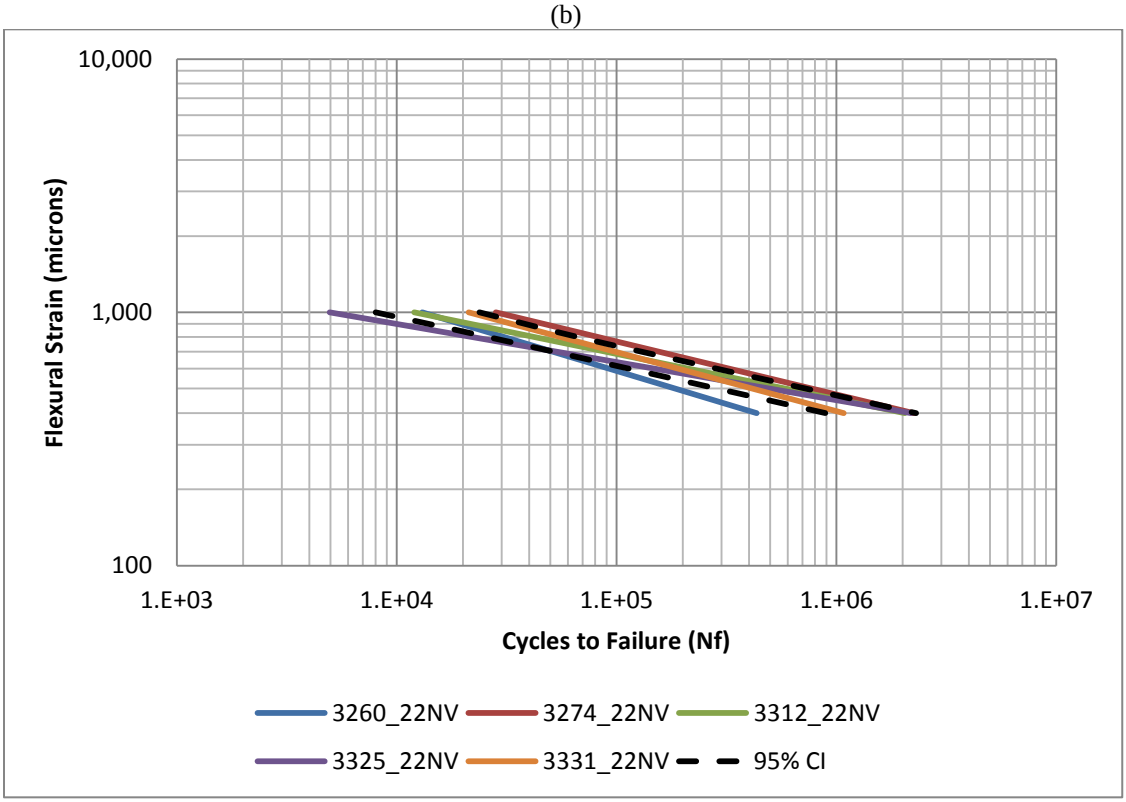

(c)

Figure 67. Fatigue Results for PG76-22NV Mixtures in Nevada (a) 55°F (b) 70°F (c) 85°F

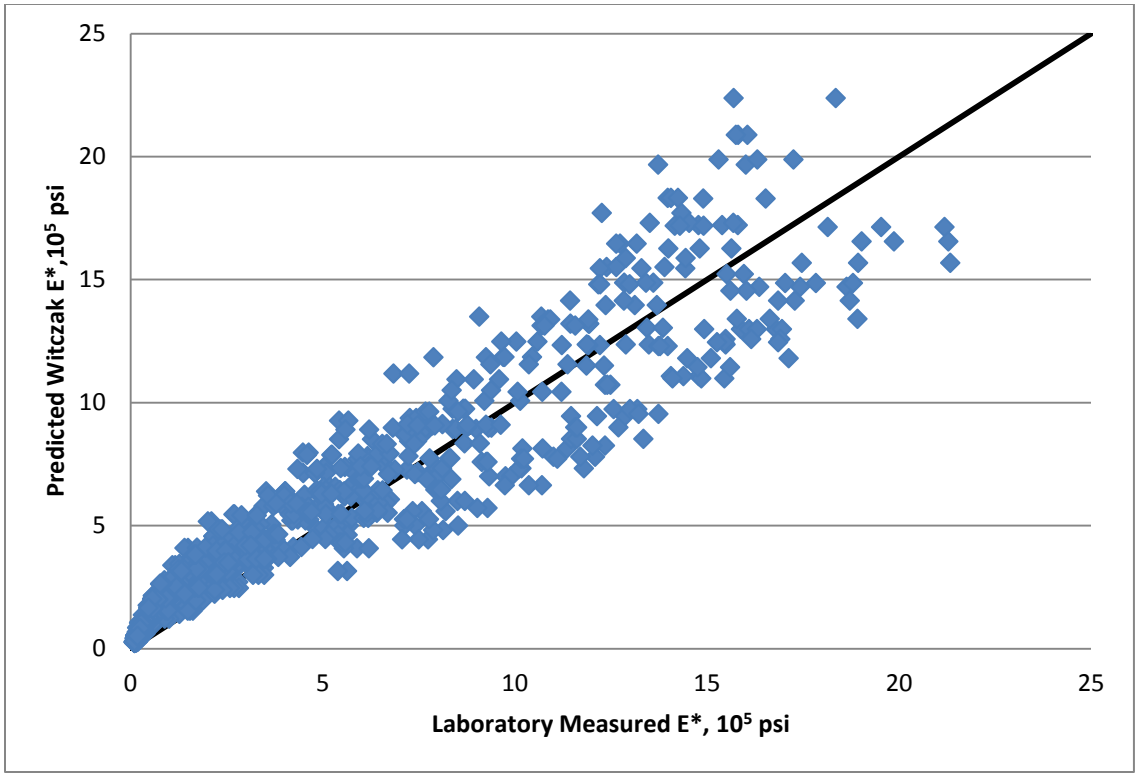

Figure 68. Witczak Model Comparison To Measured E*

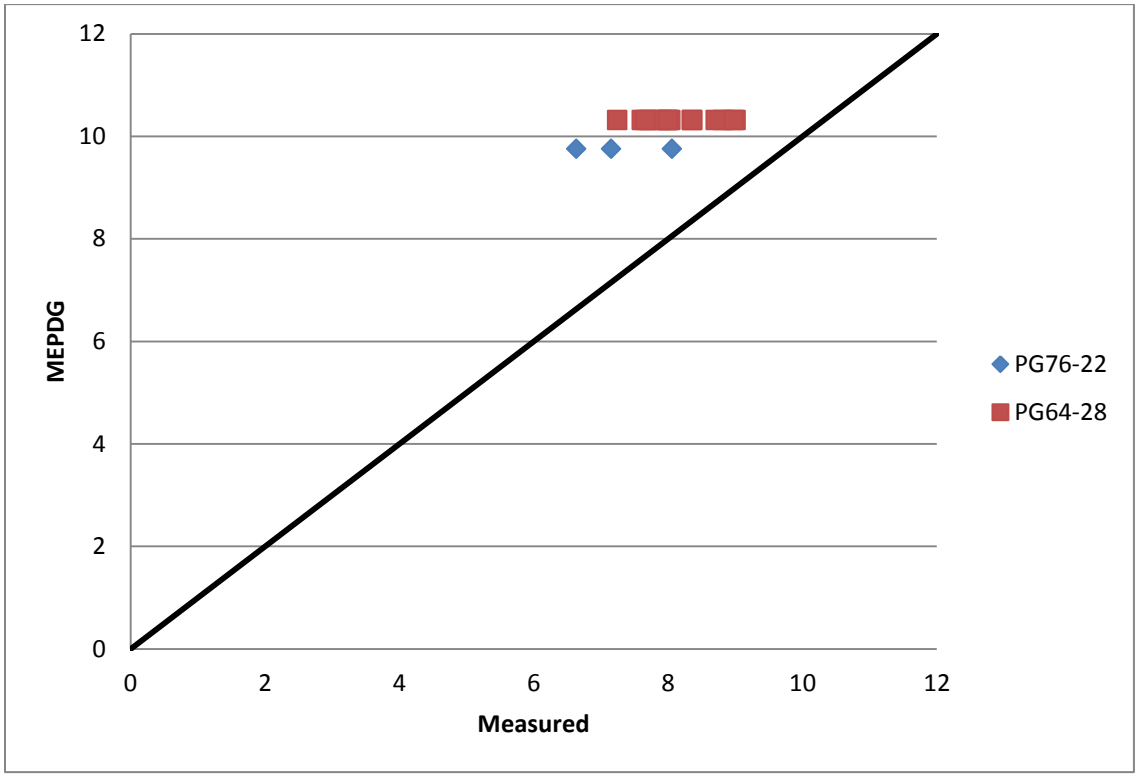

Figure 69. MEPDG Level 3 Comparison to Measured A Values

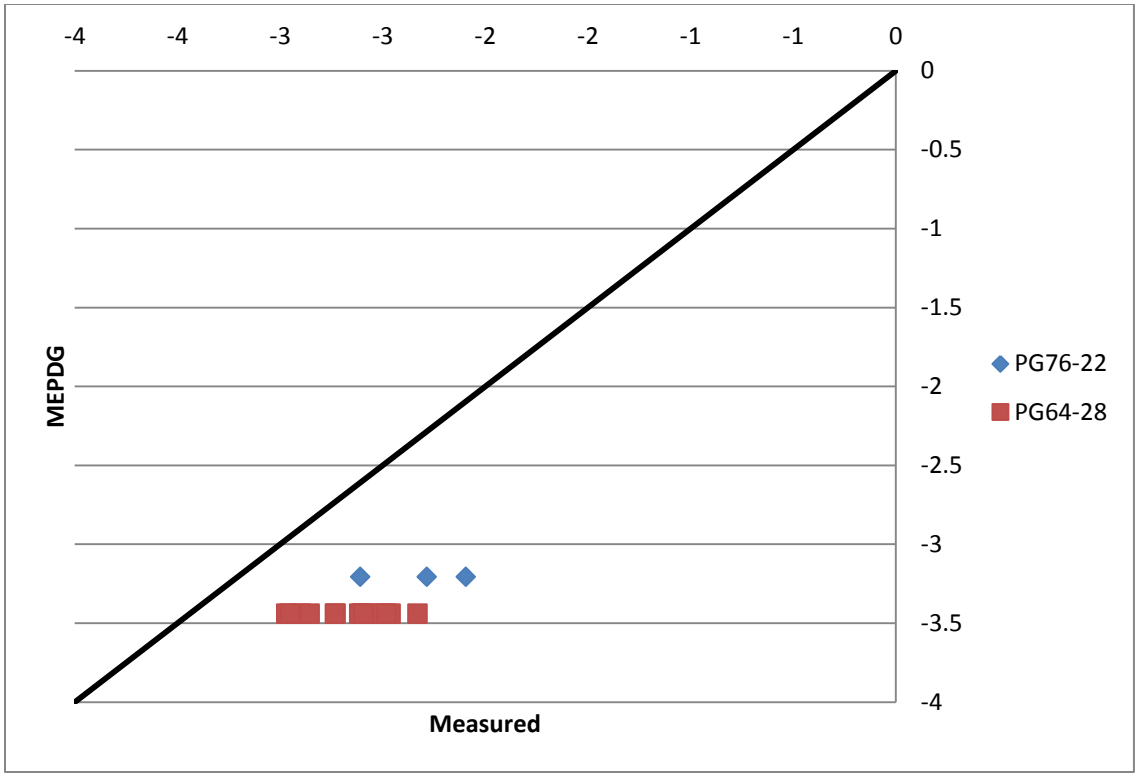

Figure 70. MEPDG Level 3 Comparison to Measured VTS Values

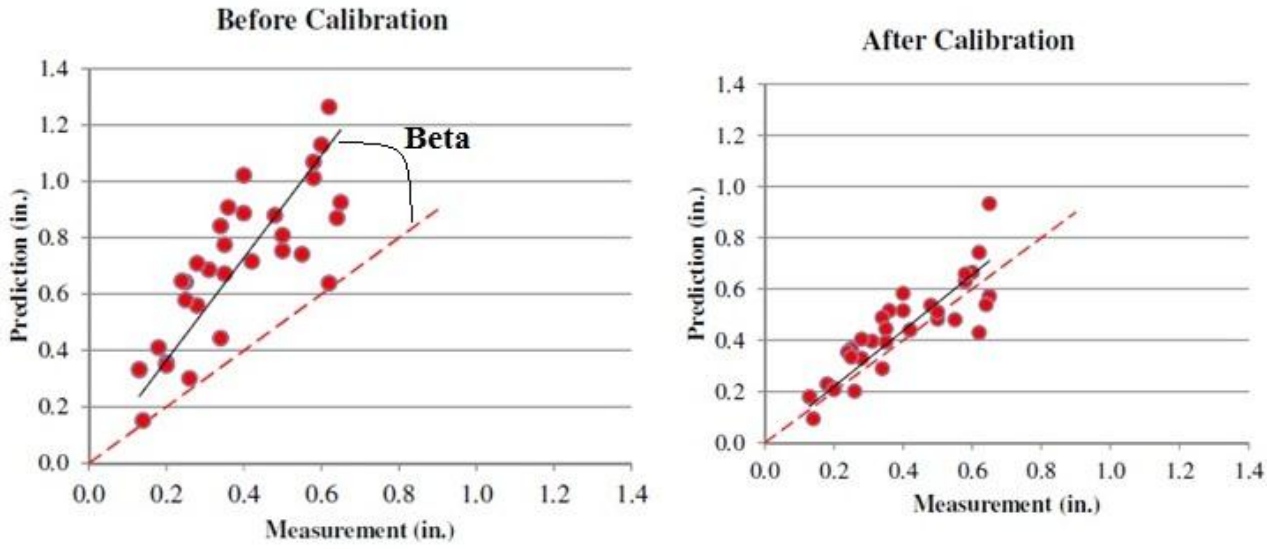

Figure 71. Shifting Predicted to Measured using a Beta Factor